FABRICATION AND PERFORMANCE ANALYSIS OF BORON NITRIDE SURFACE COMPOSITE TOOL STEEL SUBSTRATE FOR HIGH TEMPERATURE APPLICATIONS

A Thesis

Submitted in partial fulfillment of the requirements for the award of the degree of

DOCTOR OF PHILOSOPHY

In

Mechanical Engineering

By

Harminder Singh Saggu
41500104

Supervised By

Dr. Amardeep Singh Kang

Co-Supervised by

Dr. Chander Prakash
Dr. Catalin I. Pruncu

LOVELY PROFESSIONAL UNIVERSITY
PUNJAB
2021

Declaration

I hereby declare that this Ph.D. thesis entitled “Fabrication and performance analysis of boron nitride surface composite tool steel substrate for high temperature applications in Mechanical engineering in Lovely Professional University, Punjab, India” was carried out by me for the degree of Doctor of Philosophy in Mechanical engineering under the guidance and supervision of Dr. Amardeep Singh Kang and co-supervision of Dr Chander Prakash and Dr. C.I. Pruncu. The interpretations put forth are based on my reading and understanding of the original texts and they are not published anywhere in the form of books, monographs or articles. The other research papers, books, articles and websites, which I have made use of are acknowledged at the respective place in the text. For the present thesis, which I am submitting to the University, no degree or diploma or distinction has been conferred on me before, either in this or in any other University.

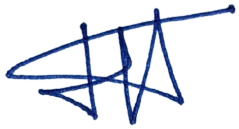

Place: Phagwara

Mr.Harminder Singh Saggu

Date: January 2021

(Research Scholar)

Lovely Professional University, Punjab, India

Certificate

This is to certify that the thesis titled "**FABRICATION AND PERFORMANCE ANALYSIS OF BORON NITRIDE SURFACE COMPOSITE TOOL STEEL SUBSTRATE FOR HIGH TEMPERATURE APPLICATIONS**" being submitted by **Mr. Harminder Singh Saggu** to the Lovely Professional University, Punjab, India for the award of the degree of **DOCTOR OF PHILOSOPHY** is a record of bonafide research carried out by him under our guidance and supervision. Mr. Harminder Singh Saggu has worked for about three and half years on the above problem and the work has reached the standard fulfilling the requirements and the regulations relating to the degree. To the best of our knowledge the work incorporated in this thesis has not been submitted to any other University or Institute for the award of any other degree or diploma.

Dr. Amardeep Singh Kang (Supervisor)
Associate Professor
Mechanical Engineering Department,

Lovely Professional University,
Phagwara, Punjab (India)

Dr. Chander Prakash (Co-supervisor)
Associate Professor,
Mechanical Engineering Department,

Lovely Professional University,
Phagwara, Punjab (India)

Dr. C. I. Pruncu (Co-Supervisor)
Research Fellow, Mechanical Engineering Department,
Imperial College of London, UK

Abstract

The current research presents the diffusion of cubic boron nitride (c-BN) on the D2 tool steel surface by the thermo-chemical process to enhance its tribological properties. The c-BN was diffused on the tool Steel surface by the thermo-chemical diffusion process using argon controlled furnace. The effect of temperature and time on the diffusion of c-BN on tool steel surface, micro-hardness, and wear resistance was studied. The field-emission scanning electron microscopy (FESEM) and energy-dispersive spectroscopy (EDS) was used to analyze the morphology and elemental composition of the as-synthesized cBN-D2 surface composite. Further, the micro-hardness of deposited coatings was investigated using Vickers hardness tester. The wear resistance of surface composite was studied using a pin-on-disk apparatus. The erosion resistance was investigated by Al_2O_3.

There was no visual diffusion observed at 550 ºC and 650 ºC at different soaking hours. This is because the re-crystallization temperature of steel is more than 650 ºC. Thereby, the c-BN was unable to dissolute on the surface. The diffusion of c-BN occurred at or more than 750 ºC after soaking at least 2 hours. At 750 ºC, the D2 steel undergone through the re-crystallization phase and get soften owing to that c-BN particles were reinforced into the substrate surface up to few microns. The diffusion depends upon the temperature and soaking hours. The increase in soaking temperature to more than 2 hours, the change in the microstructure and diffusion layer was observed. The best optimal condition for the diffusion of c-BN on the D2-steel surface was 750ºC for 2 hours and 850 ºC for 1 hour.

At 750 ºC of soaking temperature and 1 hour of soaking time, a very small diffusion layer was observed. The diffusion layer was measured upto 5 μm thick. At 850 ºC of soaking temperature and 1 hour of soaking time, very thick diffusion layer was obtained. The diffusion layer was measured upto 35 μm thick. At 950 ºC of soaking temperature and 1 hour of soaking time, very thick diffusion layer was obtained, but sample get oxidized and change its shape and profile. The diffusion layer was measured upto 43 μm thick. When the soaking time increased, the diffusion thickness increased. Still small diffusion was observed at 750 ºC of soaking temperature and 1.5 hour. The diffusion layer was measured upto 9 μm thick. At 850

ºC of soaking temperature and 1.5 hour of soaking time, very thick diffusion layer was obtained. The diffusion layer was measured upto 78 μm thick. The best optimum condition for high diffusion layer is high soaking time (2 h) and moderate soaking temperature (850 ºC).

At 750 ºC of soaking temperature and 1 hour of soaking time, a very small diffusion layer was observed as a result no significant increase in the micro hardness (H_μ) was observed. The H_μ was measured around 350 HV. At 850 ºC of soaking temperature and 1 hour of soaking time, thick diffusion layer was obtained, which improved the surface properties. The H_μ was measured around 850 HV. At 950 ºC of soaking temperature and 1 hour of soaking time, very thick diffusion layer was obtained, but sample get oxidized and change its shape and profile. As a results mechanical properties destroyed. The H_μ was measured around 650 HV. When the soaking time increased, the diffusion thickness increased, which improved the mechanical properties of surface. Still small diffusion was observed at 750 ºC of soaking temperature and 1.5 hour. As a result slight improvement in the microhardness of the surface was measured. The H_μ was measured around 500 HV. At 850 ºC of soaking temperature and 1.5 hour of soaking time, very thick diffusion layer was obtained and surface became very hard and brittle. The H_μ was measured around 1475 HV. The best optical condition for high surface hardness is high soaking time (2 h) and moderate soaking temperature (850 ºC).

It is evident from cross-section analysis of surface composite prepared at 750 ºC for 2 hours comprised of unevenly distributed micro-cracks and micro-holes of different sizes. The c-BN particles were diffused in D2 steel substrate upto 50 μm depth at operating condition of at 750 ºC for 2 hours. The as-prepared layer at 850 ºC for 1 hour comparatively thicker zone. The c-BN particles were diffused in D2 steel substrate up to 90 μm depth at operating condition of at 850 ºC for 1 hour. At higher temperatures, the D2 steel surface becomes soft and this allows c-BN to diffuse deeper in the layer. The c-BN particles in layer can be clearly seen in the cross-section micrograph, which conferred and confirmed the diffusion of c-BN particles.

The mean hardness of c-BN-reinforced surface composite developed at 750 ºC for 2 hours was measured around 1350 HV, which was 345.54% higher as compared to the un-treated sample (303 HV). Whereas, the c-BN-reinforced layer developed at

850 ºC for 1 hour was 1570 HV, which is 418.2% higher as compared to raw samples hardness 303 HV. These samples revealed slightly lower wear resistance against WC, Al_2O_3 counter surfaces and the best wear rate against Si_3N_4 counter surface. Overall, the wear resistance of pin surface treated at 850º C for 1 hour was improved with almost 89.65% by diffusion of c-BN in D2 steel, when comparing to untreated pin samples. Erosion resistance of diffused samples were maximum at impingement angle of 90° which was then increases at impingement angle of 60° and then maximum at impingement angle of 45°. Therefore, based on the present investigated data the erosion resistance at impingement angles of 45°, 60° and 90° can be arranged in the following order "**Sample-II (at** 850ºC for 1 hour) **> Sample-I (at** 750ºC for 2 hours**) > Un-treated base Steel".**

In summary, the present research study shows that c-BN diffused layer have potential of for tailoring hard and wear resistant features for high temperature applications like machine tool and turbine blade, and boiler coating.

Acknowledgements

Completion of this doctoral dissertation was possible with the support of several people. At the onset, I would like to express my sincere gratitude to all of them. Firstly, I would like to express my sincere thanks to my supervisors Dr. Amardeep Singh Kang, Dr Chander Prakash and Dr. C.I. Pruncu for their continuous support in my Ph.D study and related research, for their patience, motivation, and immense knowledge. Their guidance helped me in all the time of research and writing of this thesis. The thesis would not have come to a successful completion, without the help I received from my supervisors. Their enthusiasm on the problem and encouragement throughout the course of this work is very much appreciable.

I would like to thank Dr. Lovi Raj Gupta, Dean LTFS, Lovely Professional University, Phagwara, for creating a healthy working environment at campus and for timely help I received from him. I thank Dr. Vijay Kumar Singh, HOS, School of Mechanical Engineering for facilitating various equipment for completion of this work. I am grateful to all staff members of the department for their useful suggestions and for the help rendered to me in carrying out this work.

I would also express my gratitude to Prof. B.S. Pabla, Professor, National Institute of Technical Teachers Training & Research, Chandigarh for his cooperation during the micro-hardness testing and wear resistance experiments. I am thankful to Dr. Uday Krishna Ravella, Associate professor at Madanapalle Institute of Technology & Science, Andhra Pradesh for his guidance. I am also thankful to my fellow research scholar for their support and cooperation during my experimentation. I offer my regards and blessings to all of those who supported me in any respect during the completion of my Ph.D work. I owe a lot to my parents, who encouraged and helped me at every stage of my personal and academic life, and longed to see this achievement come true. Above all, I owe it all to Almighty God for granting me the wisdom, health and strength to undertake this research task and enabling me to its completion.

Harminder Singh Saggu

Table of Contents

List of Tables

List of Figures

LIST OF ABBREVIATIONS

c-BN	Cubic Boron Nitride
CVD	Chemical Vapour Deposition
dc	Direct Current
DLT	Diffusion layer thickness
EDS	Energy-Dispersive Spectroscopy
h-BN	Hexagonal Boron
HSS	High speed steel
PECVD	Plasma Enhanced Chemical Vapour Deposition
PVD	Physical Vapour Deposition
SEM	Scanning Electron Microscopy
W-EDM	Wire-electric discharge machining
XRD	X-ray Diffraction

CHAPTER 1

INTRODUCTION

Die steel is one of the most commonly employed engineering material contributing nearly 85% of the world's tool industry products. Carbons with relatively high strength are related to carbon steel alloys, but with low corrosion resistance, further surface treatment is required, such as surface protection coverings, when exposed to tough environments. Coatings and surface modification are the only solutions to prevent the surfaces from unfavorable external-environmental contact and resist the damage that occurred due to corrosion and other mechanical damage [1]. Tool steels have been used from the beginning of machining-era for high-temperature machine-tool applications such as a single-point cutting tool, drill bit, and milling cutter, etc. [2]. But, low surface hardness (300-330 HV) of tool steel restricts its industrial applications [3].

Tool steel is a type of steel that is used to produce tools to cut, form or otherwise form the material into a part or component adapted for certain applications. Added relatively high amounts of tungsten, molybdenum, manganese, and chromium can make the tool steels more service-intensive and provide more dimensional inspection and free from cracking during heat processing [4]. The efficiency of the tool in operation depends on the tool's nature, its exactness, the choice of the tool steel, and the heat treatment range. The heat treatment procedure is based on high-quality tool steel, appropriately built tools, and correct manufacturing methods [5].

1.1. Type of Tool steels

For comparison and evaluation, it is important to classify tool steel into relatively small numbers and to facilitate steel selection for a specific application. Since tool stones have such a variety of composition, fitting them into one category of the alloy steel system has never been easy. Tool steels have small alloy limits, and a whole series of steels is based on the varying content of carbon. The "Automotive Engineering Society" (SAE) and "American Iron and Steel Institute"(AISI) methods

are the methods the most frequently used for the classification of tool steels. AISI is more popular because it makes the instrument steel [6].

AISI W- type steel has the lowest content of the alloy and, consequently, the lowest durability of any of the steel instruments. As a result, the W-type tool steels also require water-quenching and heavy parts only harden to shallow depths. Thin segments can be hardened to minimize cracking and distortion with oil quenching. The AISI S-type steel has less carbon and a slightly higher alloy content than the stones in W. The moderate carbon content increases strength and makes type S steels ideal for shock and impact loading applications [7-8].

The cold work tooling steels are comprised of three classes, AlSI type O, A, and D. Each class has high carbon content for high hardness and wear strength in cold work, but the content of alloys vary, which impact on hardness and carbide distributions in hardened microstructures. AISI P-type tool steels are less exposed to wear than metal-working steel and are therefore low in carbon content for dies in-mold plastic. Good polishing and superb surface finish is an essential requirement [9]. The most important alloying element was the AISI h-type device, made up of chromium, tungsten, or molybdenum. The H-stalks are used to hammer, cut metal and cast metal die. Tungsten and molybdenum are the major alloying elements of the classes T and M, are the high-speed tool stalls. Tungsten and vanadium produce very high densities of stable carbides in these steels. It allows steels with high-speed machines to maintain their hardness at high temperatures and to be used widely in high-speed cutting and work applications [10].

In the past, surface engineering has been acknowledged for the safety and prevention of corrosion and other mechanical harm of surfaces against harmful chemical or physical interactions with environments. The objective of coatings is to protect the components [11]. Several processing methods were explored to synthesis coatings to protect the surface form of mechanical hazards.

1.2. Surface Engineering

A wide range of techniques were used for surface hardening. This is most widely used to boost wear-resistance without impacting the softer, tough base material required to withstand impacts during service. Materials from solid structures are

physically separated through wear. It can be classified as abrasive, adhesive, and wearing fatigue in three categories. Abrasive wear occurs when two surfaces rub together and the more difficult surface grinds away. A rough appearance will describe it. The surface can often be hardened. Unlike abrasive wear, adhesive wear is caused by rubbing together the loaded surfaces. The friction on the ends of opposing asperities on the rubber surfaces induces high localized temperatures with adhesive wear [12]. Owing to localized temperatures, these tips will deform and "weld together." They are both breaking and falling as ruins or are soaked in cold. Whenever a surface undergoes repeated high stress, fatigue wear occurs. Temperature is less influenced than corrosion by wear rates. The various surface hardening methods have three distinctly different approaches.

1.2.1 Thermal Spraying Technologies

The potential to develop high-strength surfaces has given them an increased interest in the use of thermal spraying techniques. Thermal spraying is a general term for processes that feed a chamber, torch, or weapon near or above their melting points into metal, ceramic, and some polymeric material, in wire, rod, or powder types, then accelerates into a substratum to lay the covering [16-17]. Fig. 1.1 shows the schematic representation of a thermal spray coating [18].

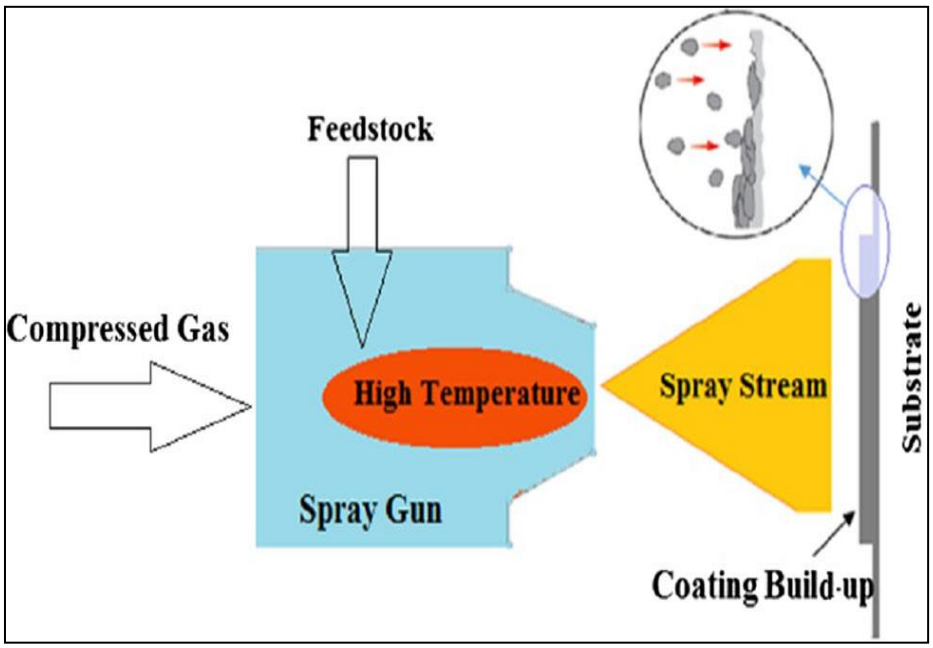

Fig. 1.1. Diffusion of forging particle through thermal spray coating [18]

The major techniques for thermal-spray are air/vacuum plasma (APS), direct-current (D.C) spraying, plasma generated radiofrequency (R.F.), arc transferred plasma (PTA), arc spray, fire spraying, high-speed oxygen (HVOF), high airspeed (HVAF), gun denotations (D-gun) and cold gaseous dynamical spraying (CS), which are the primary thermal spraying techniques. Flame, electric-arc-spray, and plasma-arc-spray were the most widely used methods in recent years for depositing corrosion-resistant coverings on steel substrates [19-20]. Flame-spray is one of the longest-standing and highly effective methods and uses fuel gasses [21]. The most well-known gasses used in this procedure include acetylene, propane, methyl acetylene propadiene, and hydrogen, and oxygen. The flame spray may occur at a low velocity and will spray both powder and wires on metals and alloys. Compressed air helps to facilitate the use of flammable materials. Flame spraying is also possible at high speeds, and in this category, HVOF is the most common technique [22-24]. HVOF uses a mixture of oxygen, namely hydrogen, propane, propylene, and kerosene, with various fuel gasses. Powdering particles in the combustion chamber are heated within a temperature range of 2500-3200 ºC and are thus softened to the substratum at high speeds of 1500-1800 m/s [25-27].

1.2.2 Thermal diffusion technologies

Thermal diffusion technology is an advanced method in surface engineering that can be used to modify the surfaces to ensure protection against extreme environmental conditions for industrial components of various sizes and shapes, in particular pipelines and high-dimensional tubes [28-29]. Thermal diffusion technology has succeeded in creating thin layers of carbides, borides, aluminides, and chromatics on the steel substrates surface which are resistant to rubbing and to hardness [30-31]. Studies and reviews of corrosion and wear of thermal diffusion coatings in this respect pave the way for further progress. This technique provides effective and modified surfaces in waste-to-energy plants and the oil and gas industry for steel substrates. The thermochemical diffusion technique, derived from the concepts of the CVD process, involves the chemical alteration of steel substrates by exposing them at elevated temperatures of 800-1100 ºC to the vaporized shape and later on the foreign particles placed on the surface get diffused in the surface [32-39].

This is the exposure of pre-heated steel substrates to different powder mixtures and the diffusion through metal substrates at high temperatures in the vaporized phases of thermal diffusion. This leads to new interconnected phases in these diffuse atoms' high-temperature interactions with the metal substrate [40-41].

Accordingly, new compounds (e.g. aluminides and chromides) such as borides or intermetallids are formed on steel substrate surfaces, depending on deposited active vapor atoms. The technology for thermal diffusion is based on diffusion processes and thus applicable to the shape of the coating are the laws for diffusion. For example, the boronization process consists primarily of two main mechanisms, namely diffusion by high-heat vacancies and interstitial diffusion of the boron selected atom [42]. Two main mechanisms for boronizing thermal diffusion in a steel substratum are shown in Fig. 1.2.

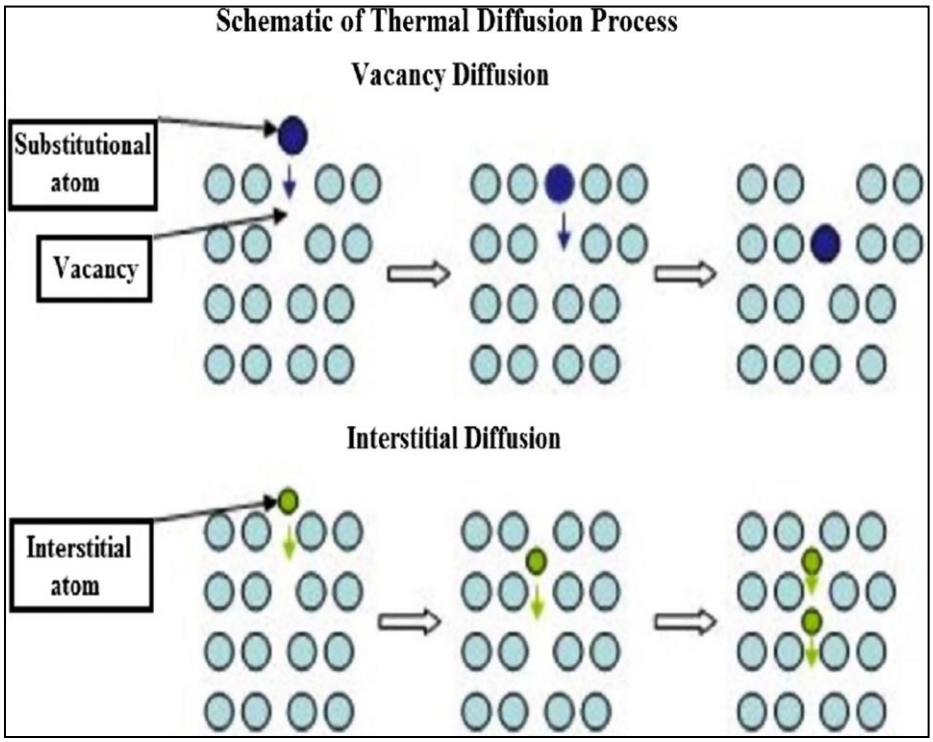

Fig. 1.2.Thermal-diffusion process [42]

Borides, aluminides, or chromides in some composition compounds simultaneously produced in the thermal diffusion coating may be included in some layers because of an inward diffusion of active coating atoms (e.g. B, Al, and Cr), and due to the external diffusion of metal substratum metals in steel (e.g. Fe, Cr, Ni, etc.). The layer can be used simultaneously for thermal diffusion. Initial mixing

compositions, substrates, and process parameters like the temperature, time-exposure, and gas pressure vary according to the structure of the forming layers, thicknesses, and compositions [43]. Fig.1.3 illustrates the microscope pictures of the cross-section of thermal diffusion coatings on low carbon steel substrates. In the case of boronization, the diffusion layer has been measured approximately 186 μm; see Fig. 1.3(a). The diffusion layer in the case of aluminisation from Fig. 1.3(b) was measured at approximately 186 μm. The diffusion layer was measured around 29 μm in the case of chromization; please refer to Fig. 1.3(c). More information is available elsewhere about the thermal diffusion process and the formation of its coating [44-45]. The thermometric diffusion process was widely used for the boronization of residual stainless steel substrates in several practical applications, particularly for waste-to-energy plants, oil & gas treatment, refining, and power generation [44-51].

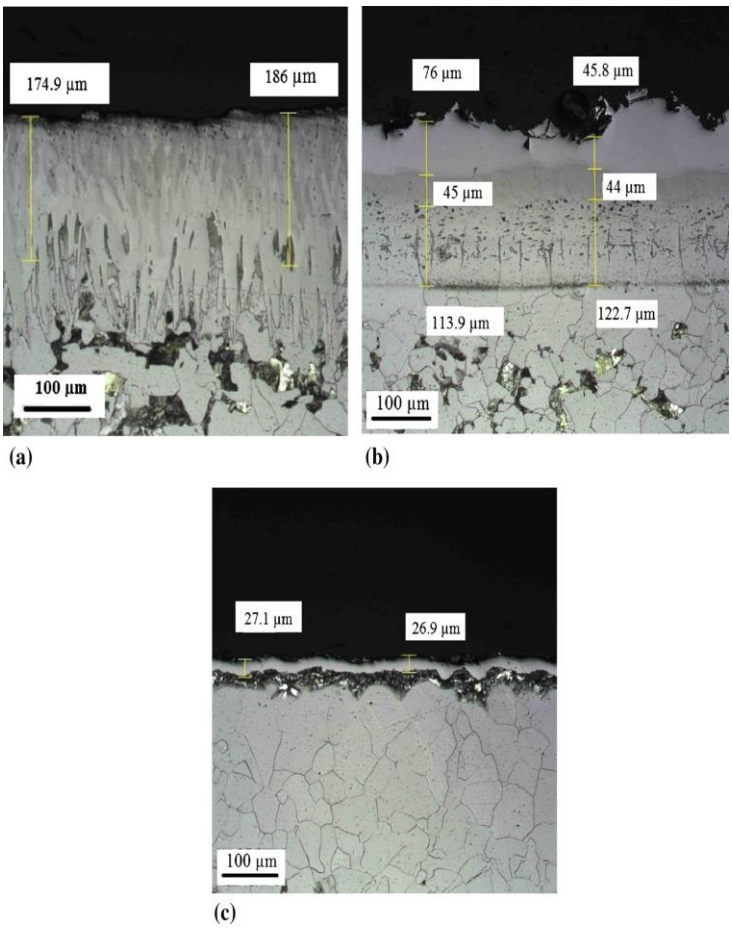

Fig. 1.3.Cross-section micrograph: (a) Boronizing, (b) Aluminizing, and (c) Chromizing [43]

Boride chemicals produced by the chemical vapor deposition and a technique of thermal diffusion were summarized by [45-46]. Metal boride materials are relatively high in hardness and chemical inertness and to be superior to those coverings in applications where corrosion and wear resistance are necessary. The corrosive resistance of the boronized steel substratum has been investigated by CVD and thermal diffusion processes [46]. It was suggested that iron borides and some other borides in the sheet protect the steel substratum effectively against corrosion at high temperatures. A study has been carried out on the surface of the boron coating of three substrates of steel, namely AISI 1018 carbon steel, AISI 4340 high-performance alloy, and austenitic stainless steel (AISI 304)[48]. Boronized coatings were exposed to hydrochloric acid (HCl) at room temperature and high temperatures (600 ° F) for oxidation resistance of coats. The boronisation of iron alloys significantly increased their corrosion resistance and oxidation resistance. Similar studies [50-51] have verified the boronated coating with AISI 1018 low carbon steel at high temperatures of up to 900 ° C. High thermodynamic characteristics, such as crystalline lattice energy and entertainment, are demonstrated in the thermal diffusion coating compounds which represent higher crystalline structure stability as well as Fe-B robust and shorter covalent bonds, which are connected with chemical stability and thermal diffusion coating integrity [52-53].

The direct result of the above phenomenon was that thermal diffusion coatings were extremely resistant to corrosion [54-55]. It was also found that, unlike stainless steel, thermally diffused boronated lacquers could not tolerate free iron (Fe) or any other constituent steel components and "introduced" (e.g., boron) elements in the covering. While considerable attention has been paid to CVD and heat diffusion boronized coatings, studies of aluminum corrosion and chromizing steels and alloys exposed to high temperatures in corrosive fluid and gaseous environments have also been carried out [56-57]. In an early analysis, the microstructures and mechanical development and the mechanistic structures and the aluminum diffusion coverage thermal stabilities were investigated on different steel substrates. Table 1.1 shows the various thermal diffusion coatings.

Table 1.1.Various layer on Steel surface using thermal-diffusion process [1]

Diffusion Process	**Substrate material**	**Temperature (ºC)**	**Findings**
Boronizing	Plain-carbon steel AISI 1018 High-strength steel AISI 4340 Austenitic stainless steel AISI 304	600	Boronizing coating significantly improved their corrosion and oxidation resistance
	Low-carbon steel AISI 1018	900	Successful corrosion resistance was observed
	Carbon steel	200-300	Boronized coatings provided a successful and promising corrosion and wear resistance under the simulated harsh Environment
	Low-carbon steel	220	Sign of corrosion was observed at elevated temperatures (500 ºC)
	316 Stainless steel	600	Boronized thermal diffusion coating on both steel substrates were slightly affected by the high-temperature corrosive attack
Aluminized	P91 ferritic-martensitic steel 800 austenitic stainless steels	650	Aluminized austenitic stainless steel substrate was corroded noticeably through via intergranular and internal chloridation-sulphidation-oxidationAluminized P91 ferritic-martensitic steel remained un-attacked
	P91 ferritic-martensitic steel	600	Two aluminide coatings, Fe1-xAl and Fe_2Al_5, were formed. Protective layer was formed

			on large parts of the $Fe_{1-x}Al$ coating, except some local failure which was associated to the dilatation of aluminum
	2.25Cr-1Mo steel	740	Aluminized coatings were not suitable for use within the application of coal gasifier atmosphere due to internal sulfidation-oxidation and detrimental cracking within the coating
	Low-carbon steel 316 Stainless steel	200	Aluminized samples have successful corrosion resistance in both low- and high-temperature molten salt—oxidation environments which was due to the formation of a thin layer of chemically inert Al_2O_3
Chromized	2.25Cr-1Mo steel	740	Chromized coating with more than 30 wt.% Cr and a thickness of 120 lm provided suitable corrosion resistance in sulfidation-oxidation conditions
	Low-carbon AISI 1020	700	Corrosion resistance of the chromized substrate improved compared to the original substrate
	Low-carbon steel	220	Chromized thermal diffusion coating on both steel substrates were not affected by the low-temperature corrosive attack; however, some phase changes after thehigh-temperature orrosive attack was observed for the chromide coatings
	316 Stainless steel	600	

In order to increase the surface hardness and galling strength, steels can be carburized [61-62]. During the carburizing process, the carbon atoms diffuse over the surface and react with the chromium in stain-less steels at high temperatures [63]. They can form carbide ($Cr_{23}C_6$) from chromium. This process is called perception. Thus, chromium may be lost and corrosion resistance may eventually be reduced. Conventional carburizing has been increasingly substituted for nitridization that does not cause sensitization issues [64]. When the material is heated to a temperature range of 600-800 ° C, sensitization takes place. Chromium and carbon are diffused at these temperatures to the grain boundaries to form chromium carboards $Cr_{23}C_6$ type. As carbides form, chrome from the base matter is depleted, but at grain borders is significantly increased. The chromium content is lower than the bulk alloy in areas that have low chromium levels, which make these areas vulnerable to corrosion. Many methods that have been proved industrial operate at lower temperatures. They work hard without affecting the original corrosion resistance, which provides a good quality base material [65-66].

The surface is not coated but is a carbohydrating area with a strong strength (up to 2–3% weight) and no risk of delamination or peeling on the surface. It is low-temperature carburizing when diffused below 450 °C. This process increases the surface hardening, nearly five times the original hardness, of the most stainless Steel to 1000 to 1200 $HV_{0.05}$. Carbon atomic interstitial solution creates high stress on the surface. All austenitic stainless steels are to be hardened [67-68].

Duplex and precipitation hardening of stainless steel grades was also successfully applied. Low temperature carburisation materials should be treated in the solution-cracking state. Sharp edges, bores and lacuna inside the process gas nitriding have no limitation. Gas nitriding is a case-hardening operation, by holding the steel in contact with a nitrogen gas, usually ammonia, in the air. For hard case production, quenching is not necessary. For most steels the nitriding temperature ranges from 500 °C to 550 °C [69]. While nitridization has adverse impacts on corrosion, similar to carburizing, it improves the toughness of the surface and provides less friction, hence improvement of the resistance to abrasion. Austenitic stainless steels and ferritic stains should be cured and removed from machining stresses before being gas-nitrided (as is also recommended prior to carburization). Usually, standard annealing

treatments for obtaining optimum resistance to corrosion are adequate [70-71]. There are other thermal diffusion and coating process such as plasma nitriding [72-80], liquid nitriding [81-100], nitro carburizing [101-120], and induction hardening to improve the surface properties of steel to enhance the wear resistance and heat resistant application.

1.3 Need and importance of thermal diffusion

Surface engineering procedures are used to create wear-resistant exteriors. In literature review various surface hardening methods were discussed. For surface modification carburizing, nitriding, nitrocarburising, carbonitriding, chromizing and thermal diffusion techniques were used. Amongst all thermochemical diffusion method alters the external surface's chemical composition with carbon, nitrogen and boron-like hardening species effectively. By diffusion one can achieve the surface to be extremely hard. They can be used for single elements as well as for batches. A thermal diffusion procedure involves the purposeful construction of the metal substratum of a new deposit over the substrate. The diffusion layer thickness obtained from the thermal diffusion can be effectively controlled by the controlling temperature and soaking time. The wear resistance, abrasion wear, adhesive wear, erosive wear and corrosion resistance improved in thermal diffusion process.

Chemical vapour deposition (CVD) and physical vapour (PVD) are the most commonly used methods used universally for depositing low-corrosive and non-abrasive coatings because of their large variety of elements to be deposited on ferrous and non-ferrous substrates with accuracy and more of purity in terms of chemical composition. But the cost of CVD, PVD, and magnetron sputtering is quite high as compared to the thermal diffusion. In thermal diffusion there exist an atomic bond in between substrate and the depositing element on the diffusion layer which shows a greater strength and anti-abrasive wear as compared to other thin coatings which are having high internal compressive stresses and thus responsible for low adhesion in between the coatings and the substrate material.

In case of thermal diffusion the deposited material have capacity to be applied to the substrate of any intricate shape and size without applying high pressure. With all these advantages over other processes thermal diffusion was chosen as surfaces hardening process.

CHAPTER 2

LITERATURE REVIEW

2.1 Introduction

Boron Nitride is an industrial ceramic material of limited but important applications mainly in electrical insulators and cutting tools. BN is a temperature and chemically reluctant composite which generally occur in dual forms (cubic and hexagonal). Cubic BN analogous to diamond is castoff in producing typically fused materials. Cubic BN is the second hardest material. It has good thermal and element stability, high resistance to mechanical properties **[1]**. hBN is most stable and is similar to graphite. It is used in manufacturing refractory materials. BN nanotubes can be produced with a similar structure to carbon nanotubes.By virtue of its unique and excellent thermal, electrical, and mechanical properties; it has received considerable scientific interest.

Industrial applications of BN thin film/ BN coatings are numerous. Application of BN as a thin film and BN as key constituent of composite have been tried and are being used industrially. BN being ceramic can withstand temperatures above 2000 ^{o}C and especially in cubic morphology, exhibits hardness better than diamond, making it an economical option as cutting tool material. The wear resistance and corrosive resistance even at elevated temperature is of the charts, making it a more suitable for applications, which demand high temperature corrosion, erosion resistance and hardness.

2.2 Boron Nitride coatings

Cubic boron nitride is used now a days as an important coating material on cutting tool applications as it is having very good mechanical and chemical properties. It is also used as it is having good hardness properties, very good thermal resistance, and good electrical resistance at elevated temperatures. In contrast, owing to its chemical balance, diamond is typically progressed at high temperatures as opposed to

oxygen and ferrous materials. Hexagonal boron nitride has good lubricating residences at high and low temperatures (up to 900 ^{o}C, even when the atmosphere is oxidizing) [5].

2.3 Review of thin films

Gocmanet al. studied the structure, morphology, and mechanical activity of thin films of boron nitride through the use of pulsed laser deposition on different metal substrates. Substrates are subjected to gas nitriding to improve adhesion and reduce internal stresses. Stable, crystalline, multi-phase coatings have been purchased with excellent adhesion to the metal substrate [121].Fig. 2.1 shows the diffused layer of thin boron nitride.

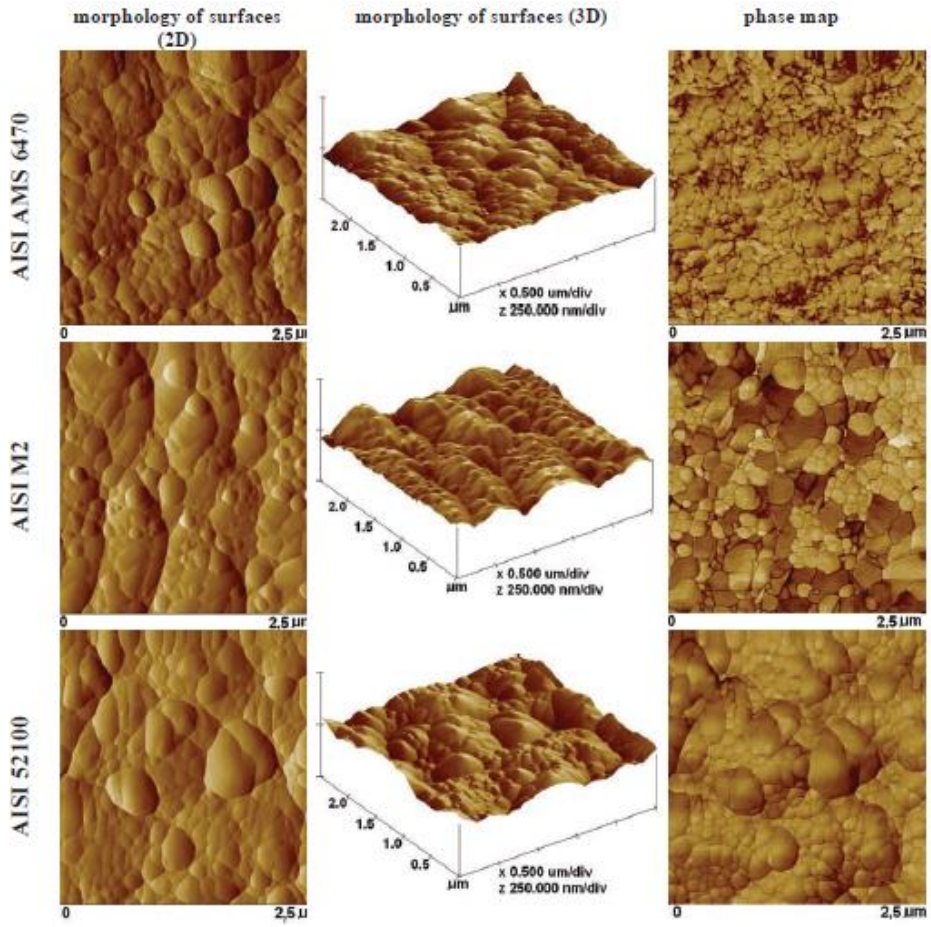

Fig. 2.1. AFM image of boron-nitride layer of steel surface [121]

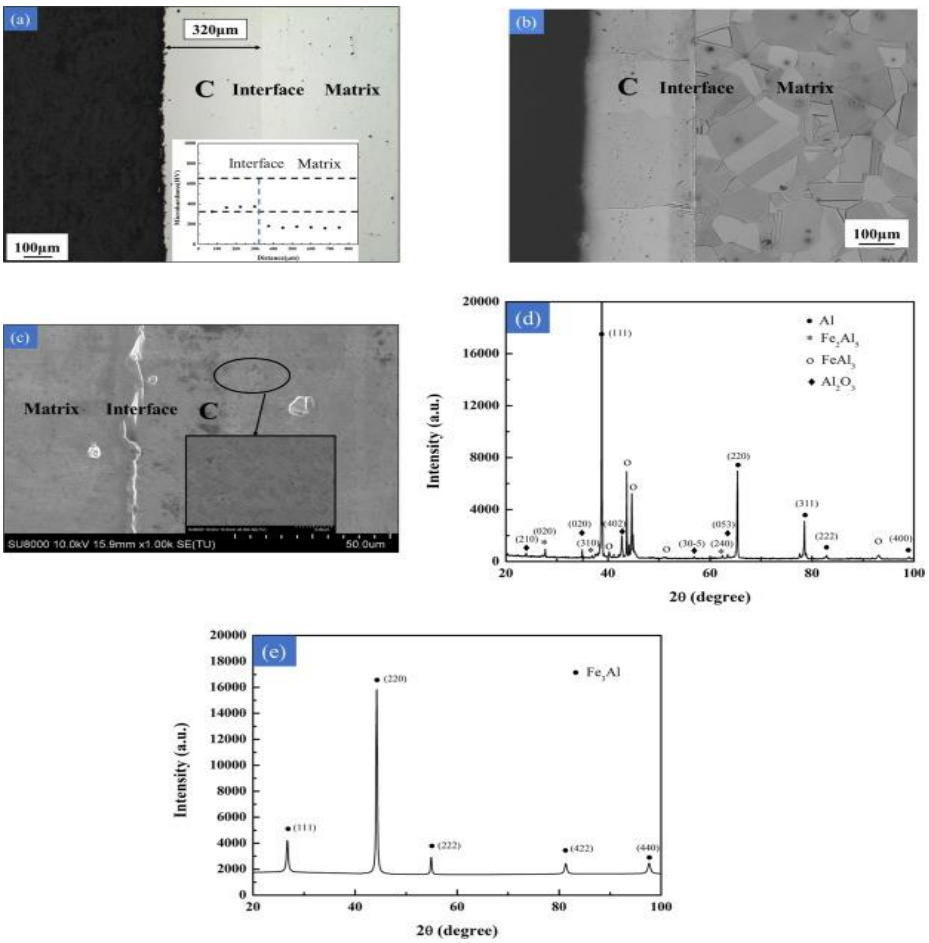

Fig. 2.2.Coating morphology of Fe-Al inter-metallic surface [122]

Wang et al. developed Iron-Aluminum (Fe-Al) intermetallic layer on steel using hot dipping aluminium followed by a thermal diffusion process. After the hot-dip process $FeAl_3$, Al, and Fe_2Al_5 intermetallic phases were developed, while after the thermal diffusion process only Fe_3Al left. The diffusion layer was developed in the range of 320 μm thick, which has excellent mechanical properties and corrosion resistance. Fig. 2.2 shows the cross-section morphology of the diffused layer of Fe-Al inter-metallics before and after thermal diffusion. After the thermal diffusion layer becomes more dense and brittle. From the XRD pattern, it can be seen that several Al-Fe phases were formed before thermal diffusion, while after thermal diffusion only Fe_3Al phases exhibit in the layer [122].

Rosa et al. studied the effect of thermal diffusion alloying of alumina/iron-Aluminium (Al_2O_3/FeAl) intermetallic layer on the steel. The efficient growth in locations of the intermetal thermal diffuse layer has been expected to depend

specifically on many variables, such as the development enthalpy of alloy-element aluminides, as well as the elemental fractions and diffusion rate of the specified alloy element in the steel substrate. Fig. 2.3 shows the cross-section microstructure and morphology Al_2O_3/FeAl intermetallic layer on the steel. The diffused layer thickness was measured around 150-200 μm thick. The diffused layer possessed high surface hardness and possessed excellent mechanical properties [123].

Xiang-Yu et al. diffused a copper (Cu) layer through plasma spray followed by a thermal diffusion process on the steel surface. The objective of the study was to improve the antibacterial and mechanical properties of steel. The layer of Cu was diffused up to 2.7 μm depth and comprised 5.7% percentage of total surface elemental composition [124]. **Medvedovski** critically reviewed and presented the boride coatings using a thermal diffusion process to enhance the corrosion resistance of steels. It has been reported that Fe-B based coatings are potentials and enough strong to withstand high-temperature applications such as steam containers [125]. Furthermore, **Medvedovski et al.** studied the application of a boride-based coating to enhance the tribological performance of steel for oil, gas, and power-plant industries. In these industries, large size steel components were used, which are under the high temperature sever conditions. The tribological tests were conducted to test the endurance strength of boride-based coatings. Wear resistance and structural-changes were investigated under dry and wet conditions. Fig. 2.4 shows the cross-section morphology of coating using 950 ºC at 12 h.

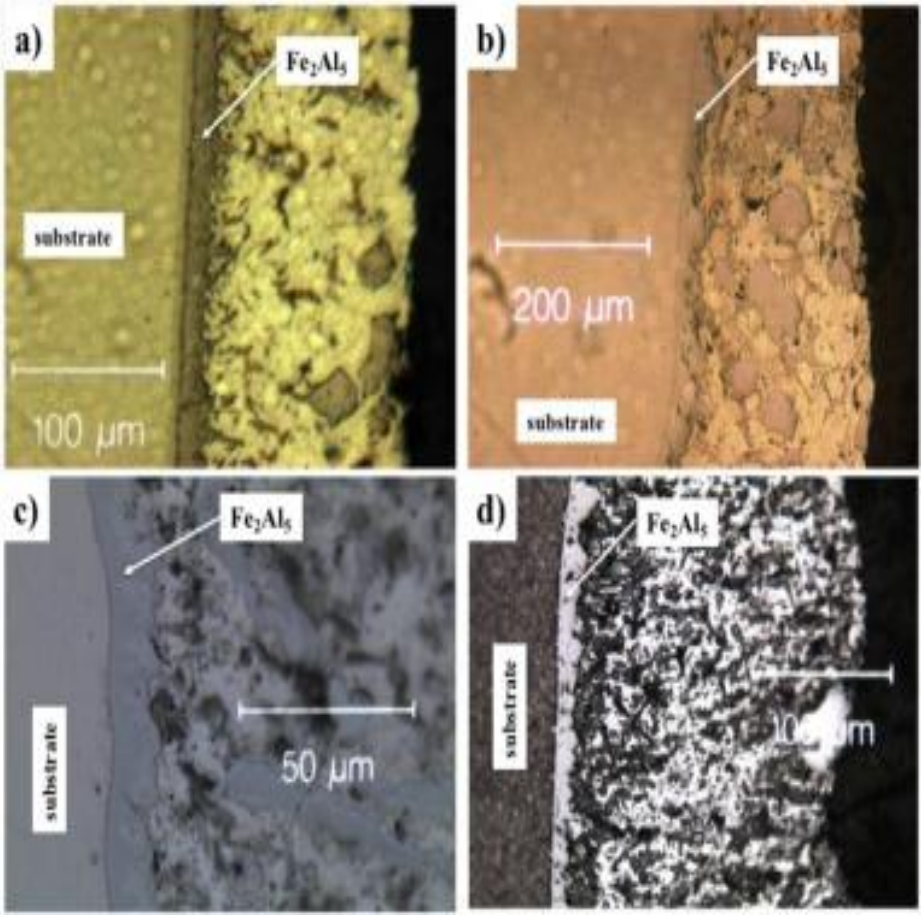

Fig. 2.3.Cross-section of coatings on different steel-substrates [123]

The boride coatings obtained were shown to have a substantially lower loss of friction than untreated steel without peeling and flaking. The boride coefficients of friction are consistent over the length of the test. The effect of the thickness on the efficiency of the boride coating is seen. Moreover, the effect of processing time on the diffusion depth was also investigated. The coating thickness was increased with processing time [126].

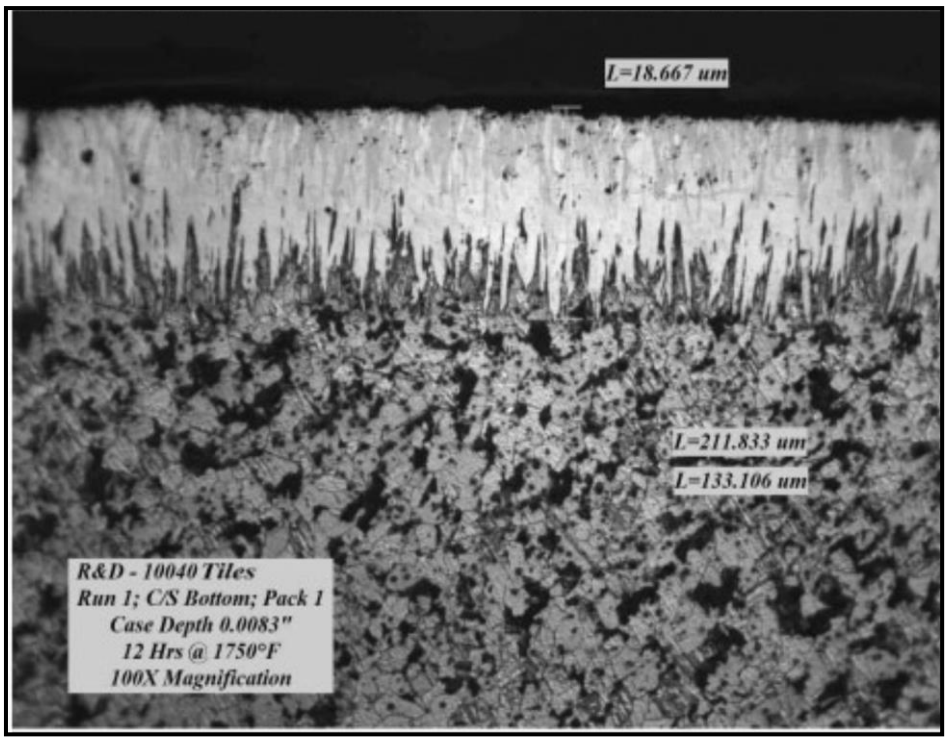

Fig. 2.4.Cross-section of boron-diffused layer [125]

Ghadi et al. developed a composite layer of chromium (Cr) and vanadium (V) carbide on CK-45 steel using a thermal reactive diffusion process. The diffusion of CrC and VC in the layer was homogenous. The diffused layer was measured around 6-10 μm thick. The micro-hardness of the diffused layer was measured around 3200 HV, which improved the wear resistance of steel. Fig. 2.5 shows the cross-section micrograph of the CrC and VC diffused layer. The CrC rich phases and VC rich phases can be seen in the diffused layer as can be seen in Fig. 2.5 (a) and (b), respectively [127].

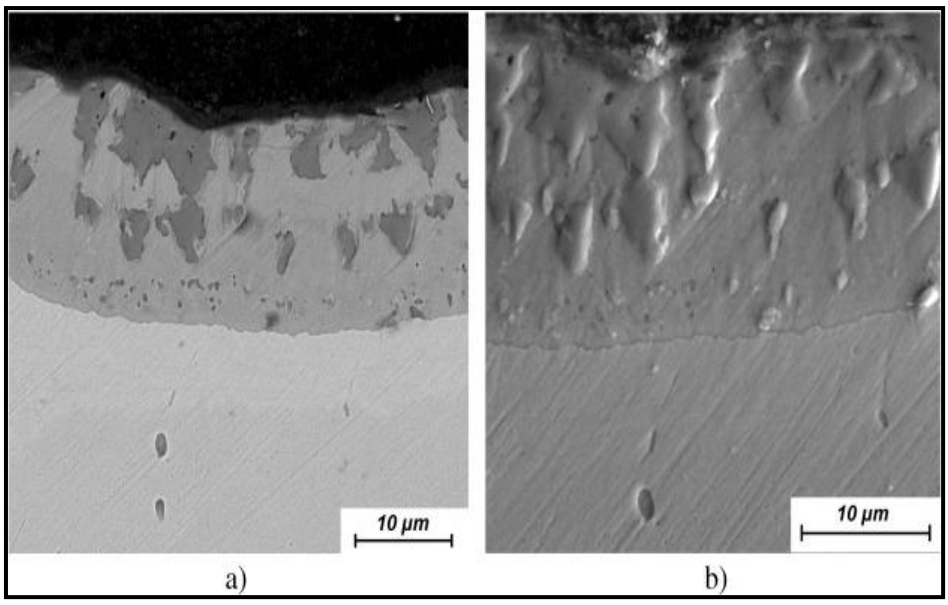

Fig. 2.5 (a) CrC rich phases and (b) VC rich phases in the diffused layer [127]

Huang et al. developed a molybdenum (Mo) rich vanadium-carbide (VC) coating on die steel using thermal diffusion treatment process. The effect of Mo-content reinforcement on the microstructure and mechanical properties of VC-coating was studied. The alloying/ reinforcement Mo-content prevents the carbide formation in the diffused zone and promotes the grain growth. A defect free and dense diffused layer was obtained with uniform microstructure. From the cross-section the thickness was measured around 10-15 µm thick. Fig. 2.6 shows the molybdenum (Mo) rich vanadium-carbide (VC) coating on die steel using thermal diffusion treatment process at different steel substrates. The micro hardness was increased to 2800 HV after reinforcement of MO-content [128].

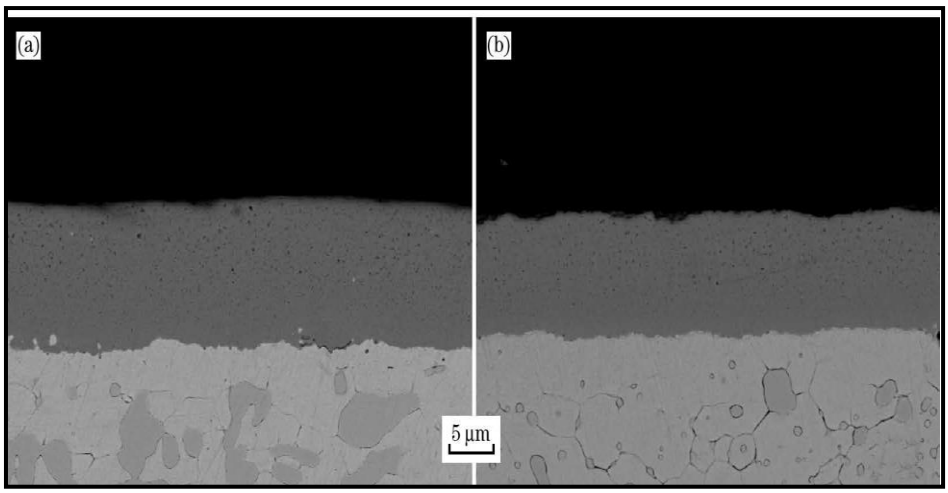

Fig. 2.6. Mo-rich VC coating on (a) type-I and (b) type-II steel substrate [128]

Hollis et al. deposited a thick layer of zirconium coating on the steel surface using the thermal spray diffusion technique. The effect of thermal spray diffusion on the microstructure, surface integrity, porosity, and mechanical properties studied. It has been reported that microstructure properties are the function of the diffusion process. The very thick, dense, and low porous coating was developed on the steel surface. The diffusion layer was measured about 15 to 30 µm thick. A very fine grain structure was developed in the layer, which enhanced the mechanical properties of the coating. The effect of transferred arc (TA) current of a thermal spray diffusion process on the temperature, porosity, diffusion depth, and grain growth was investigated, as can be seen in Fig. 2.7. From the results it can be seen that the diffusion temperature increased with the increase in TA-current [129].

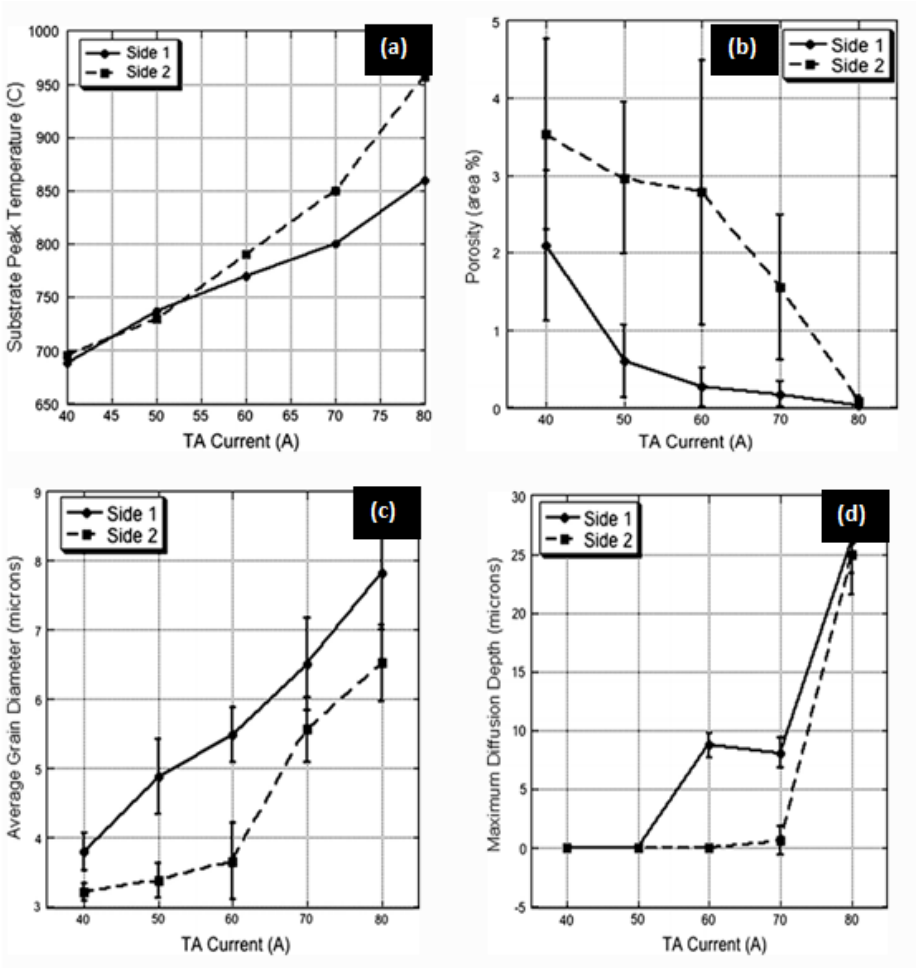

Fig. 2.7. (a) Temperature vs. TA current, (b) porosity vs. TA current, (c) average grain size vs. TA current, (d) Diffusion depth vs. TA current [129]

With the increase in current thermal energy increased, which further increased the temperature generation in the process. With the increase in TA-current, the generation of porosities in the diffused layer was decreased significantly. With the increase in the TA-current, the temperature increased, which further help to densify the coating; thus reduced the porosities generation. The average grain size increased with the increase in TA-current because the grain structure becomes course with the increase in the temperature. With the increase in TA-current, the diffusion depth increased. This is attributed because with the increase in the TA-current, the top surface layer of materials becomes soft and Zr-powder is reinforced in the layer.

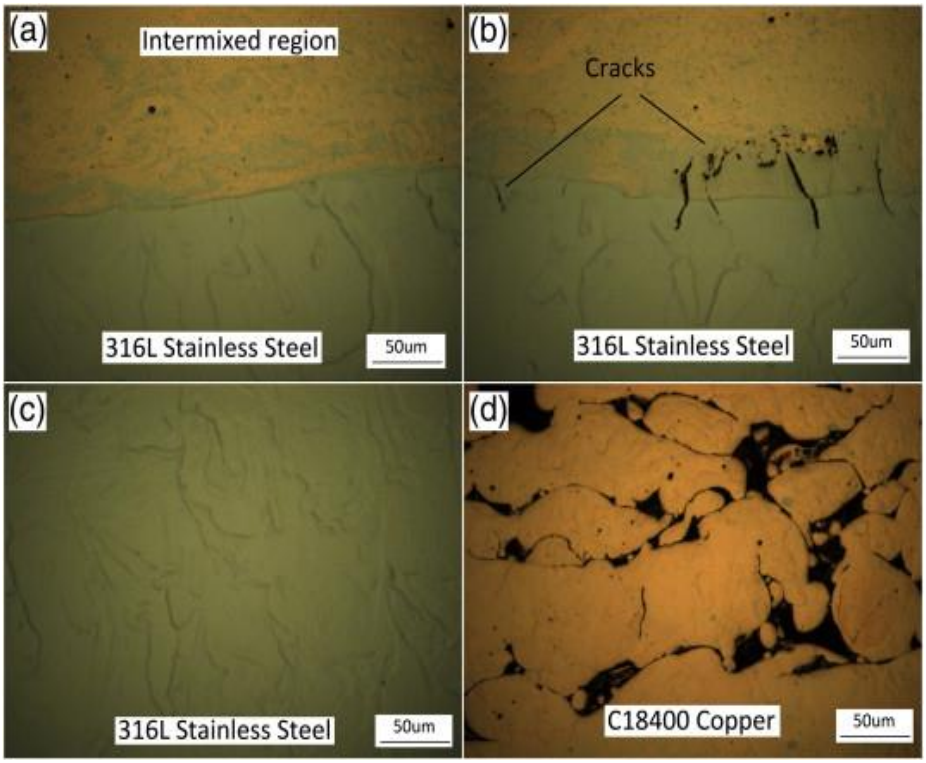

Fig. 2.8. Cross-section morphology of steel-Cu diffused layer [130]

Liu et al. investigated the diffusion of 316L-steel and C18400 Copper alloy using selective laser melting. The microstructure and mechanical properties of the diffused zone were studied. Excellent metallurgical bonding between 316L-steel and C18400 Copper alloy was obtained. The disused zone possessed a fine grain microstructure, which improves the mechanical properties of diffused substrates. The tensile strength and micro-hardness of the diffused region were measured around 310 MPa and 256 HV, respectively. Fig. 2.8 shows the microstructure of copper, Steel, and diffused region [130].

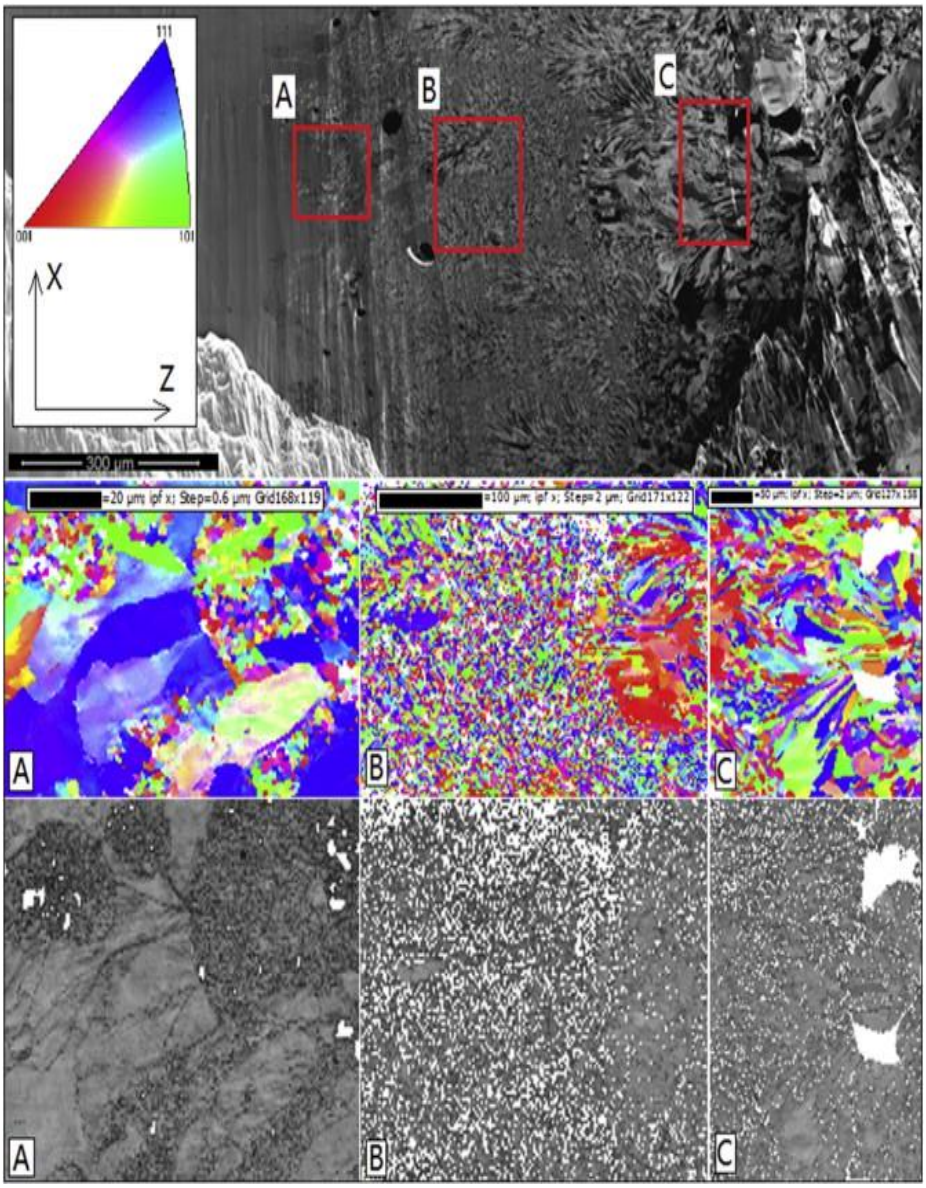

Fig. 2.9.Microstructure of steel-Cu surface [130]

It can be clearly seen that the diffused zone intermixed region of both elements, refer Fig 2.8(a). The diffused zone is 50 µm wide and comprised cracks and porosities due difference in elemental composition, refer Fig 2.8(b). The steel microstructure is dense; refer Fig 2.9(c). The copper microstructure is porous; refer Fig 2.8(d). Fig. 2.9 shows the backscattered image of 316L-steel/C18400 diffused layer.

Ozbek et al. reported the development of boride-rich AISI-M2 high-speed-steel using thermal diffusion process. The effect of temperature and processing time

was studied on the microstructure, micro-hardness, diffusion layer thickness, and fracture toughness.

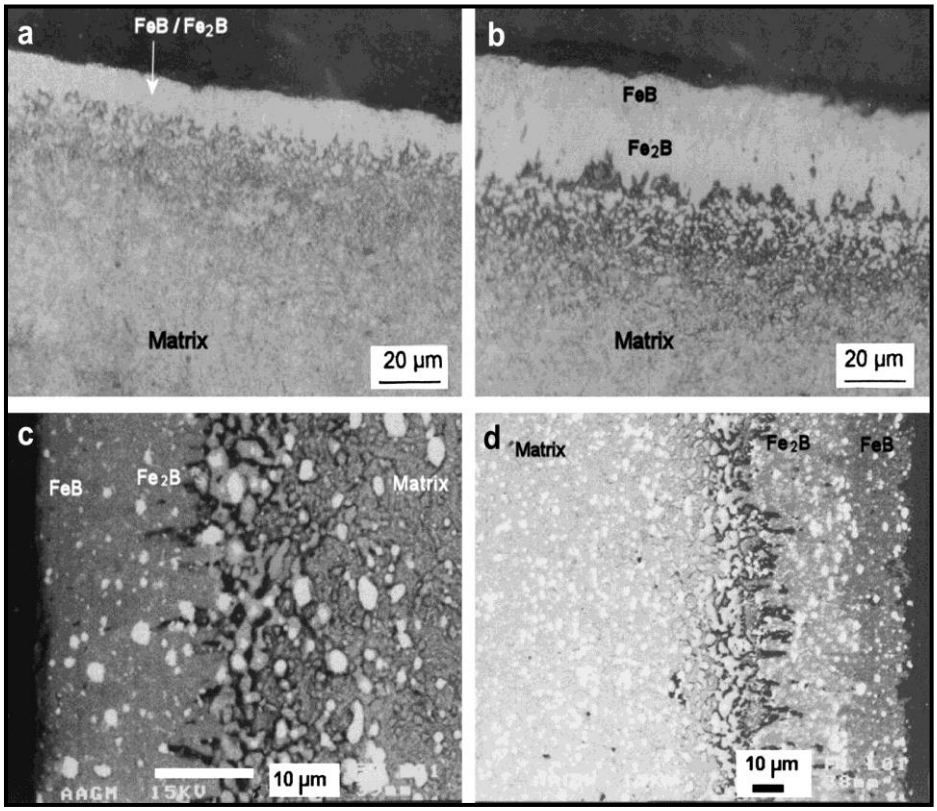

Fig. 2.10 Cross-section morphology of diffused layer on steel [131]

The microstructure results confirmed the formation of FeB intermetallic compound phases in the layer. The diffused layer was compact, dense, and smooth. The diffusion layer thickness was measured from 20 to 40 µm thick. The micro-hardness of the diffused layer was measured from 1600-1900 HV. The fracture toughness of boride-rich AISI-M2 high-speed-steel was measured in the range of 4.8-5.21 MPa/M^2. Fig. 2.11shows the microscopy and SEM images of borided AISI M2 at 850 °C for 2 h, 950 °C for 4 h, 950 °C for 1 h, and 950 °C for 4 h. From the optical images, a clear picture of FeB intermetallic phases can be seen. From the SEM-micrographs, refined grain structure in the diffused zone can be seen [131].

Henryk et al. reported the development of a Zinc-based thick layer on low-carbon steel using the thermal diffusion process. The effects of diffusion temperature (300-450 ºC) and time (30-240 minutes) on the microstructure, mechanical properties

were investigated. A two-layered structure was developed with Fe-Zn intermetallic phases. The temperature and processing time significantly affect the formation of various compositions of Fe-Zn intermetallic phases. The fine-grain structure was developed in the layer, which improves the coating mechanical properties. The diffusion depth/layer was dependent on the temperature and processing time [132].

Ganji et al. developed chromium carbide and vanadium carbide coating layer on tungsten-tool-steel using a thermal diffusion process. The molten salt bath was used for the coating process. The effect of salt-bath temperature (800 ºC) at different processing times 8, 10, and 12 h on the microstructure, diffusion layer, and mechanical properties were studied. With the increase in processing time, the microstructure of the diffused layer was changed significantly. Fig. 2.11 shows the effect of processing time on the microstructure and depth of the diffusion layer. In the case of the VC layer, at a high processing time 12 h, more carbides will be formed and the layer comprised more cracks. The diffusion layer thickness was increased with an increase in processing time. The diffusion layer thickness was measured in the range of 30 to 50 μm thick. Fig. 2.12 shows the effect of processing time on the microstructure and depth of the diffusion layer. On the other hand, the CrC layer microstructure becomes more refined with the increase in processing time. The diffusion layer thickness was measured in the range of 30 to 50 μm thick. The coating layer was smooth and free from cracks [133].

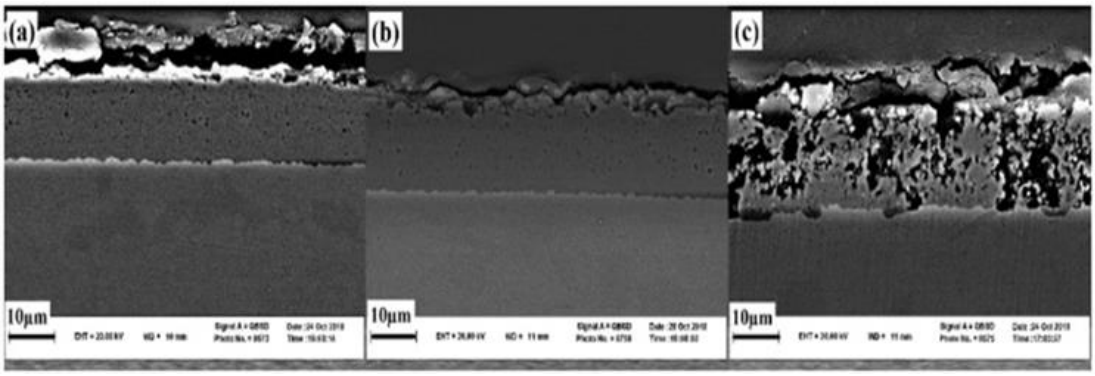

Fig. 2.11. Cross-section morphology of VC-coatings [133]

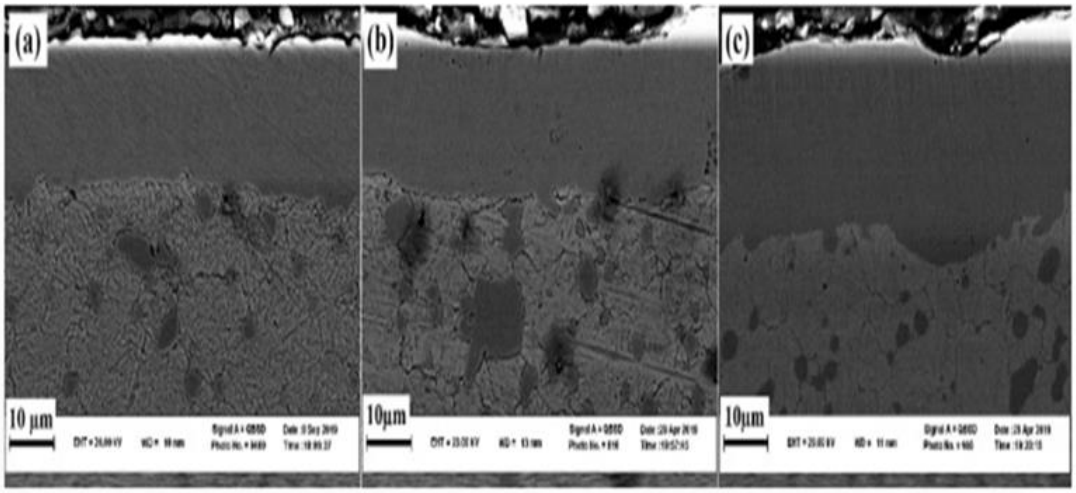

Fig. 2.12.Cross-section morphology of CrC-coatings [133]

The hardness of coatings layer increased with the processing time of diffusion. The CrC layer possessed high handedness as compared with VC. This is because CrC layer has better compactness and FCC structure.

Sabetghadam et al. investigated the joining of SS410-steel with copper using thermal diffusion process. For the diffusion of two dissimilar metals, a rich layer of nickel was used for better adhesion. The effect of temperature on the microstructure and mechanical properties were studied. Fig. 2.13 and Fig. 2.14 shows the effect of various temperature on the change of microstructure of diffused region [134].

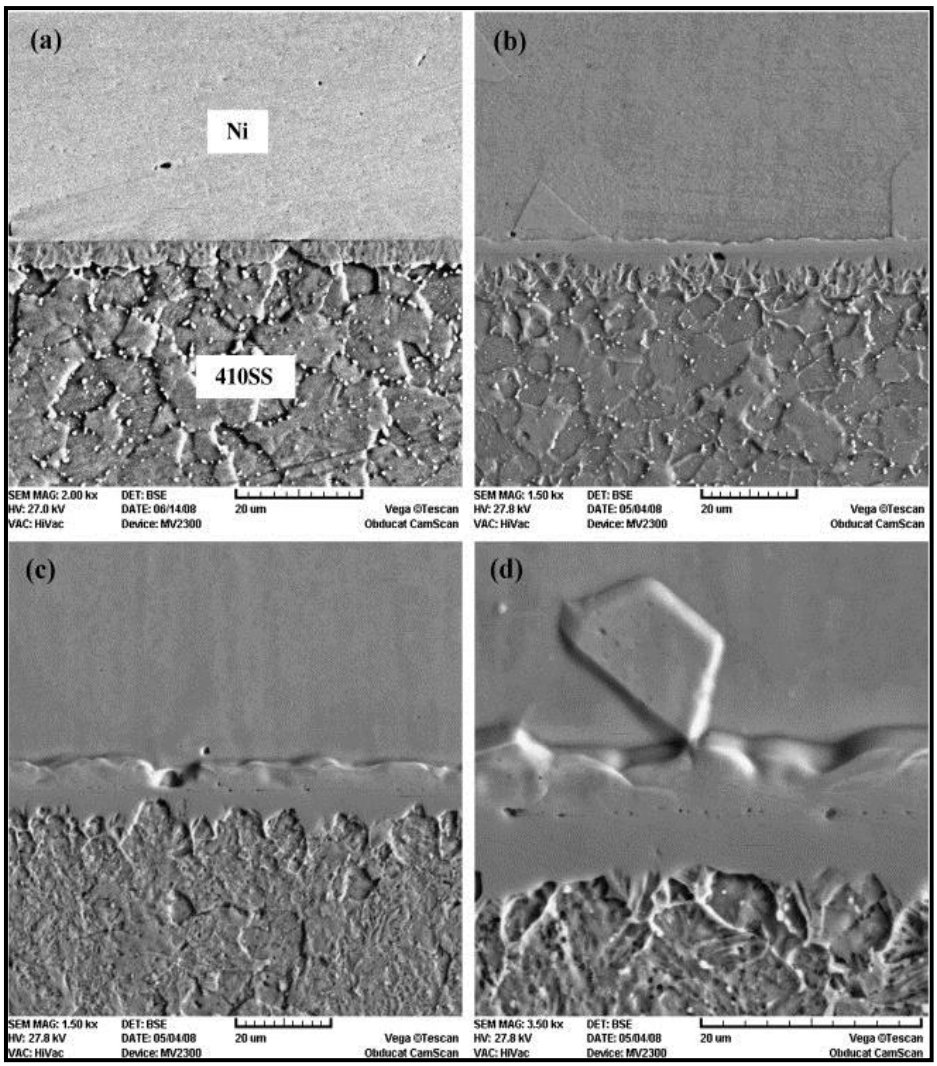

Fig. 2.13.Cross-section morphology of steel-Ni interface [134]

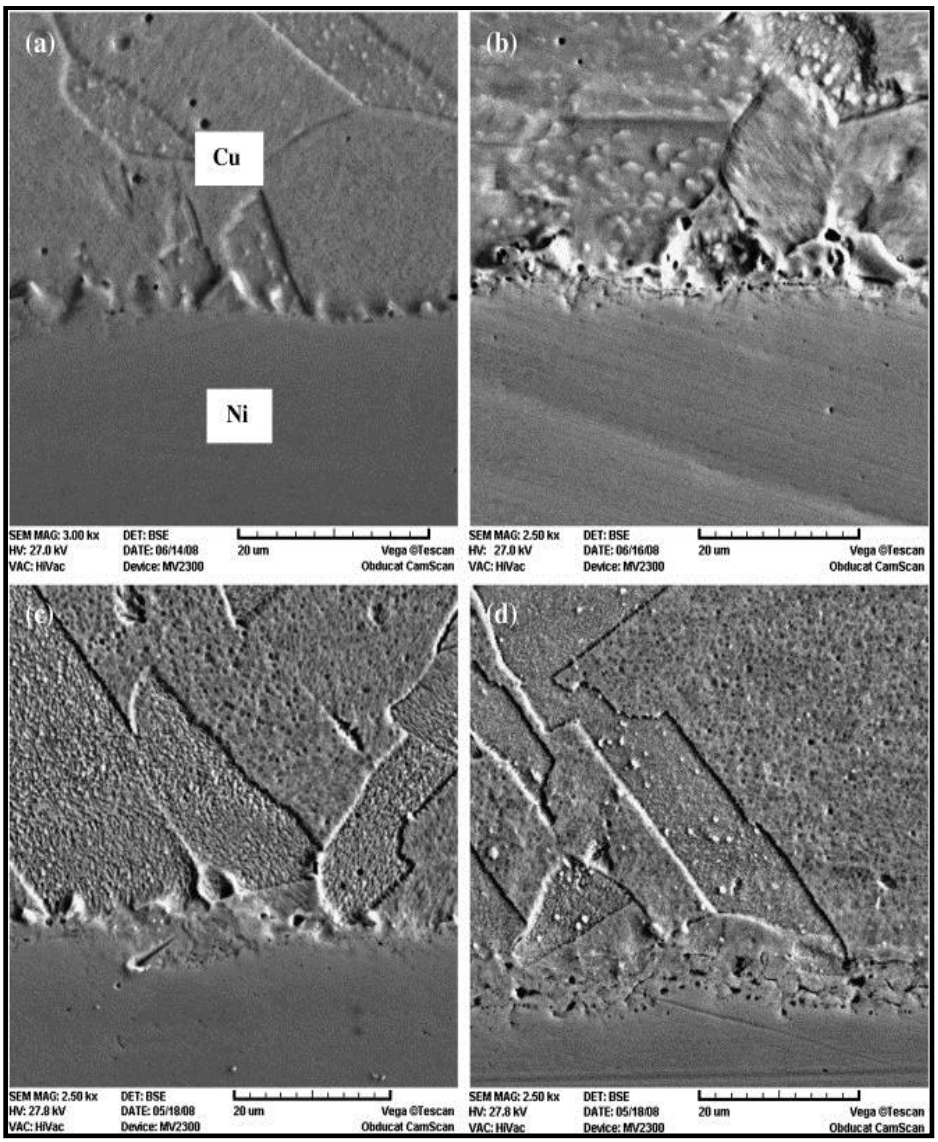

Fig. 2.14.Cross-section morphology of Cu-Ni interface [134]

It shows the clear interface of the SS410-Ni and Ni-Cu. At the interface of SS410-Ni, a brittle structure was formed and at Ni-Cu interface ductile structure was formed. Various intermetallic phases were formed during the diffusion process. Best microstructure was obtained at 900 ºC temperatures, where the diffused zone possessed excellent mechanical properties and fine microstructure. The effect of bonding temperature on the shear strength and micro-hardness of the diffused zone was studied. The highest shear strength at 900 ºC temperatures was measured around 145 MPa and highest micro-hardness was measured around 432 HV. With the

increase in bonding temperature, the diffused layer become more dense and compacted, which provide the resistance to delamination.

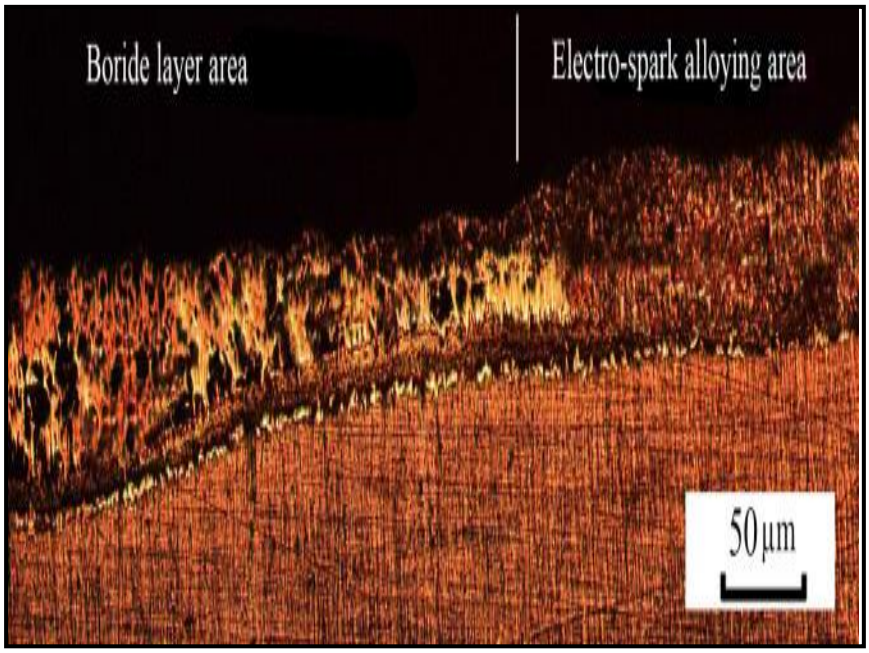

Fig. 2.15. Microstructure of the composite coating layer of coating boron [135]

Dashkevich et al. presented the new approach for the diffusion of composite layer of Cu-Boride on steel surface using hybrid manufacturing process. In the research work electro-spark alloying and thermal spray diffusion has been integrated in order to take the advantages on one process to the other process. Fig. 2.15 shows the cross-section of the composite layer of Cu-Boride. The thickness of diffused layer was measured around 100 μm thick. A clear interface was be seen, which is metallurgical bonded with substrate surface. The diffused layer possessed excellent mechanical properties. The hardness is very high and recorded around 550 HV [135].

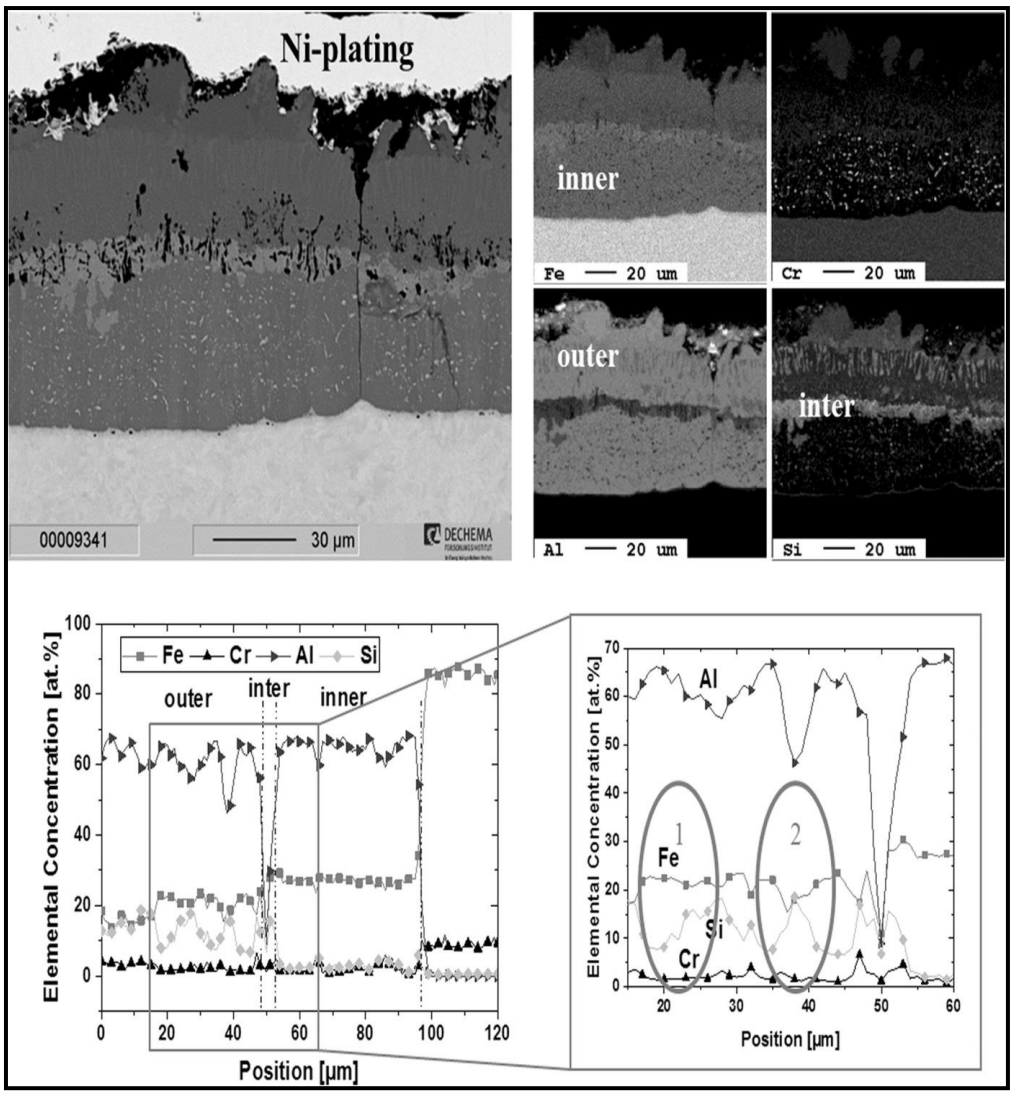

Fig. 2.16.Micro-structure of diffused layer and elemental composition [136]

Fähsing et al. investigated the deposition of Cr-layer on steel surface using thermal diffusion process to enhance the corrosion performance for solar-power applications. The microstructure, layer thickness, mechanical properties, and corrosion resistance of diffusion layer was studied. Fig. 2.16 shows the cross-section morphology, elemental, and phase composition of Cr-rich diffused layer.

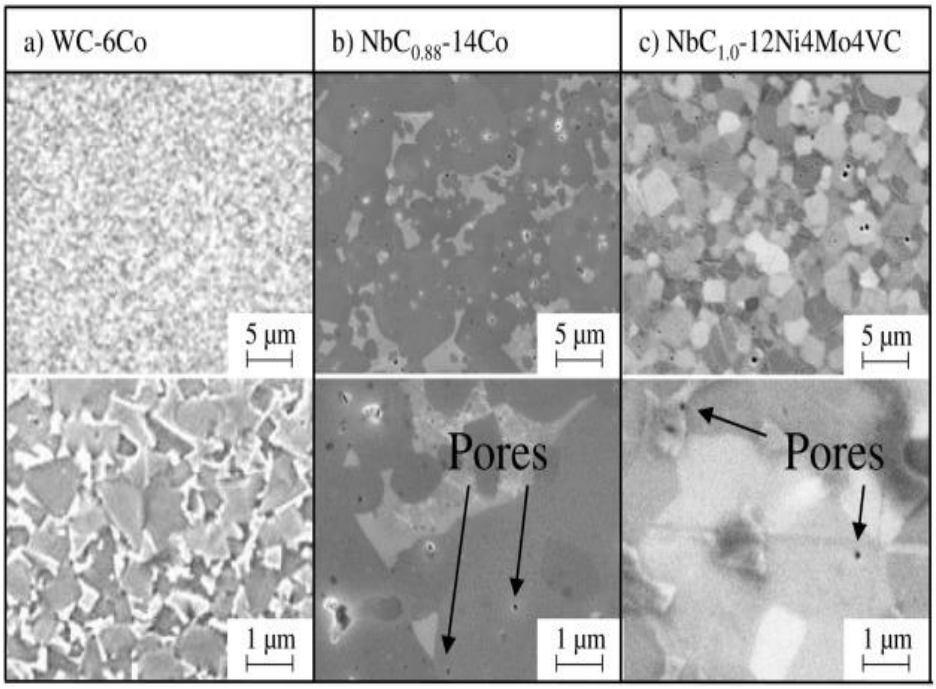

Fig. 2.17.Morphology of different coating techniques [137]

Form the SEM micrograph it can be seen that very dense and defect free layer was obtained. The diffusion layer thickness was measured in the range of 55 µm thick. The layer comprised various intermetallic-phases which improved the mechanical and corrosion resistance of layer. The Cr-rich layer was metallurgical bonded with the steel substrate and possessed excellent adhesion strength, which further provide resistance to delamination. Moreover, the layer also possessed also possessed excellent corrosion resistance [136].**Uhlmann et al.** investigated the development of NbC coating on tungsten-carbide (WC) tool using thermal diffusion process for cutting tool inserts applications. The aim of deposition of NbC-coating to enhance the wear resistance of on WC tool. The microstructure, mechanical properties, wear resistance was studied. Fig. 2.17 shows the coated morphology of NbC-coated WC surface. It can be seen that various phases were developed in the coating which has fine microstructure. At high magnification, submicron-scale pores were observed in the coating. The diffusion coating thickness of layer was measured around 3 µm thick. The micro hardness of NBC-coatings was measured in the range of 1275-1790 HV [137].

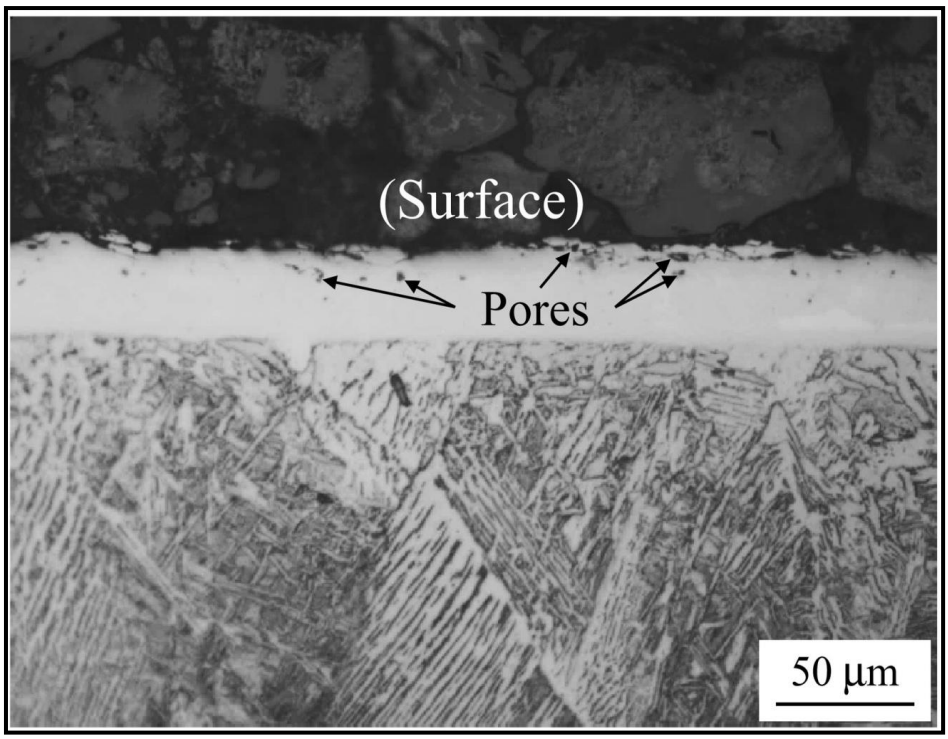

Fig. 2.18. Cross-section micrograph of Cr-rich layer [138]

Kikuchi et al. investigated the deposition of Cr and Mo elements on AISI-1045 steel surface using thermal diffusion process. The microstructure, diffusion layer thickness, and corrosion resistance has been studied. From the SEM-micrograph, it can be seen that Cr-rich layer possessed dense structure, refer Fig. 2.18. No visible cracks were identified form the diffused surface. The diffusion layer thickness was measured around 30 μm thicknesses, which has excellent metallurgical bonding with the surface. The Cr-rich layer prevents the surface form degradation and acted as barrier to corrosion resistance. The corrosion resistance of Cr-deposited layer was very high as compared with base steel surface [138].

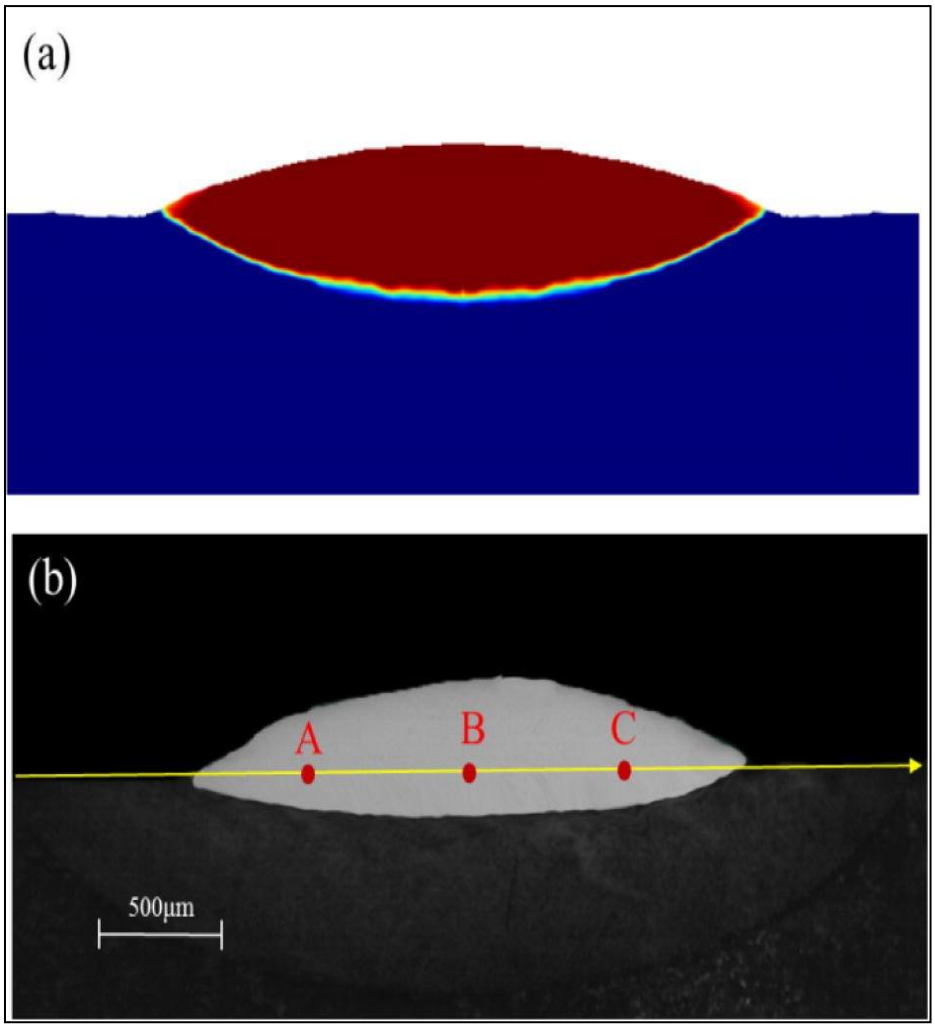

Fig. 2.19. Cross-section of C-based layer cladded on the Steel surface (a) Numerical simulation and (b) experimental [139]

Gan et al. explored the capability of numerical simulation of cladding of Co-based alloy layer on the steel surface using thermal diffusion process using laser cladding technique to validate the experimental results. Form the numerical simulation and experimental study, it has been observed that a very thick layer can be cladded on the steel-surface, which has excellent metallurgical bonding with substrate. Fig. 2.19 shows the cross-section of Co-based layer cladded on the Steel surface using numerical simulation and experimental study [139].

Maruno et al. developed a diamond-like carbon (DLC) layer on the aluminium surface using plasma-enhanced chemical vapour deposition (PECVD) technique, which is a thermal diffusion process. The microstructure, layer thickness,

micro-hardness, adhesion strength, and wear resistance was studied. In order to enhance the adhesion strength of coating, various intermediate coating layers of various intermetallic alloys were deposited, as can be seen in Fig. 2.20. Form the cross-section micro-graph it can be seen that the DLC-layer possessed coating thickness in the range of 0.85 to 1.50 μm. The mechanical and wear performance of DLC-coating has been compared with intermediate bond-coatings. The coating layer exhibit nano-scale surface roughness in the range of 7-11 nm. The coating also possessed excellent wear resistance [140].

Biesuz et al. investigated the development of a composite coating of CrC, VC, CrN, and VN layer on the steel using thermal diffusion process. The effect of different processing temperature on the microstructure and mechanical properties was studied. Various intermetallic carbide and nitride were developed in the layer. The effect of processing time on the microstructure, diffusion thickness, and mechanical properties were studied. The cross-section morphology shows that the layer comprised fine grain structure without any surface defects. Fig. 2.20 shows the cross-section micrograph of CrC coating layer with respect to processing time. It can be seen that diffusion layer increased with the increase in processing time. The diffusion layer was measured in the range of 5-10 μm thick. Fig. 2.21 shows the cross-section micrograph of VC coating layer with respect to processing time. It can be seen that diffusion layer increased with the increase in processing time. The diffusion layer was measured in the range of 3-10 μm thick. The surface micro-hardness of coating was recorded in the range of 1800 to 2500 HV, which prevents the surface form mechanical hazard [141].

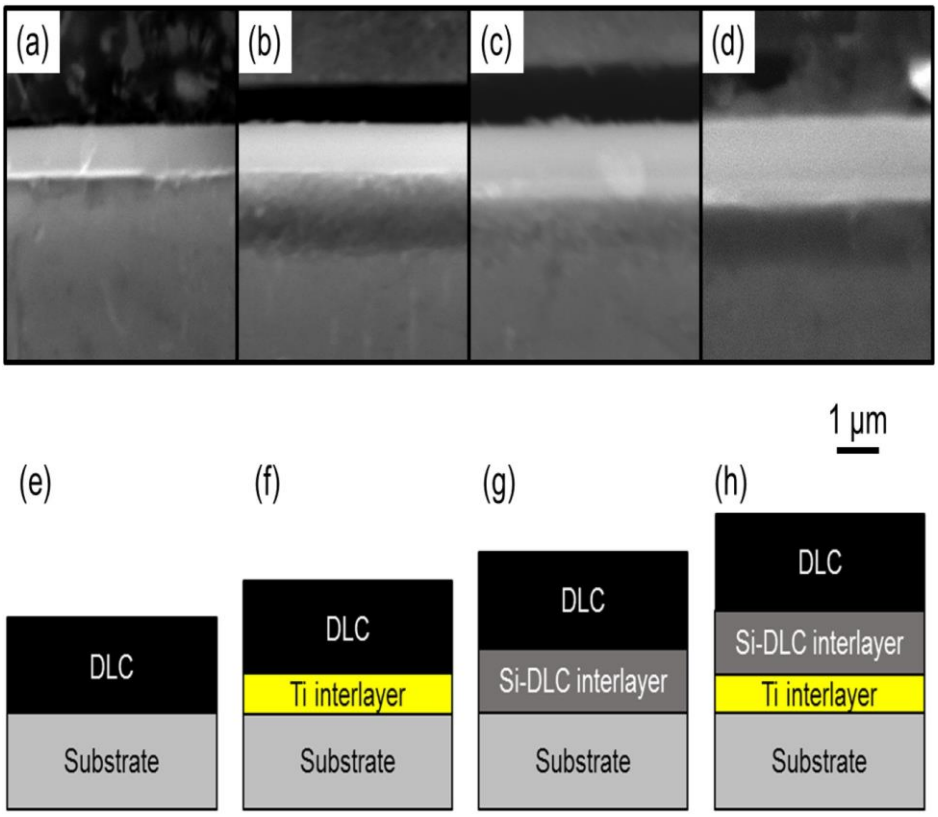

Fig. 2.20. DLC coating with various intermediate coating layers [140]

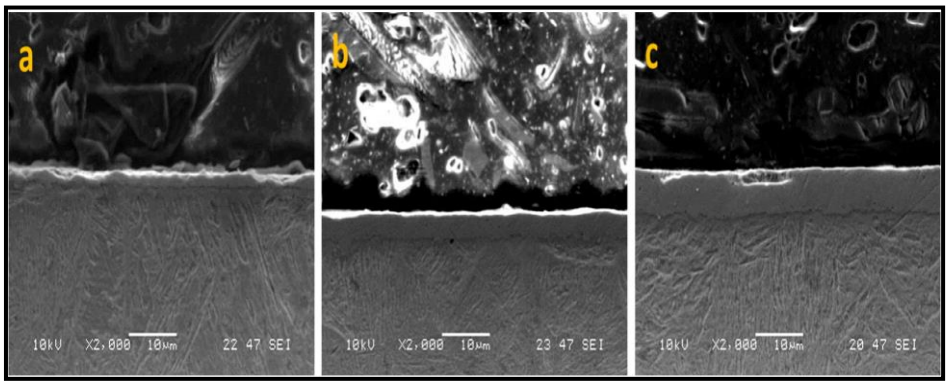

Fig. 2.21. The cross-section morphology of CrC layer at 900 ºC for different processing time (a) 2 h, (b) 4 h, and (c) 16 h [141]

Rayane et al. developed boride layer on XC38-steel surface using thermal diffusion process for high temperature applications. The microstructure has been studied by HT-TEM and FE-SEM techniques. The micro-hardness of diffused layer was also been studied. Microstructure examination of diffusion layer showed the 200

μm thick layer. The boride-rich layer comprised excellent mechanical properties [142].

Ortiz-Domínguez et al. developed a iron-based boride (Fe-B) layer on the steel surface using thermal diffusion process. The effect of process temperature and time was studied on the microstructure and mechanical properties of FeB-rich layer. The microstructure was refined with the increase in temperature and processing hours. But, diffusion of boride layer at 1272 K at 5 hours processing time is the best optimal condition for the development of dense and defect free layer. The diffusion layer thickness was measured around 50-200 μm thick. Fig. 2.22 shows the cross-section morphology and XRD phase composition of FeB-layer on Steel at 1123 K 2 h and 8 h of processing time [143].

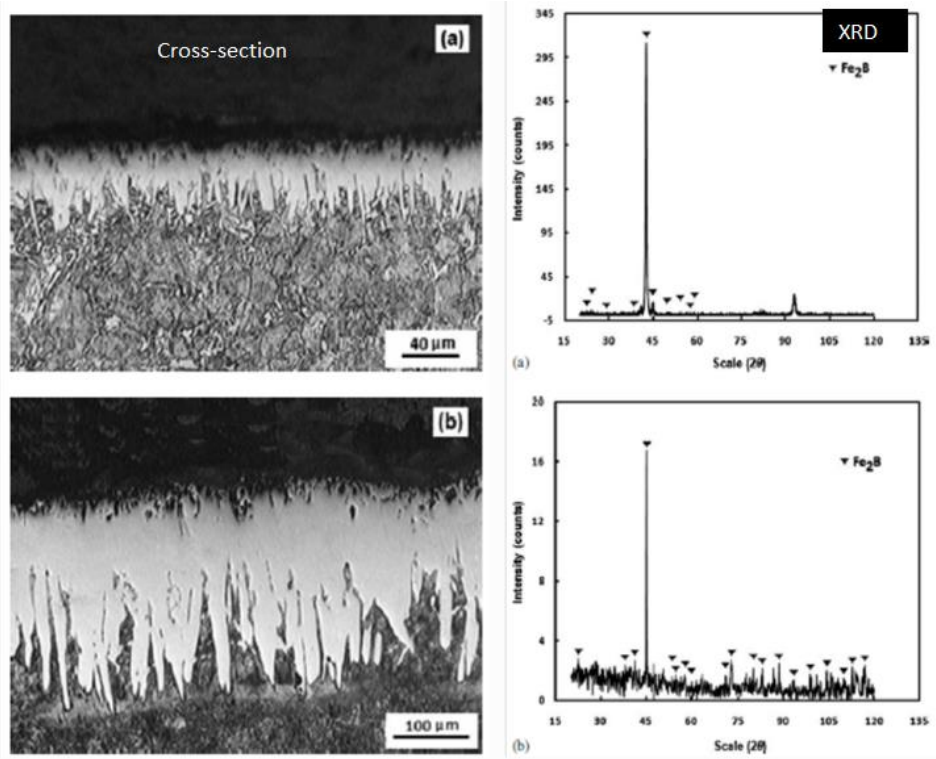

Fig. 2.22. Cross-section morphology and XRD phase composition of FeB-layer on Steel at 1123 K (a) 2 h of time and (b) 8 h of time [143]

Strahin et al. developed a VC coating on AISI-5100-steel by thermal diffusion process for tribological performance. The microstructure, layer thickness, phase composition, crystallographic structure, hardness, and elastic modulus were

studied. The tribological performance was studied using pin-on-disc wear test. Fig. 2.23 shows the SEM morphology of steel before coating, after coating, cross-section micrograph. The thickness of diffusion layer was measured around 4 μm thick and rich layer of VC was observed. The average grain size of the VC formed in the layer was 33 nm, which improve the mechanical properties of coating. The hardness and elastic modulus of coating was determined using nano-indentation technique. The hardness and elastic modulus of coating was measured around 35 GPa and 350 GPa, respectively. The coating also exhibit excellent wear resistance [144].

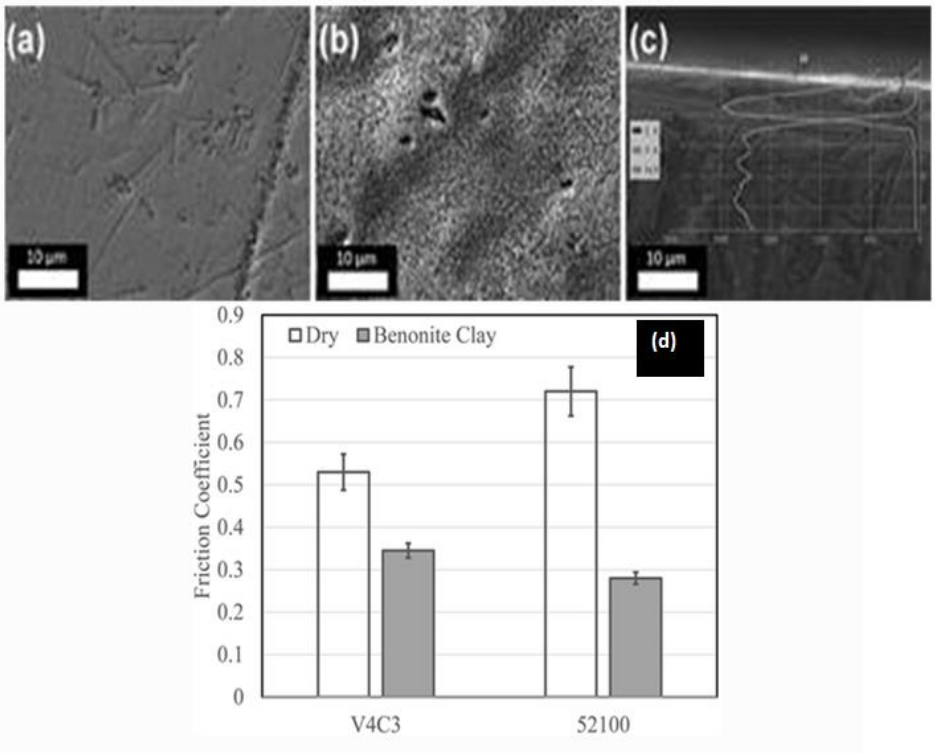

Fig. 2.23. SEM morphology of steel (a) before coating, (b) after coating, (c) cross-section micrograph, and (d) wear performance [144]

Xiuju Song **et al.** investigated installation of Boron nitride on Si and metal substrates in an Ar and N2 combination (5:1) with the aid of utilising radio frequency magnetron sputtering manner. Most often they studied bias voltage values starting from a hundred to 200 V and temperature varied between 200-250 ºC within the deposition of boron nitride along with their outcomes. They concluded that further

modifications for the period of deposition system could expand the cubic ratio in the films. XPS outcome show that almost stoichiometric films have formed [145].

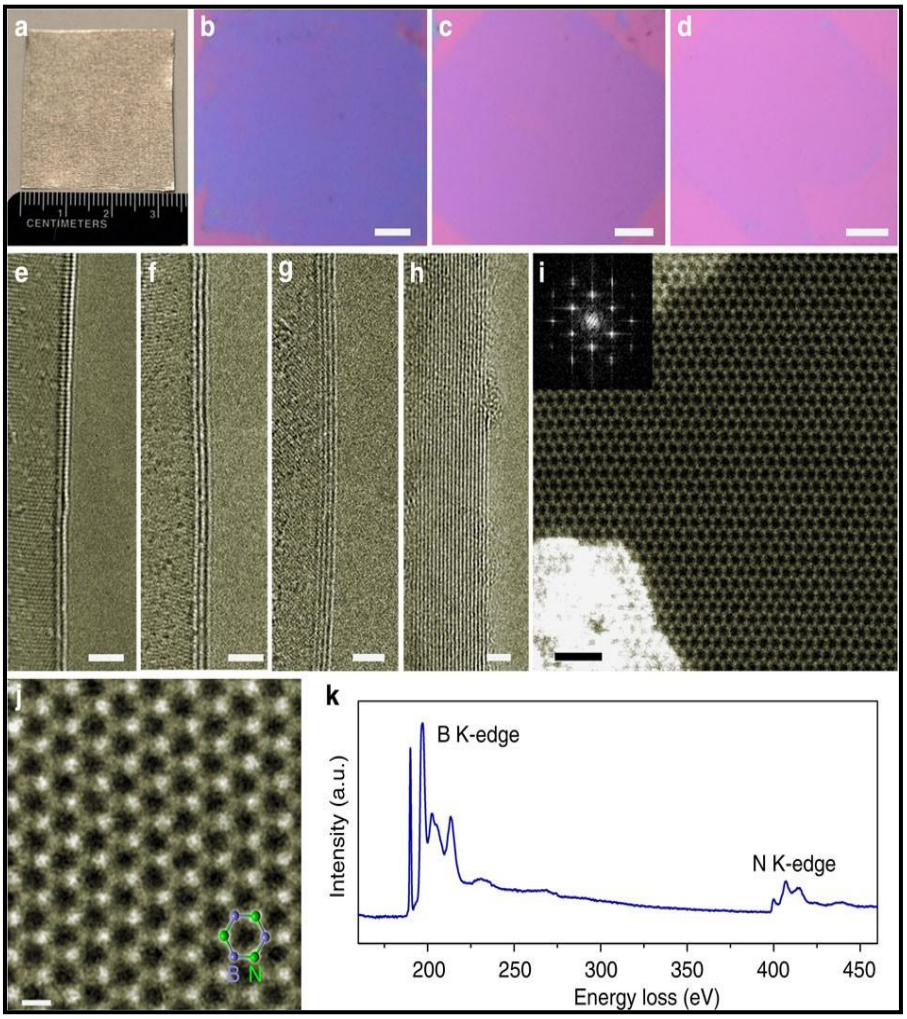

Fig. 2.24. Optical and TEM characterizations of CVD h-BN layers [147]

Liu et al. investigated that even at extreme temperatures such ultra-thin hexagonal nitride films are impermeable to oxygen diffusion and may function in oxidizing atmospheres with great efficiency oxidation-resistant nickel coatings up to1100^{o}C [146]. **Song et al.** Developed h-BN coatings that are the thinnest coatings interminably to be castoff at such extreme temperatures, last steady and shield metal surfaces beside oxidation. [147].Fig. 2.24 shows the h-BN layer on steel surface.

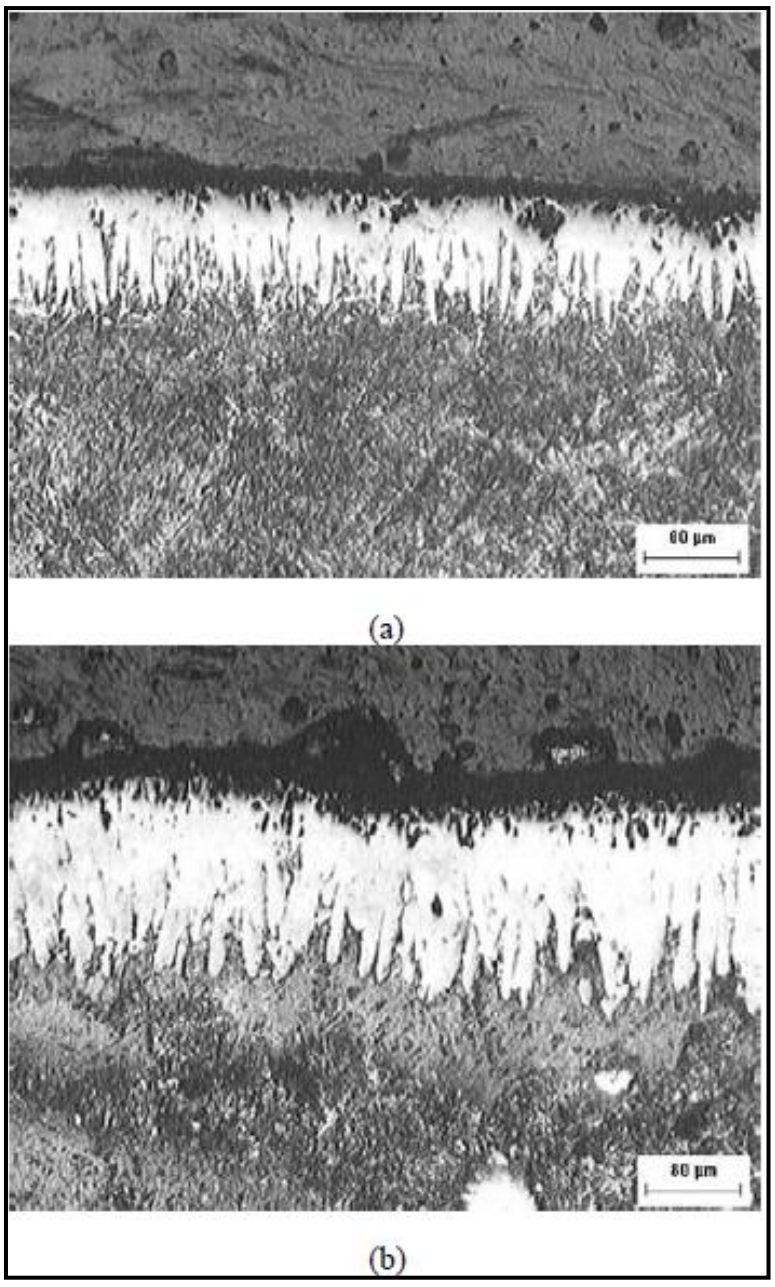

Fig. 2.25. Cross-section micrograph of boride layer at 1223 K with (a) 4 h and (b) 8 h processing time [148]

Silva et al. developed a FeB-hard coating by thermal diffusion process at steel surface. The effect of temperatures and processing time on the microstructure and mechanical properties were studied. The coating layer possessed dense structure and layer thickness was changed with respect to processing time. With the increase in

processing time 4 h to 8 h the diffusion layer thickness was increased from 80-150 μm thick, refer Fig. 2.25 [148].

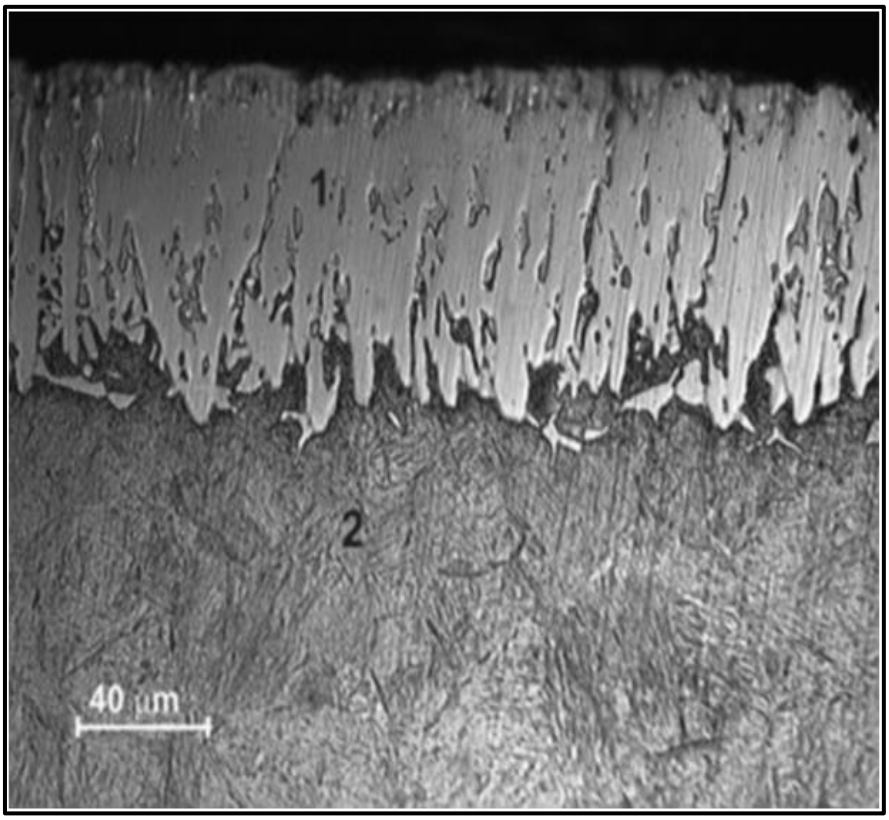

Fig. 2.26. Cross-section morphology of FeB-rich surface using thermal diffusion process [149]

Kulka et al. developed a boride-rich layer on 41Cr4-steel surface using laser-boriding technique and thermal diffusion process. Microstructure, surface characteristics, phase composition, micro-hardness, and wear resistance was studied. Fig 2.26 and Fig 2.27 shows the cross-section morphology of FeB-rich surface in the case of laser bording and thermal diffusion process, respectively.

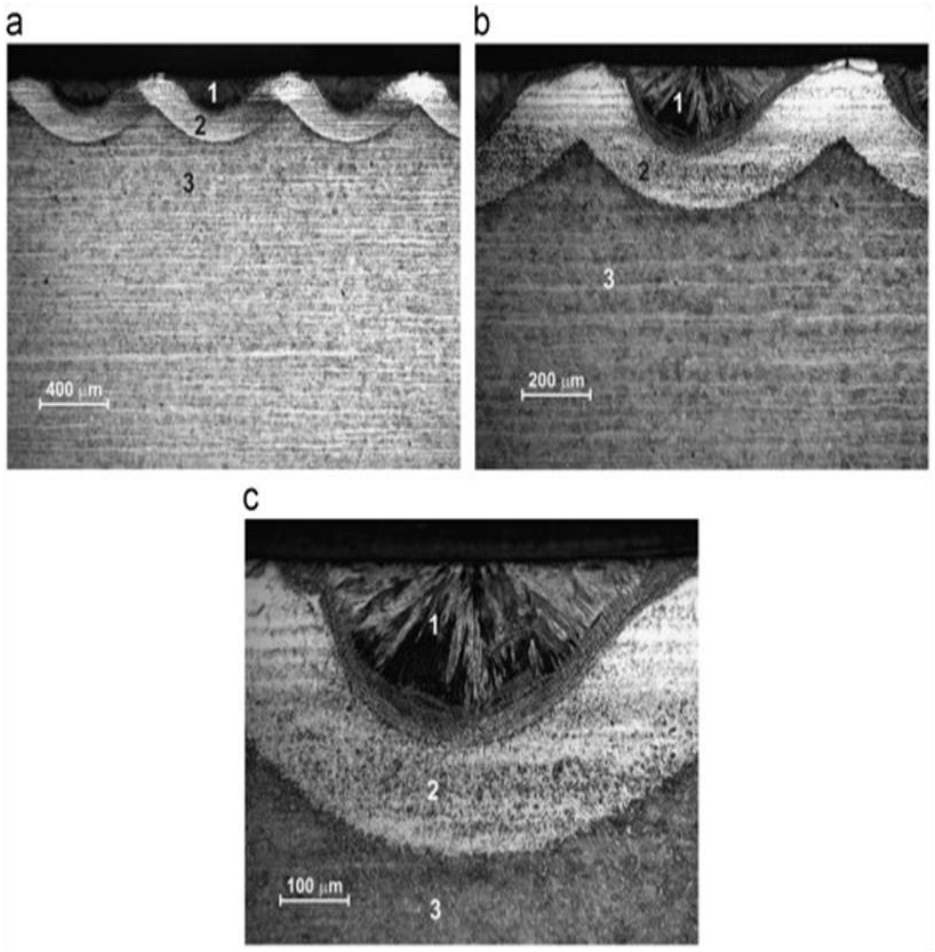

Fig. 2.27. Cross-section morphology of FeB-rich surface using laser bording process [149]

From the microstructure examination, the laser-bording cross-section image shows the three-layers. First layer comprised the borided-rich zone, second layer comprised medium-carbon zone and heat-treated zone, and this layer comprised heat-affected zone. Eutectic-phase microstructure formed suing the process in the layer, which was responsible to increase in the surface hardness. The diffusion layer thickness was measured around 200 μm thick. On the other hand, it can be seen that FeB are formed near to the top surface of layer in the case of thermal diffusion process. The marsenties-type microstructure was formed in the thermal diffusion process. The layer was measured around 80-100 μm thick [149].

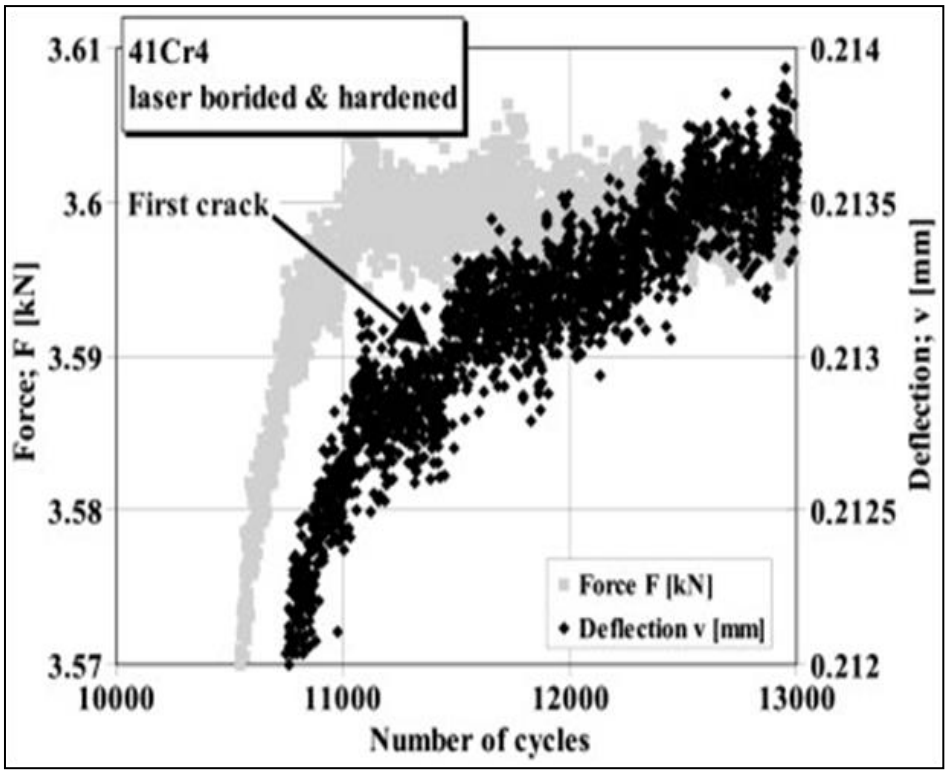

Fig. 2.28. Fatigue performance: (a) thermal diffused and (b) laser borided surface [149]

The micro-hardness of FeB-rich layer in the case of thermal diffusion process was measured in the range of 1350-1850 HV, which is very high in comparison with laser borided surface (1100-1600 HV). The thermal diffused boride layer possessed excellent abrasion resistance as compared to laser borided surface. Moreover, the fatigue strength of thermal diffused boride layer is high in comparison with laser borided surface, refer Fig. 2.28.

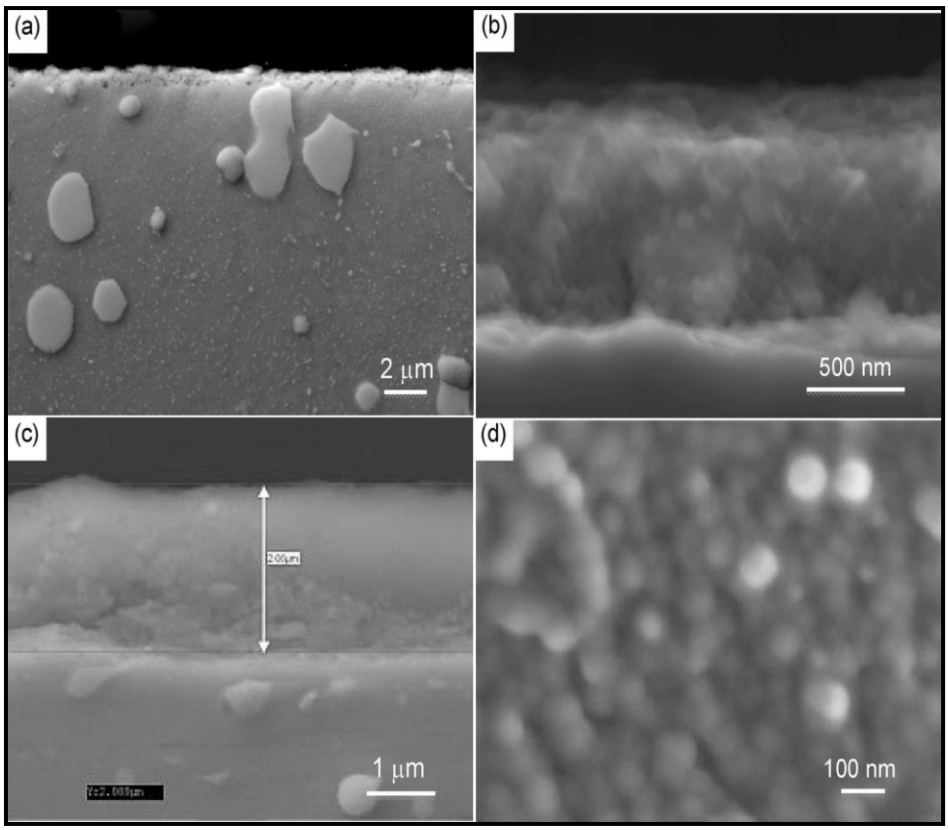

Fig. 2.29. Cross-section of B/C/N coating on steel surface at low-temperature on MS (a-b) and HSS (c-d) [150]

Chauset. al. developed a composite and complex coating of boron-carbide/Nitride on steel surface and MS using thermal diffusion process for the high temperature applications. The effect of temperature and processing time was studied on the microstructure, morphology, surface roughness, micro-hardness, residual stresses, and machining. It can be seen that very thin coating was developed on the substrate surface. The layer thickness was measured in the range of 1-2 μm. Very fine-grain microstructure was developed in the layer and grain size was recorded in the range of 50-100 nm. Fig. 2.29 shows the cross-section of B-C-N diffused layer at low temperature. When the processing temperature increased the diffusion layer thickness increased and microstructure changed [150].

Fig. 2.30 and Fig. 2.31shows the cross-section of B-C-N layer diffused on steel surface at 880 ºC in the case of HSS and MS substrate. The layer thickness increased to 8 μm. The layer is very dense and comprised crack free needle-like

structure. EDS-spectrum conformed that the carbon-rich layer were formed which enhance the mechanical properties.

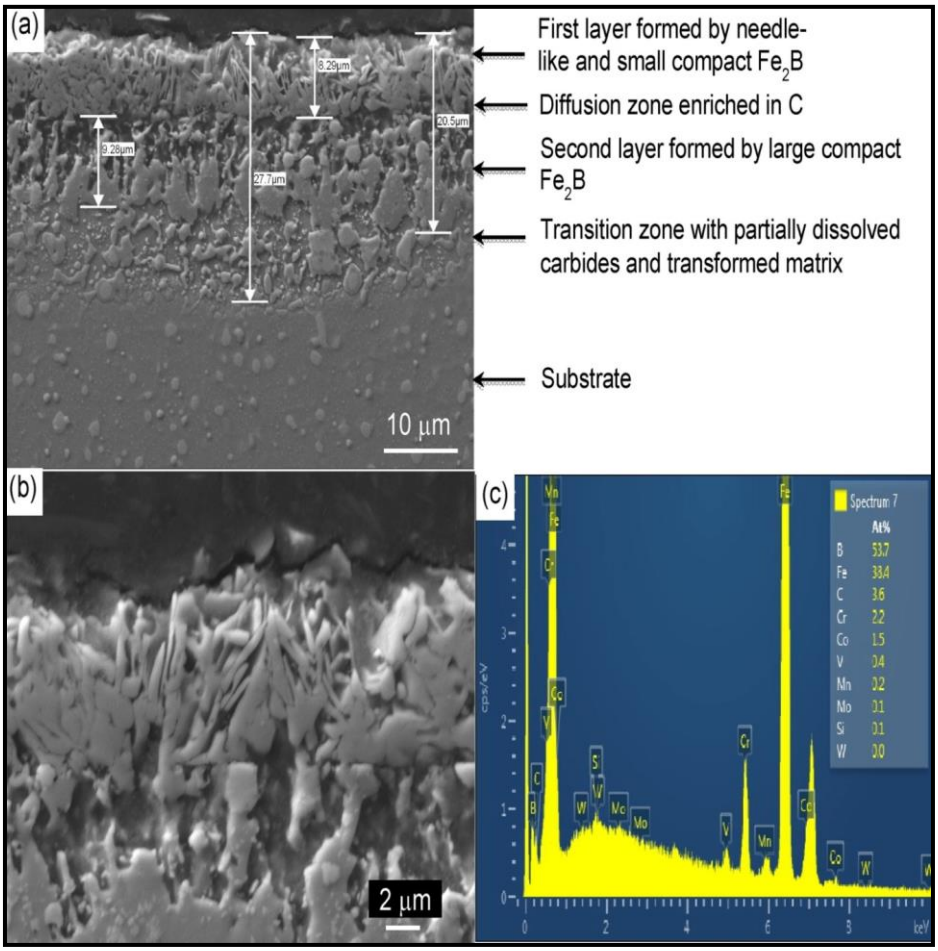

Fig. 2.30. Cross-section of B-C-N layer diffused on steel surface at 880 ºC in the case of HSS substrate [150]

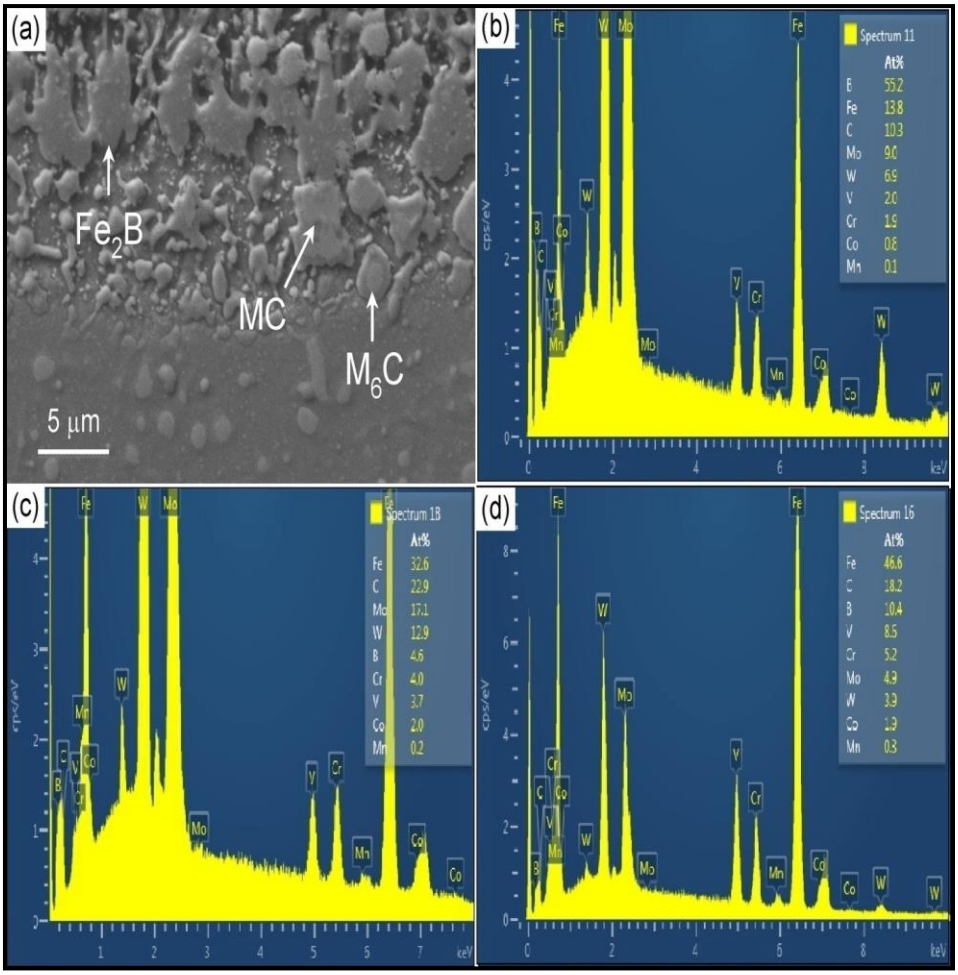

Fig. 2.31. Cross-section of B-C-N layer diffused on steel surface at 880 ºC in the case of MC substrate [150]

Suri et al. critically reviewed the formation of boron-carbide layers on various metals for various industrial applications. Moreover, authors also presented the formation of boron-carbide for coating/deposition using powder metallurgical process. It has been reported that boron-related carbides coated material possessed excellent mechanical properties and could be used for high temperature industrial applications [151].

Zhong et al. investigated the double layer of W/Ni with SiC on ferritic-steel using thermal diffusion process. Fig. 2.32 shows the cross-section micrograph of multilayer diffused zone. In the diffused zone No-W rich phases were developed, which enhanced the mechanical properties. The tensile strength of layer was measured in the range of 55 MPa [152].

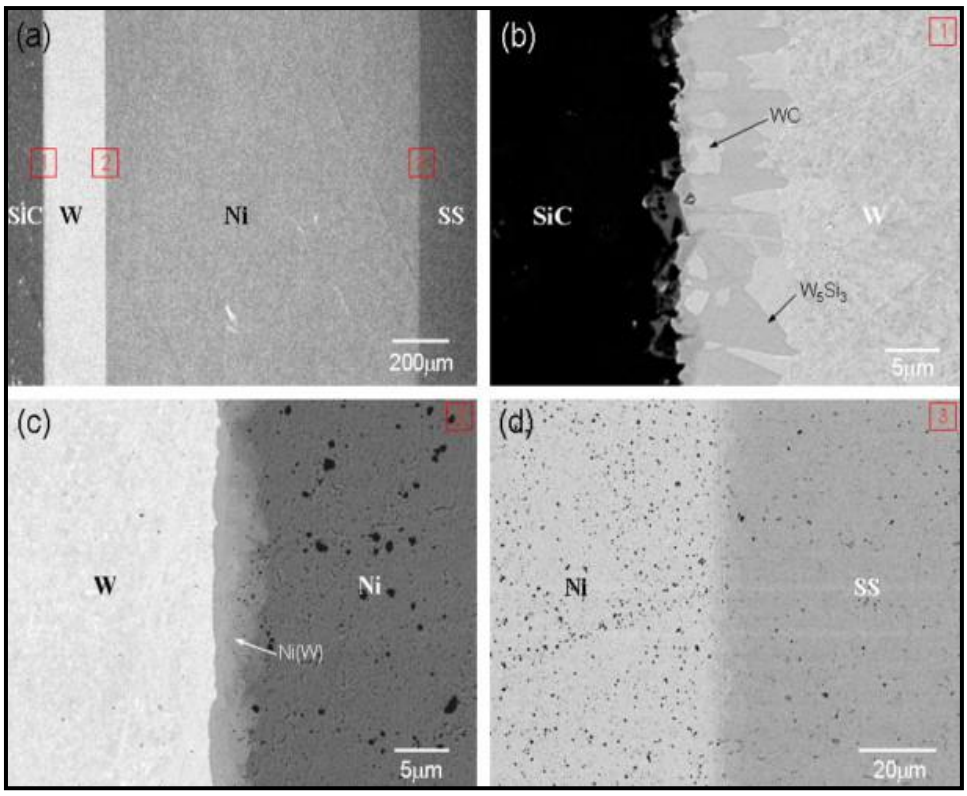

Fig. 2.32 Cross-section micrograph of multilayer diffused zone [152]

Galedari et al. critically reviewed the application of various intermetallic oxide and carbide for various heat resistance applications. Most common coatings such as Al, WC, Cr, Zn, Ni, and boron-based used to enhance the corrosion, wear and fatigue performances. Among these, coating boron-based coating has excellent mechanical properties [1].Fig. 2.33 shows the application of various metallic and ceramic coatings for various industrial applications.

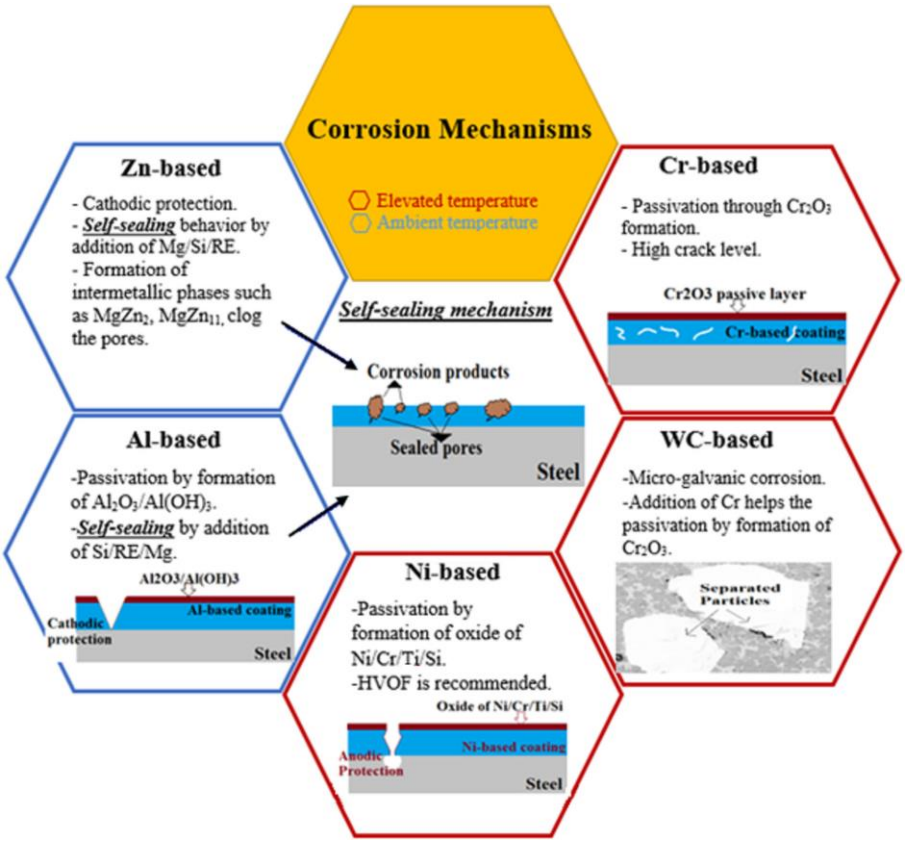

Fig. 2.33. Applications of various coating [1]

Table 2.1. Shows the review of boron nitride films using various techniques/instruments used, parameters, properties examined and observations.

Table 2.1. Review of Boron Nitride BN thin films

Research Group/s (year)	**Deposition Technique**	**Variable Parameter**	**Properties Examined**		**Instruments used**	**Advantage/limitation**
			Tribological	**Mechanical**		
H. Cesur et al.[145]	RF Magnetron Sputtering	temperature was varied between 200-250 ºC bias voltage	COF:0.5 Wear resistant of the films were quite high	Thickness of 0.5 µm for 2 hr duration.	Fourier transform infrared spectroscopy (FTIR), X-Ray photoelectron spectroscop	High wear resistance

		from 100 to 200 V.			y (XPS) and Scanning Electron Microscopy (SEM)	
Zheng Liu et al.[120]	Chemical Vapour Deposition Method(CVD)	temperatures ranging from 200 ^{0}C to 1,100 ^{0}C	NIL	Thickness of 7.5 μm	Optical microscopy and TEM	excellent oxidation protection
Xiuju Song et al.[158]	LPCVD	Precursor evaporation temperature (Tp) range of 65 °C ~ 120 °C.	NIL	Thermal resistant 1100 degree C Thickness of t ~72 μm	The scanning electron microscope (SEM), optical microscope (OM) Spectroscopic characterizations, including X-ray photoemission spectroscopy (XPS), Raman spectroscopy and UV-visible spectroscopy (UV-Vis)	High-quality h-BN monolayer films with the large single-crystalline domain size up to ~72 μm in edge length have been achieved on Cu foils
Krzysztof Gocman1 et al.[121]	Pulsed Laser Deposition (PLD)	temperatures ranging from 470 °C	NIL	Hardness, Young's modulus)	Atomic force microscopy (AFM), Fourier transform	Stable, crystalline, multiphase coatings with good adhesion to

		to 510 °C		proved that obtained coatings has two-phase structure.	infrared spectroscopy (FTIR).	the steel substrate were obtained. in case of 52100 bearing steel critical load was twice smaller than other materials
J. L. Anduj ar et al.[159]	Plasma-enhanced chemical vapor deposition	rf power density (W/cm2): Anode-0.25–0.5. Cathode-0.3–0.5 Gas pressure (Pa): Anode-30, 60 Cathode-20–60	NIL	Micro hardness of around 15 GPa.	X-ray photoelectron, infrared, and Raman spectroscopies; scanning and transmission electron microscopies; and optical transmittance spectrophotometry.	These films were chemically stable to moisture, even after an exposition period of two years. In contrast, the films grown on the anode from the B_2H_6–N_2 mixture showed tensile stress failure and were very unstable in the presence of moisture. However, the films grown on the cathode from B_2H_6–H_2–NH_3 gases suffered from compressive stress failure on exposure

						to air.
Halil Caliskan et al.[160]	Physical Vapor Deposition (PVD)	Cutting speed, Vc- 30 m/min Feed rate, fz- 0.05 mm/tooth	Abrasion and adhesion wear.	No significant effect on the surface roughness	scanning electron microscopy, energy dispersive spectroscopy.	Approximately two times longer tool life was obtained with the BN coated carbide tools.
M. Kandeva et ai.[161]	EFTOM-Ni technology method	heating during 6 h at 300 °C)	NIL	Thickness of 10 μm	disk-abrasive roller test rig	Decreases the abrasive wear rate (by approximately 54%).
Tharajak, J.et al.[162]	flame spray coating technique.	mean particle size of 0.5 micrometer was varied from 2 to 8 wt%	specific wear rate and friction coefficient	NIL	Ball-on-Disc sliding wear test.	Composite coatings could improve friction Coefficient and specific wear rate at elevated temperature.
Henrik Pedersen et al.[163]	CVD	pressure in the 10-4 Pa (10-6 mbar) range,	NIL	NIL	Fourier transform infrared spectroscopy, elastic recoil detection analysis,XRD	This growth behavior is believed to be caused by an uncontrolled release of water and/or oxygen in the deposition

						chamber and highlights the sensitivity of the BN CVD process towards oxygen and water.
K.P. Budna et al.[164]	Unbalanced DC magnetron sputtering	Varying the nitrogen partial pressure (pN2) between 0 and 64% of the total pressure (pAr+pN2),	yield only a moderate friction coefficients between 0.5 and 0.7.	the hardness and indentation modulus rapidly decrease from 40.6 and 397 GPa for CrB2 to 13.4 and 108 GPa for CrB2.0 N0.5.	X-ray diffraction, Transmission Electron Microscopy and X-ray photoelectron spectroscopy	The missing h-BN based lubricity is due to a lack of a significant long-range order.
Anden et Alemu et al.[165]	Ion assisted physical vapor deposition(IAPVD)	low substrate Temperatures (150 -250 °C).	NIL	constant index of refraction (2.8)	Auger electron spectroscopy (AES),Atomic force microscopy (AFM)	Negligible transmission losses over the useful range of the solar spectrum.
T. Wittkowski et al.[166]	RF-magnetron sputtering with simultaneous ion plating.	The emitted laser power is 200 to 400 mW.	NIL	From ten loading - unloading cycles at	Auger electron spectroscopy (AES), Fourier transform infrared spectroscop	Brillouin light scattering is shown to be an excellent method to characterize the elastic behaviour of

				different positions the hardness is found to be 14.6 ± 0.3 GPa for the h-BN films	y (FTIR).	hard films especially if the maximum thickness is less than a μm.
Quan Li et al.[167]	RF magnetron sputtering and DC plasma jet	Substrate Temperatures (450 -1000 °C),-120 to -50 Substrate Bias Voltage from 100 to 200 V.	NIL	NIL	XTEM	They found that theoretical calculations together with the experimental observations suggest that the availability of reactive tBN environment, along with other factors such as the integral stress in the films, contribute to the cBN nucleation process.
S. Nakhaie et al.[168]	Molecular Beam Epitaxy	temperatu refrom 730^0C to 835^0C over 3 to 5 h.	NIL	NIL	Raman spectroscopy, Atomic force microscopy, Scanning	The morphology of h-BN was found to evolve from dendritic,

					electron microscopy	star- shaped islands to larger, smooth triangular ones with increasing growth temperature.
Alan F. Jankowski et al,[169]	RF magnetron sputtering	200^0C to 600^0C substrate Heating and 300 V negative bias.	NIL	NIL	Auger electron spectroscopy, transmission electron microscopy, Nano indentation, Raman spectroscopy and x-ray absorption Spectroscopy.	41 GPa hardness is measured for a BN film consisting of 80% (cBN) $\mathbf{sp^3}$ bonding.

CHAPTER 3

PROBLEM FORMULATION

3.1. Gaps in Literature

The following research gaps were identified from the analysis of a comprehensive literature survey.

1. The literature available indicates that extensive knowledge of enhancing the surface properties of stainless steel is only accomplished by thermal treatment, coating, and cladding.
2. Very limited research studies are available on the development of surface composites using the thermochemical diffusion process.
3. There is no study available which reports the diffusion of cubic boron nitride (c-BN) on the D2 tool steel surface by the thermal diffusion process.

3.2. Proposed Research and Problem formulation

Tool steels have been used from the beginning of machining-era for high-temperature machine-tool applications such as a single-point cutting tool, drill bit, and milling cutter, etc. But, its low surface hardness (300-330 HV) restricts its industrial applications. Several techniques such as heat treatment, coating, and cladding, have been made to improve the surface properties of tool steel to make it useful for the industrial application exceptionally for high-temperature machine-tool applications. Plenty of metallic and ceramic materials such as CrN, Al_2O_3, WC, TiAN, and TiC, etc., has been explored and used as coating and reinforcements to achieve the desired mechanical properties. The thermal diffusion technique is an advanced surface-modification technique that can be used to improve the surface properties by developing surface-composite to provide safety against harsh environmental conditions for industrial components.

The present study aims to diffuse the cubic boron nitride (c-BN) powder on D2 tool steel surface by the thermal diffusion process to enhance its wear resistance for high temperatures applications.

3.3. Research Objectives

Following a comprehensive literature survey, the following priorities were chosen to tackle the study gaps in the existing study:

1. To develop a BN based surface composite on tool steel via thermal diffusion.
2. To characterize the microstructure of BN diffused steel using various techniques.
3. To study the effect of diffusion parameters (time and temperature) on the thickness of BN layer.
4. To study the hardness and wear behavior of developed BN based surface composite.

3.4. Research Design and Methodology

1. The D-2 steel work piece has been procured and elemental composition was tested.
2. The additive powders (c-BN) have been procured and characterized in terms of purity level.
3. Then experimentation has been performed by spreading c-BN powders on the D2-Steel surface. The effect of temperature and socking time (hour) on the diffusion layer thickness was investigated.
4. The surface micro-hardness and diffusion layer thickness was investigated.
5. The diffused layer was investigated using various characterization techniques.

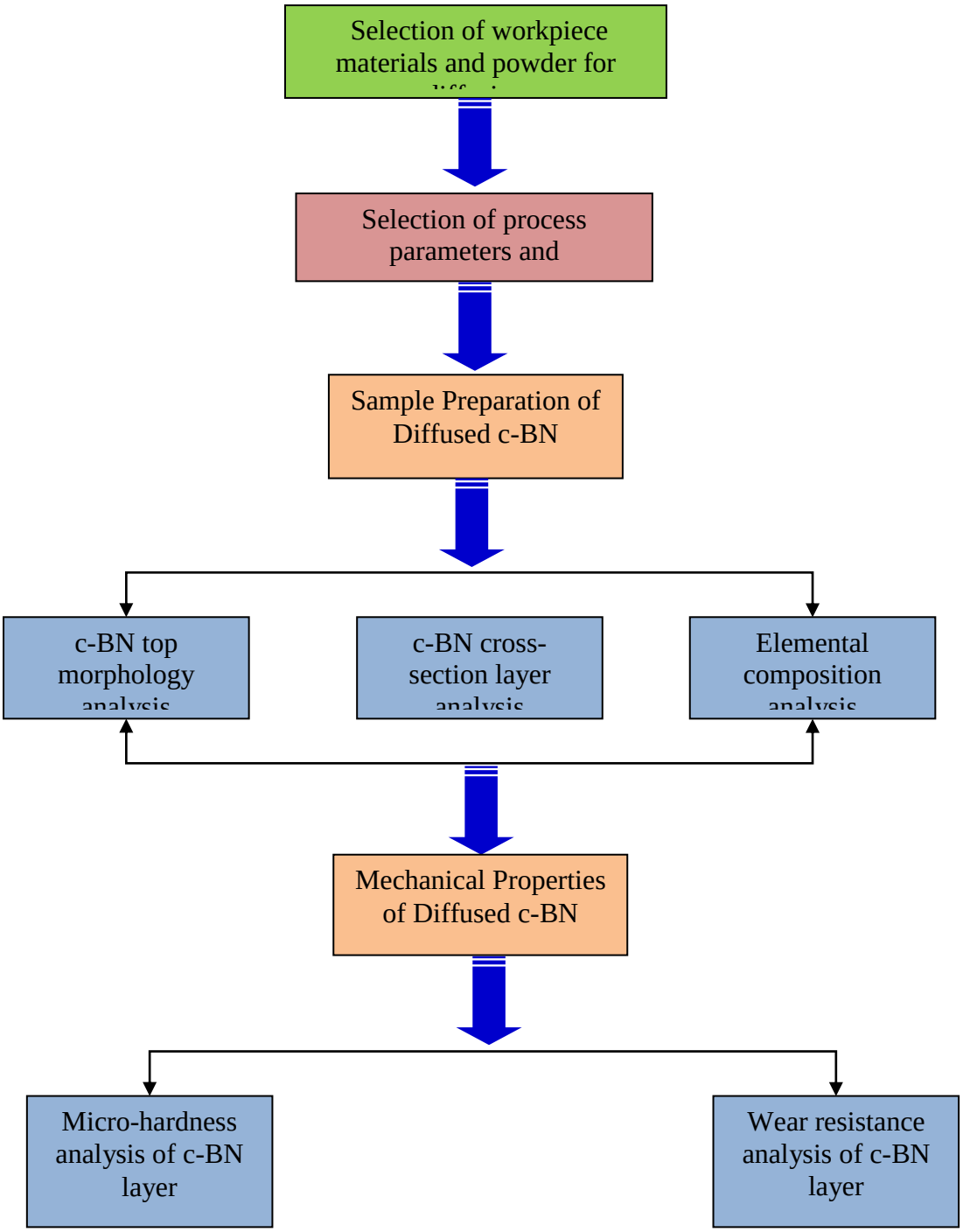

Fig. 3.1. Flowchart of the methodology adopted for c-BN layer diffusion and analysis

CHAPTER 4

EXPERIMENTATION AND CHARACTERIZATION

This chapter covers the details of the materials, methods, experimentation and characterization. This chapter also summarizes the specific technical information about materials, procedures and equipment used in the experimental work. It gives an overview of the different characterization techniques used.

4.1. Selection of work piece Materials

Thermal Diffusion is a technique to improve the surface properties such as hardness, of different kinds of steels. The contact between low carbon steel and an atmosphere high in carbon increases the carbon content of the steel and hardens the work piece. D2-die steel was chosen as a work piece material for its excellent consistency. D2 steel is a high chromium air hardening tool that is very durable. Fig. 4.1 optically displays the 10 mm diameter sample.

Fig. 4.1. Photograph of D2-steel material

In order to analyze the micro-structural characteristics the samples were well polished with the aid of correct polishing methods, and then nital (2% nitric acid and 98% ethyl alcohol) reagents were graded in around 15s. The JEOL 7600F optical microscope and field scanning microscope were examined for the microstructure. In the ready-made shape of the D2-steel cast, energy-dispersive X-ray (EDAX) and X-ray diffraction (XRD) technologies were analyzed. This method has been chosen for microstructure examination. Fig. 4.2, Fig. 4.3 and Fig. 4.4 display the optical micrograph, the EDS spectrum and the D2-Steel XRD.The microstructure of the sample was also shown in Fig. 4.2, showing the grain boundary pattern clearly. Fig. 4.3 displays the corresponding EDS spectrum and may confirm the presence of simple D2-steel elements. The related XRD pattern for D2 steel with strong iron-based phases (Fe) appears in Fig. 4.4.

For cubic boron nitride (c-BN), the divert powder was chosen over hexagonal boron nitride because it is second hardest substance next to diamond hence it is having good wear resistance and abrasion resistance. Cubic boron nitride is having very good thermal stability at elevated temperatures. Hexagonal boron nitride is having laminar structure like graphite. Due to this property it can be used as lubricant material. For laminar hexagonal sheet structure its adhesive wear is low as compare to c-BN. c-BN has sphalerite atomic structure similar to diamond. It is thermal stable up to 2800 ^{o}C in inert environment. c-BN melting point is 3500 ^{o}C. Fig. 4.5, Fig. 4.6 and Fig. 4.7 demonstrate the actual powder, dimensions and composition of c-BN powder particles.

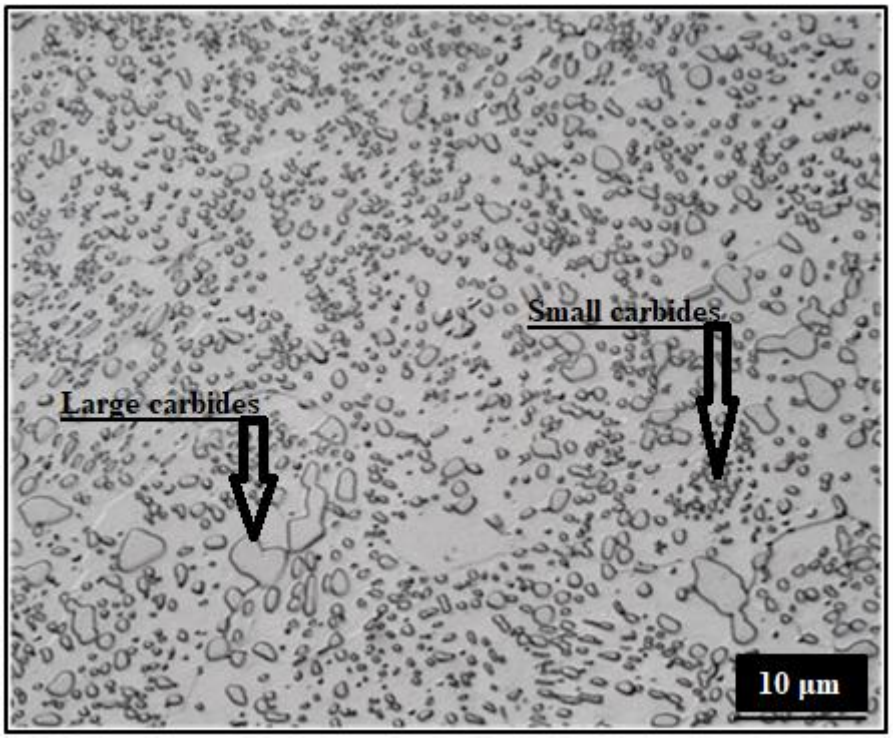

Fig. 4.2. SEM image of AISI D2-Steel

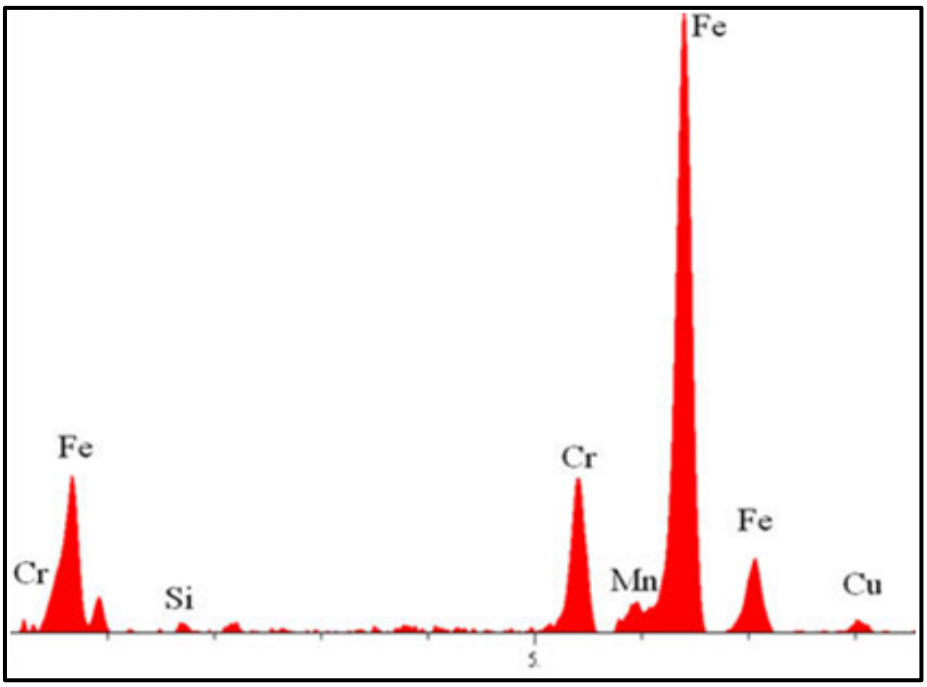

Fig. 4.3. EDS Spectrum of AISI-D2 Steel

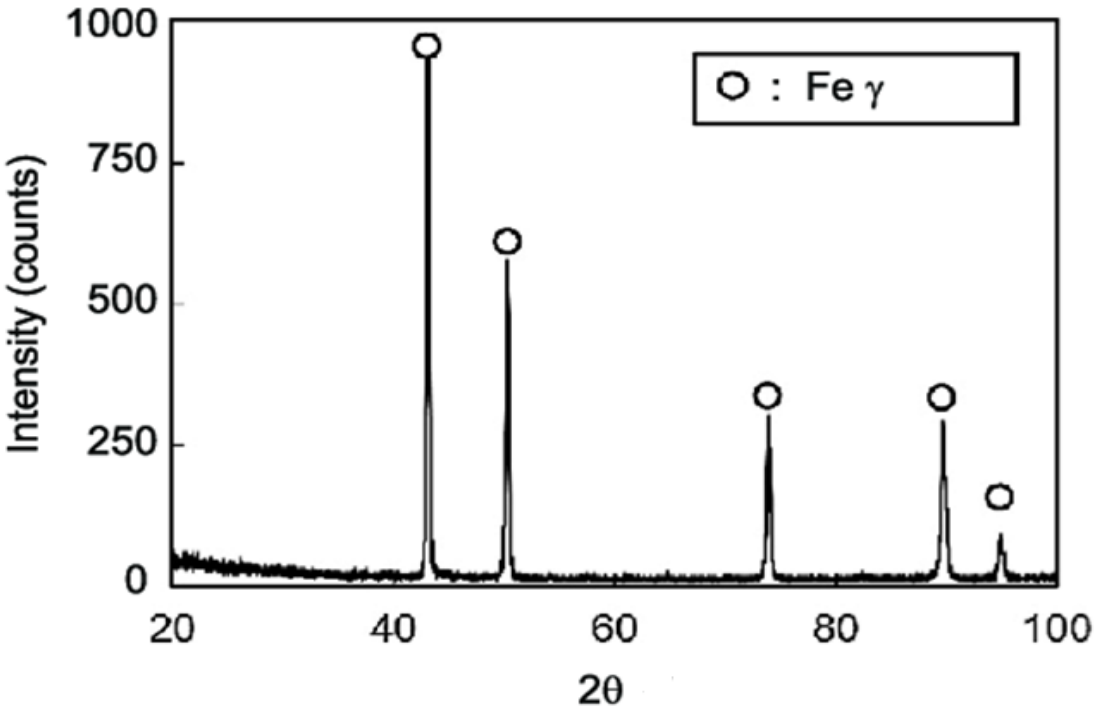

Fig. 4.4. XRD pattern of D2-steel

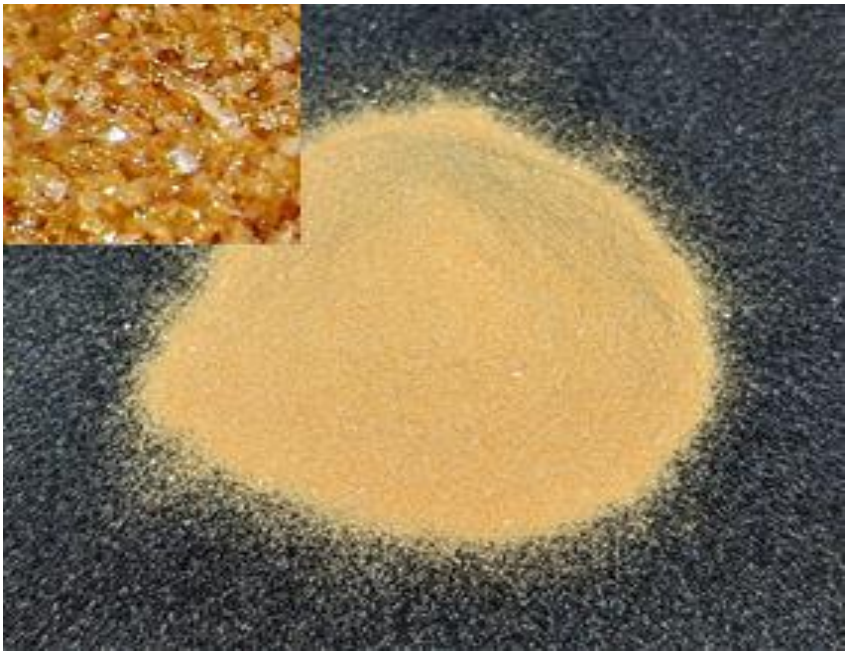

Fig. 4.5. Cubic boron nitride powder

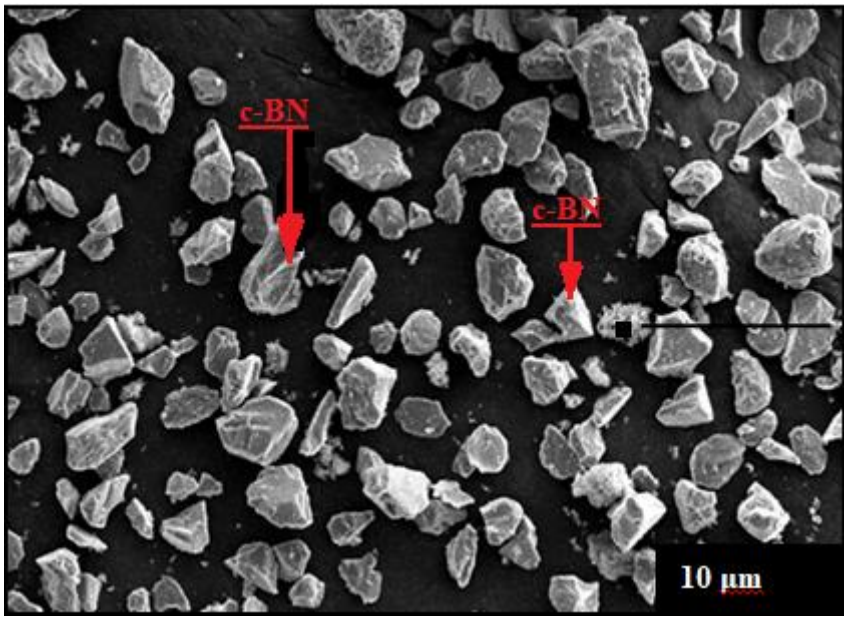

Fig. 4.6. SEM image of c-BN powder

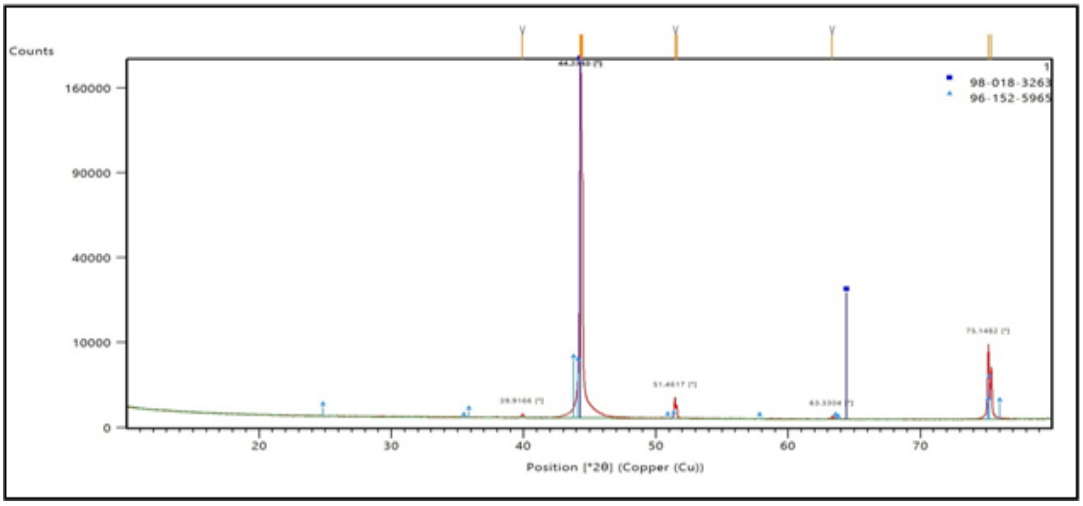

Fig. 4.7. XRD pattern of c-BN powder

4.2. Preparation of work piece specimens

The sample for further processing was cut from the steel using W-EDM process. Fig. 4.8 shows photograph of W-EDM machine, [153-154].After cutting the specimen filing operation was done then emery paper was used for achieving the fine surface. The grain sizes of emery paper (220, 550, 1000, and 1500) were used to get smooth surface. Emery consist of natural oxide of aluminum called corundum were used. Impurities present (iron oxide) on the surface of work piece act as an abrasive too. Diamond paste was used to allow the material to be extracted as quickly and as

clearly as possible. Different results were made from any other abrasives available. Both textures and diamond phases were remarkably well made, regardless of their hardness. During polishing, a smaller chip size was preferred so that a surface was finally reached without scratch and deformation. More flexible Velvet fabric was used to achieve zero chip sizes in addition to the small sizes of grain (e.g. 1.0 μm). A lower force reduced the size of the chip during polishing.

Fig. 4.8. Photograph of Wire-electric discharge machining (W-EDM) process

Fig. 4.9 shows the photograph of disc-polishing machine and diamond paste. The diamond paste is used to remove the unwanted scratch from the surface. It helps to obtain the mirror like surface.

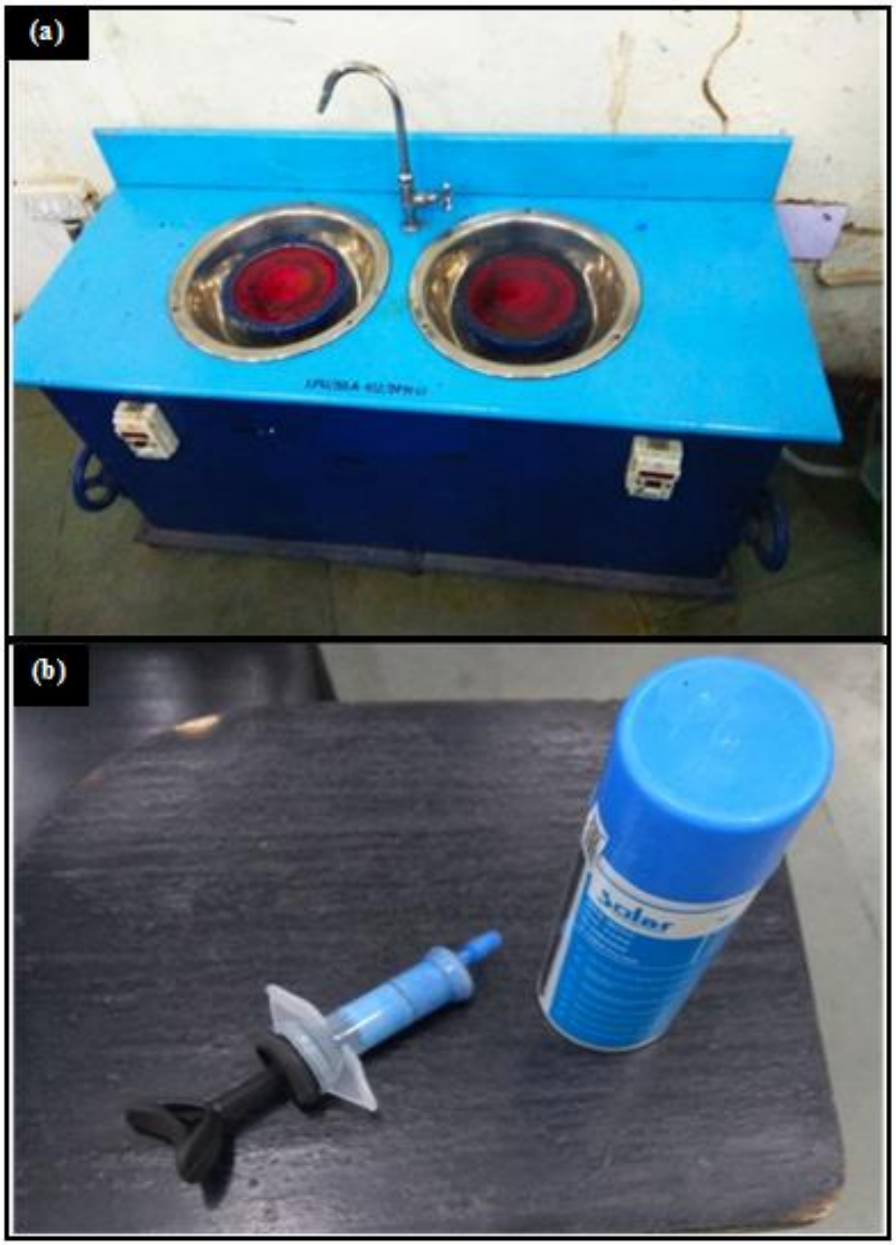

Fig. 4.9. (a) Disc polishing machine; (b) Diamond syringe & Developer

4.3. Experimentation

Before diffusion, the surface of D2 tool steel samples was grounded to produce plane surface and surface roughness (Ra) of value 1.5 μm. To develop

surface composite, first, the D2-tool steel samples were placed in a controlled vacuum furnace. First the vacuum furnace was pre-heated and c-BN powder particles were sprinkled on the surface of D2-steel samples. The diffused samples were then cooled for 18 hours in the furnace. Fig. 4.10 shows the photograph of vacuum controlled furnace. Fig. 4.11 shows the schematic representation of the diffusion process via a vacuum furnace. Table 4.1 shows the thermal diffusion process parameters.

Fig. 4.10. Experimental set-up of thermo-chemical diffusion

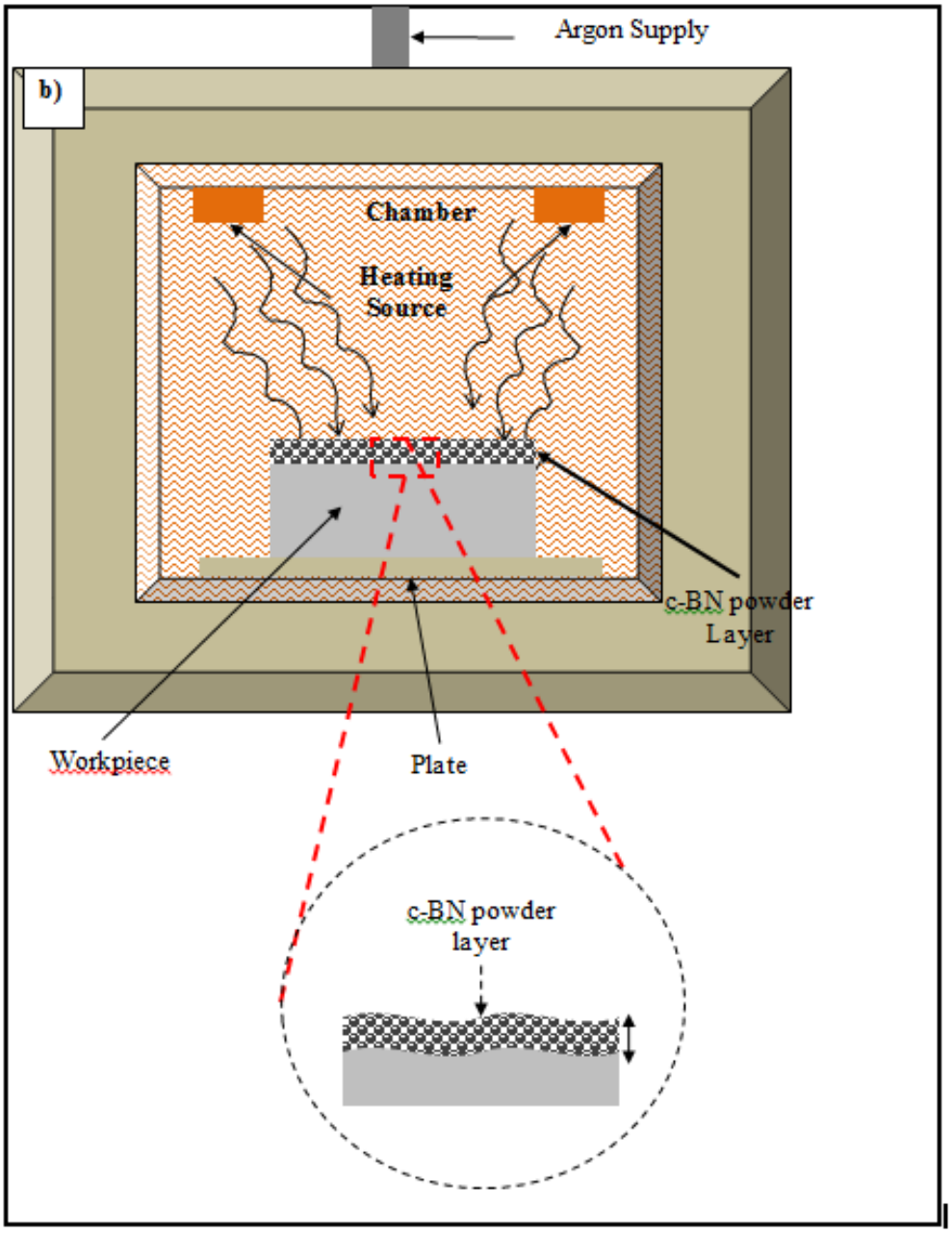

Fig. 4.11. Schematic representation of diffusion mechanism of c-BN on D2 Steel surface via vacuum furnace

Table 4.1. Input Process parameters for experimentation

Input Parameters	**Levels**				
Temperature	**550^{0}C**	**650^{0}C**	**750^{0}C**	**850^{0}C**	**950^{0}C**
Soaking time	**½ hr**	**1 hr**	**2 hr**	**3 hr**	**5 hr**

According to table 4.1 trial experimentation were performed as per following steps:

1. Identify the time and temperature of initiation and termination of diffusion process.
2. Cool the specimen in the furnace.
3. Took the specimen out.

Fig. 4.12 shows the c-BN diffused samples. A clear picture of diffused layer of c-BN on the D2-steel surface can be seen.

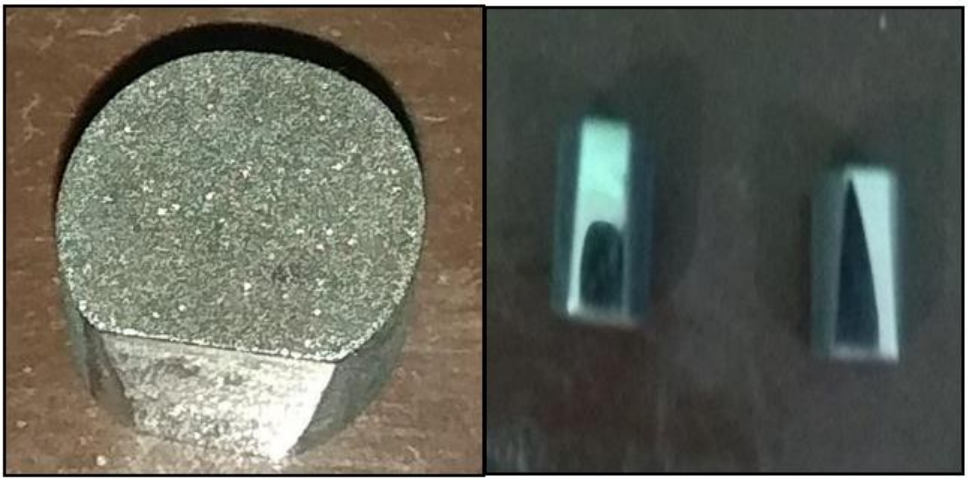

Fig. 4.12. (a) Top surface image of c-BN diffused layer; (b) Side view of c-BN diffused layer

4.4. Characterization

The c-BN diffused layer was investigated in terms of surface morphology, topography, microstructure, elemental composition, and mechanical properties

(micro-hardness and elastic modulus). Moreover, the wear resistance was also investigated to claim the anti-wear resistance.

4.4.1. Microstructure examination

After diffusion of c-BN layer, the morphology was investigated by optical micro-scope and field emission-scanning electron microscope (FE-SEM) made of JEOL model-7600F. The elemental composition of c-BN diffused layer was analyzed by energy-dispersive X-ray spectroscopy (EDS). Fig. 4.13 shows the image of FE-SEM coupled with EDS. The analysis was carried out at 15 KeV [155].

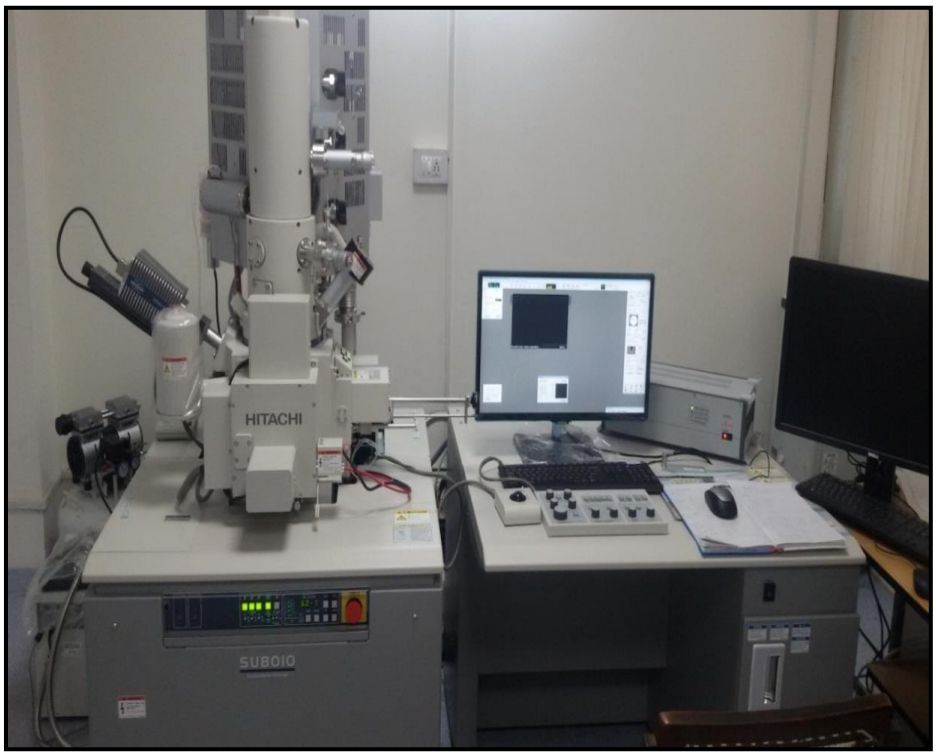

Fig. 4.13.FE-SEM machine

The phases composition of specimens, before and after diffusion were investigated by X-ray diffraction (XRD) with CuK radiation at an incident angle range of 20–80º.Fig. 4.14 shows the image of XRD-machine.

Fig. 4.14. XRD equipment for Phase Composition Analysis

4.4.2. Surface Microhardness (Hμ)

The test surface was measured according to ASTM standard (ASTM-E384-11) using appropriate polishing and grinding methods. The sample consists of a section with a low-speed screw and polished emery paper on a cross section of 220, 600, 800, 1200 and 2000 grade. Afterwards, it was polished with the help of diamond paste to get the mirror finish. In the microhardness test conducted on the Vickers hardness tester (Mitutoyo HM-125), the cross section of the sample was tested. A breakdown load of 2.45 N was applied and the holding time was 10 s. From recast to substrate, the hardness readings of each sample were recorded as five straight lines. Fig. 4.15 (a) and (b) show the microhardness and the uniformly distributed microhardness calibration area of the intersecting surface [156].

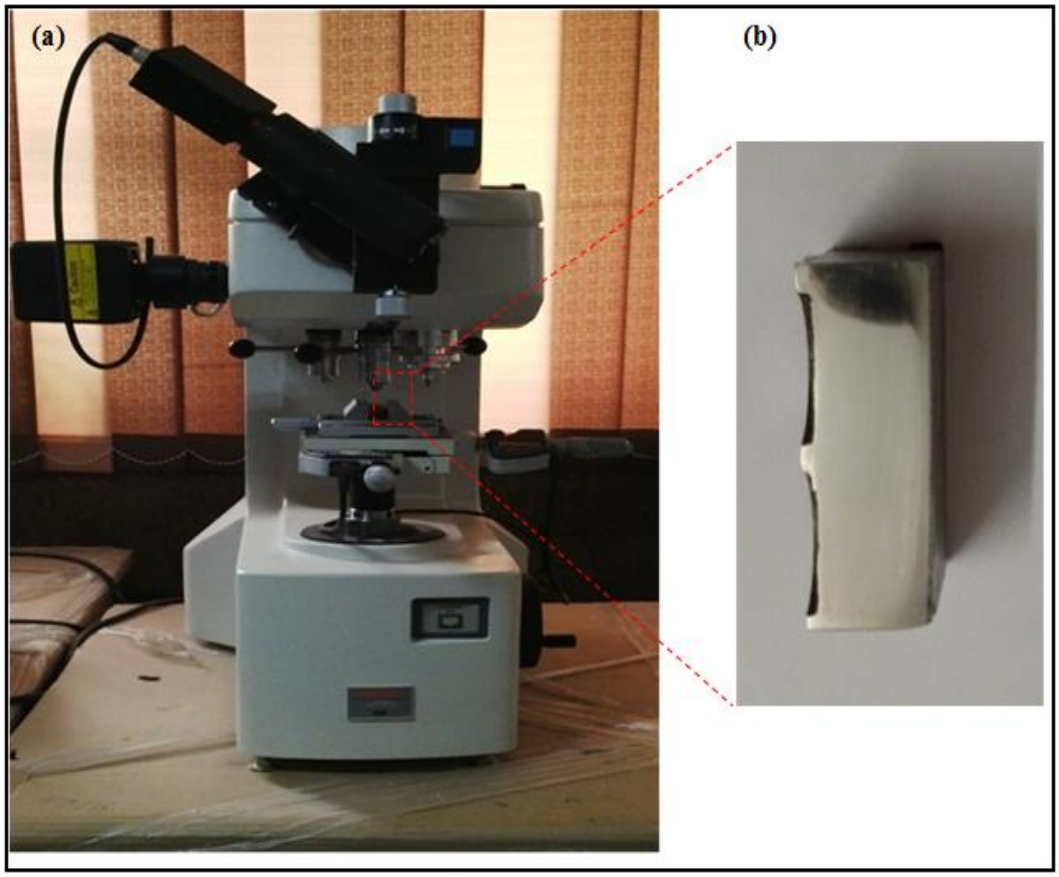

Fig. 4.15. (a)Mitutoyo microhardness tester and (b) Cross-section of polished-surface

Fig. 4.16 displays the diamond-index indentation mark used for the determination of micro-hardness.

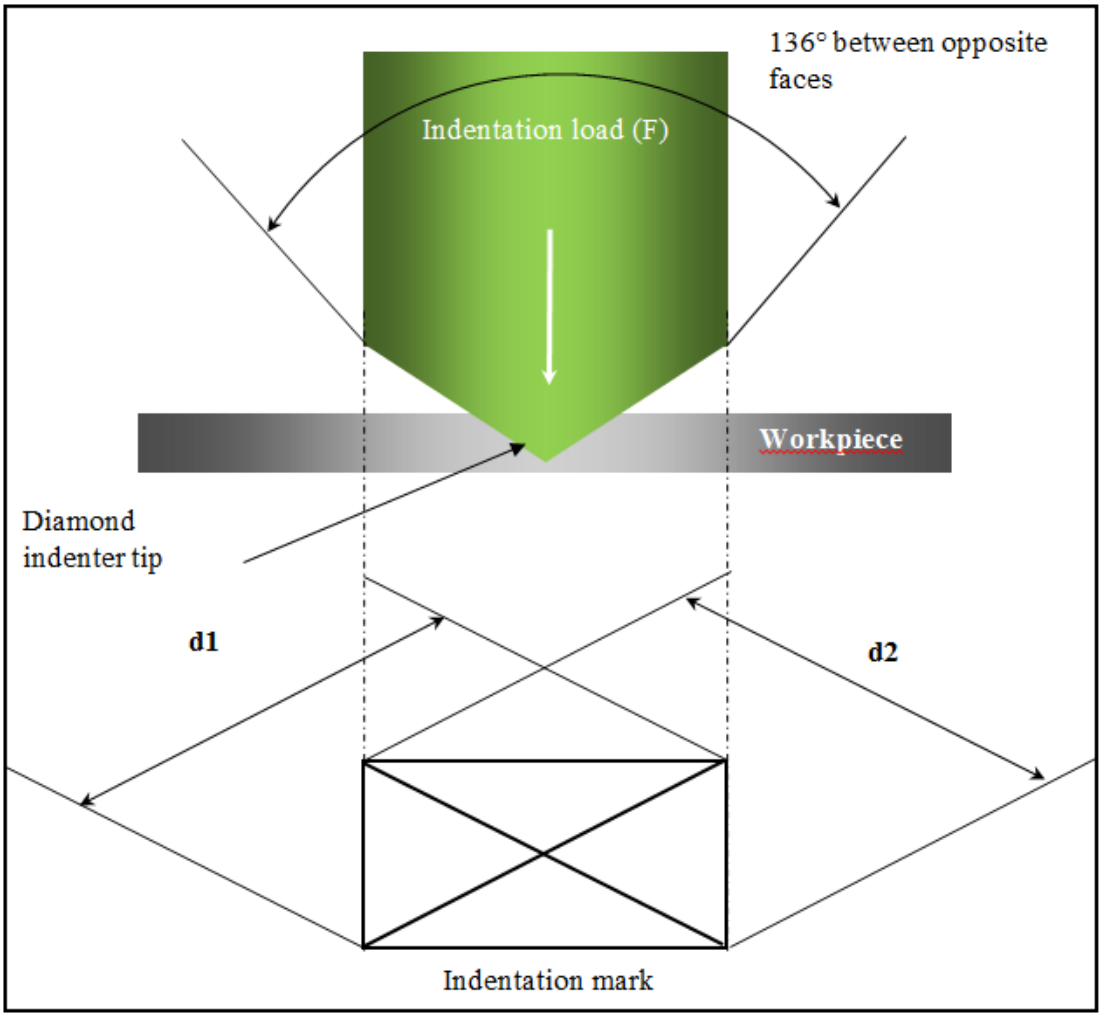

Fig. 4.16.Micro-hardness measurement process [156]

Microhardness means the strength of a material measured with small indenters. The thinner sheets or smaller test materials, which cannot depend on standard measurements, were then applied to a lower resistance compared to conventional measuring instruments.

F= Load in kgf

d = Arithmetic mean of the two diagonals, d1,and d2 in mm

HV = Vickers hardness

$$HV = \frac{2FSin\frac{136^\circ}{2}}{d^2} \qquad [156]$$

$$HV = 1.854\frac{F}{d^2} \qquad [156]$$

When the mean diagonal of the indentation has been determined the Vickers hardness may be calculated from the formula, but was more convenient to use conversion tables.

4.4.3. Wear Testing

The tribological performance of untreated and c-BN diffused specimens of D2-steel was investigated by frictional wear test. The test was carried out with a load of 10 N in air at room temperature using a pin-on-disc frictional wear-testing system (DUCOM, Instruments Pvt. Ltd, Bangalore, India), as can be seen in Fig. 4.17. To perform wear test, a pin of ϕ 10 × 50 mm was prepared from the diffused samples. The pin was rubbed against WC, Al_2O_3, Si_3N_4 counter surface material and sliding distance was taken 500 m. The sliding velocity for wear test was considered 0.1 m/s. The amount of specific wear rate K ($mm^3.N^{-1}.m^{-1}$) and the coefficient of friction were determined. The details to calculate the volume loss (V_{loss}) and specific wear rate [156].

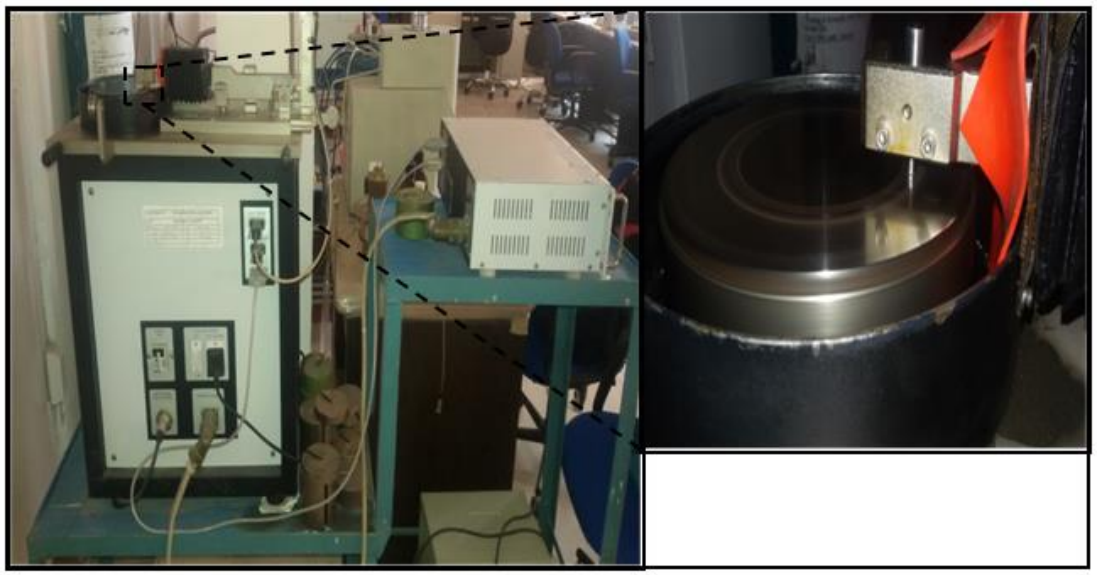

Fig. 4.17. Photograph of wear test rig

4.5. Erosion Analysis

The erosion studies were conducted to study the relative erosion-resistance and behavior of bare samples and coated specimens. Under this investigation, standard erosion test conditions were utilized and reported in Table 4.2. To achieve

the identical conditions on all the test specimens, bare sample and coated samples were polished with 1μm alumina wheel cloth polishing before the specimen was subjected to the test rig. The test specimens were cleaned with acetone, dried, and weighed to an accuracy of 1×10^{-5}g using an electronic balance before the test run. The specimens were subject under the test conditions for about 30 minutes and then weighed again to determine the weight loss. The erodent particles used in the present study were standard alumina 50 μm. The SEM analysis shows the morphology of the erodent particles (Al_2O_3) and EDAX analysis depicting its elemental composition.

Table 4.2. Conditions at erosion testing carried out

Erodent Material	Alumina (Irregular shape)
Erodent Specification	50 Micron Al_2O_3
Particle Velocity(m/s)	30 m/s
Erodent rate(g/min)	2 gm/min
Impingement angle	45°,60° and 90°
Nozzle diameter	1.5 mm
Test time	30 min.
Test temperature	150°C–Sample temperature 180°C- Air temperature

To measure the erosion resistance the weight of the specimen was measured before the erosion test and after the test. The erosion rate and erosion resistance were calculated.

CHAPTER 5

RESULTS AND DISCUSSION

This chapter addresses the observations in two stages. In the first segment, the experiment results were analyzed, which analyzed the surface features of the c-BN diffused layer. Further, the analysis of microstructure, surface morphology, micro-hardness, and diffuse layer thickness were carried out comprehensively. The second step was planned to determine the efficacy of the thermo-chemical diffusion method of manufacturing high-temperature surface layers to determine the surface strength and wear resistance of the c-BN diffuse layer.

5.1. Effect of process parameters on the diffusion of c-BN

The diffusion of c-BN was assessed by a cross-sectional view and the diffused layer of c-BN was measured using SEM microscopy. Fig. 5.1 and Table 5.1 show the effect of temperature and soaking time on the diffused layer. There was no visual diffusion observed at 550 ºC and 650 ºC at different soaking hours. This is because the recrystallization temperature of steel is more than 650 ºC. Thereby, the c-BN was unable to dissolute on the surface. The diffusion of c-BN occurred at or more than 750 ºC after soaking at least 2 hours. At 750 ºC, the D2 steel undergone through the re-crystallization phase and get soften owing to that c-BN particles were reinforced into the substrate surface up to few microns. The diffusion depends upon the temperature and soaking hours. The increase in soaking temperature to more than 2 hours, the change in the microstructure, and diffusion layer was observed. The best optimal condition for the diffusion of c-BN on the D2-steel surface was 750 ºC for 2 hours and 850 ºC for 1 hour.

Fig. 5.2 and Fig. 5.3 shows the diffusion layer on specimen after thermal diffusion at 750 ºC and 850 ºC at different soaking time from ½, 1,2,3,5 hours. Fig. 5.4 shows the optical micrograph of surface composite at 750 º C for 2 hours and 850 ºC for 1 hour. From the micro-graph the diffusion of c-BN was clearly observed and

distribution of c-BN on the whole surface was found. At low temperature diffusion of CBN was less and at high temperature the diffusion of CBN was more.

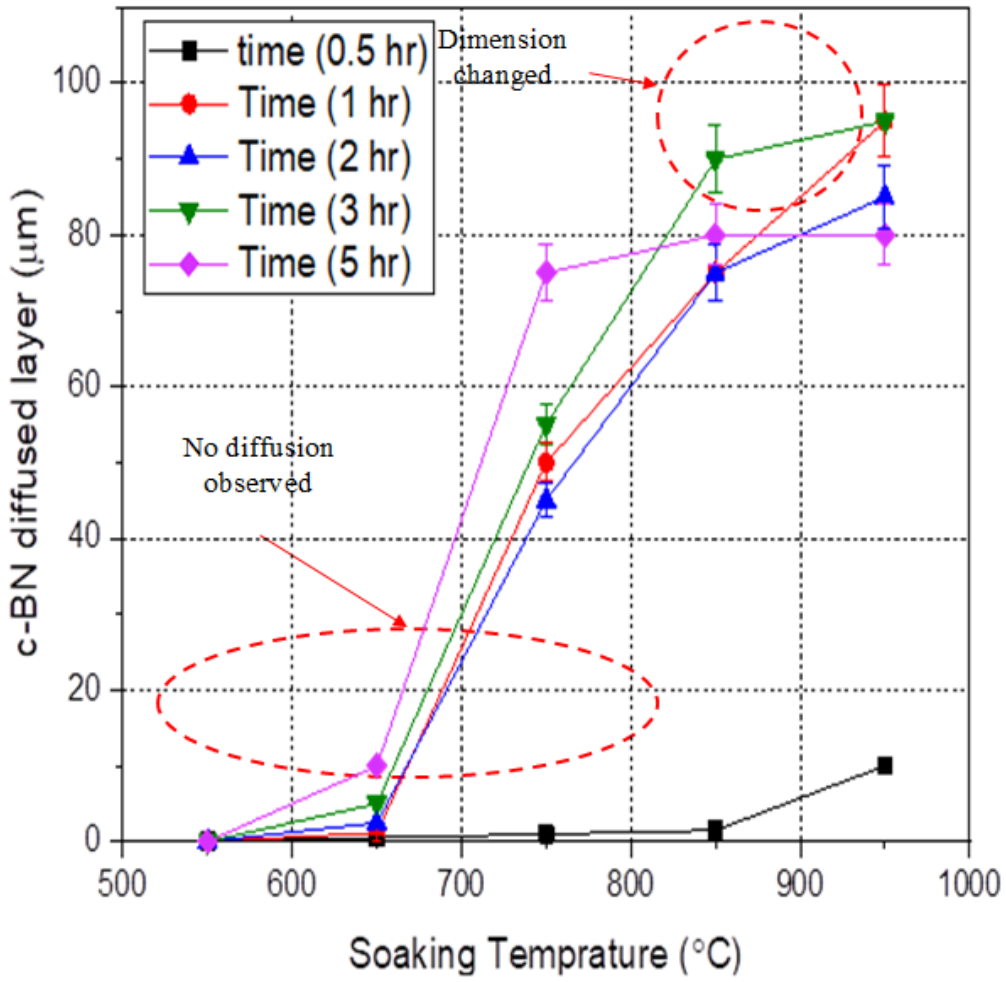

Fig. 5.1. Effect of temperature on the c-BN diffusion layer

Table 5.1. Effect of temperature and soaking hours on the diffusion of c-BN

Soaking Time (Hours)	**Diffusion Temperature (°C)**				
	550°C	**650°C**	**750°C**	**850°C**	**950°C**
½ hour	No visual change/diffusion	No visual change/diffusion	No visual change/diffusion	No visual change/diffusion	Diffusion occurred /change in dimensions
1hour	No visual change/diffusion	No visual change/diffusion	No visual change/diffusion	Diffusion occurred	Diffusion occurred /change in dimensions
2 hour	No visual change/diffusion	No visual change/diffusion	Diffusion occurred	Diffusion occurred /change in dimensions	Diffusion occurred /change in dimensions
3 hour	No visual change/diffusion	No visual change/diffusion	Diffusion occurred /change in dimensions	Diffusion occurred /change in dimensions	Diffusion occurred /change in dimensions
5 hour	No visual change/diffusion	No visual change/diffusion	Diffusion occurred /change in dimensions	Diffusion occurred /change in dimensions	Diffusion occurred /change in dimensions

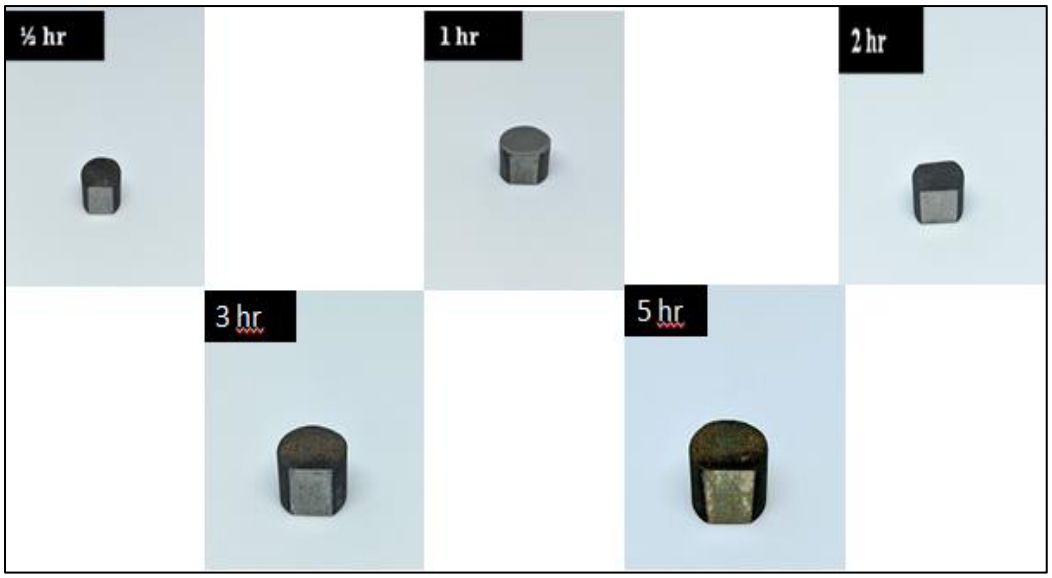

Fig. 5.2 Diffusion samples at 750 ºC for different soaking times

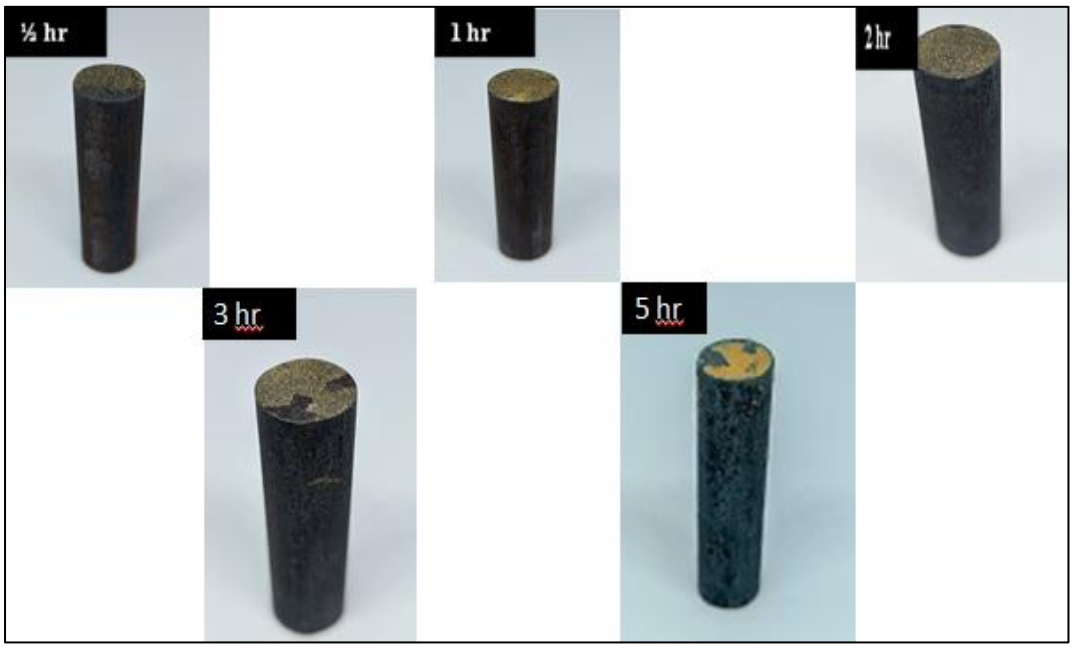

Fig. 5.3 Diffusion samples at 850 ºC for different soaking times

Fig. 5.5 shows the optical micrograph of surface composite subjected to 750 ºC and 850 ºC for 1/2 hour. It reveals details of the microstructure formation and the diffusion layer. From this micro-graph, it can be seen that at 750 ºC and 850 ºC for soaking time ½ hour, the c-BN particles were not diffused on the surface, no changes were observed. The c-BN particles were found placed on the top surface.

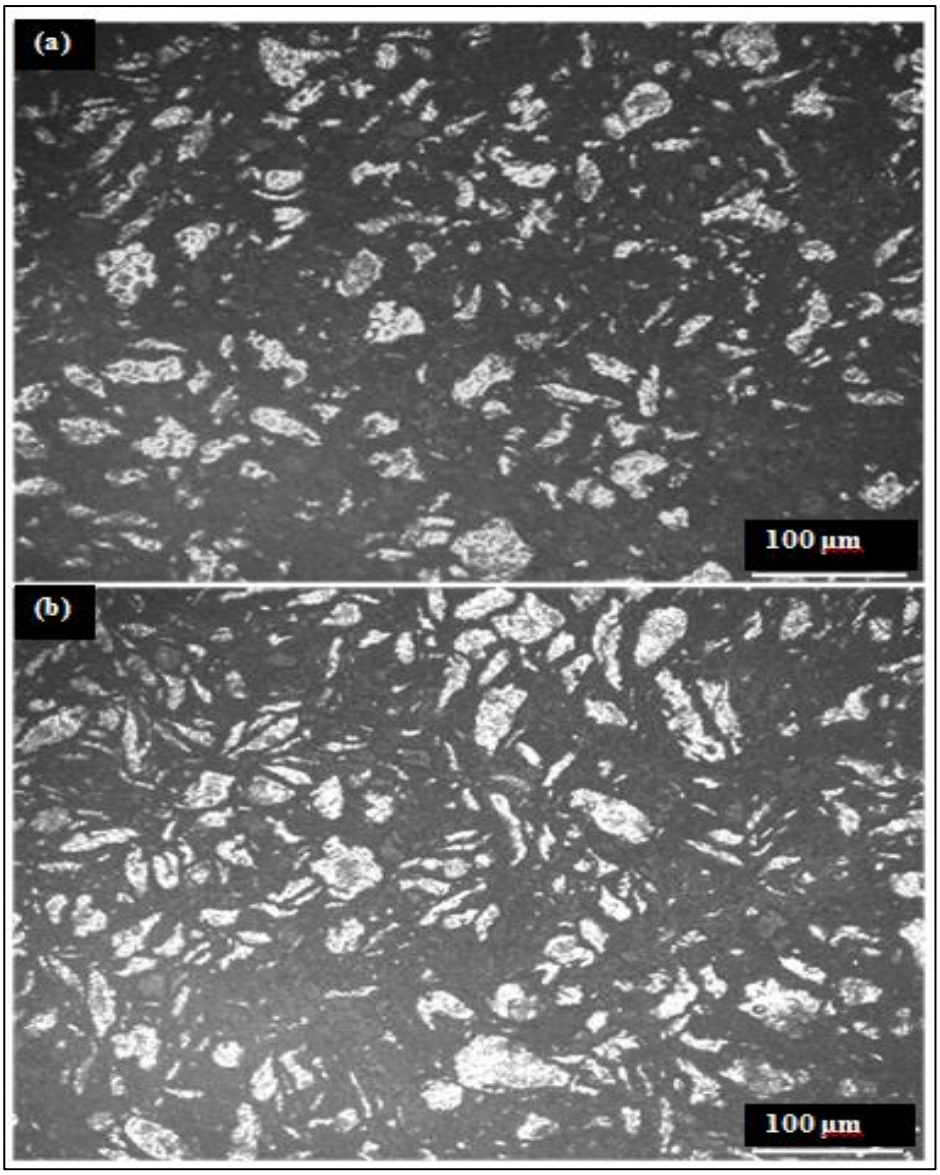

Fig. 5.4. Optical micro-graph of surface composite prepared at (a) 750 º C for 2 hours and (b) 850 ºC for 1 hour

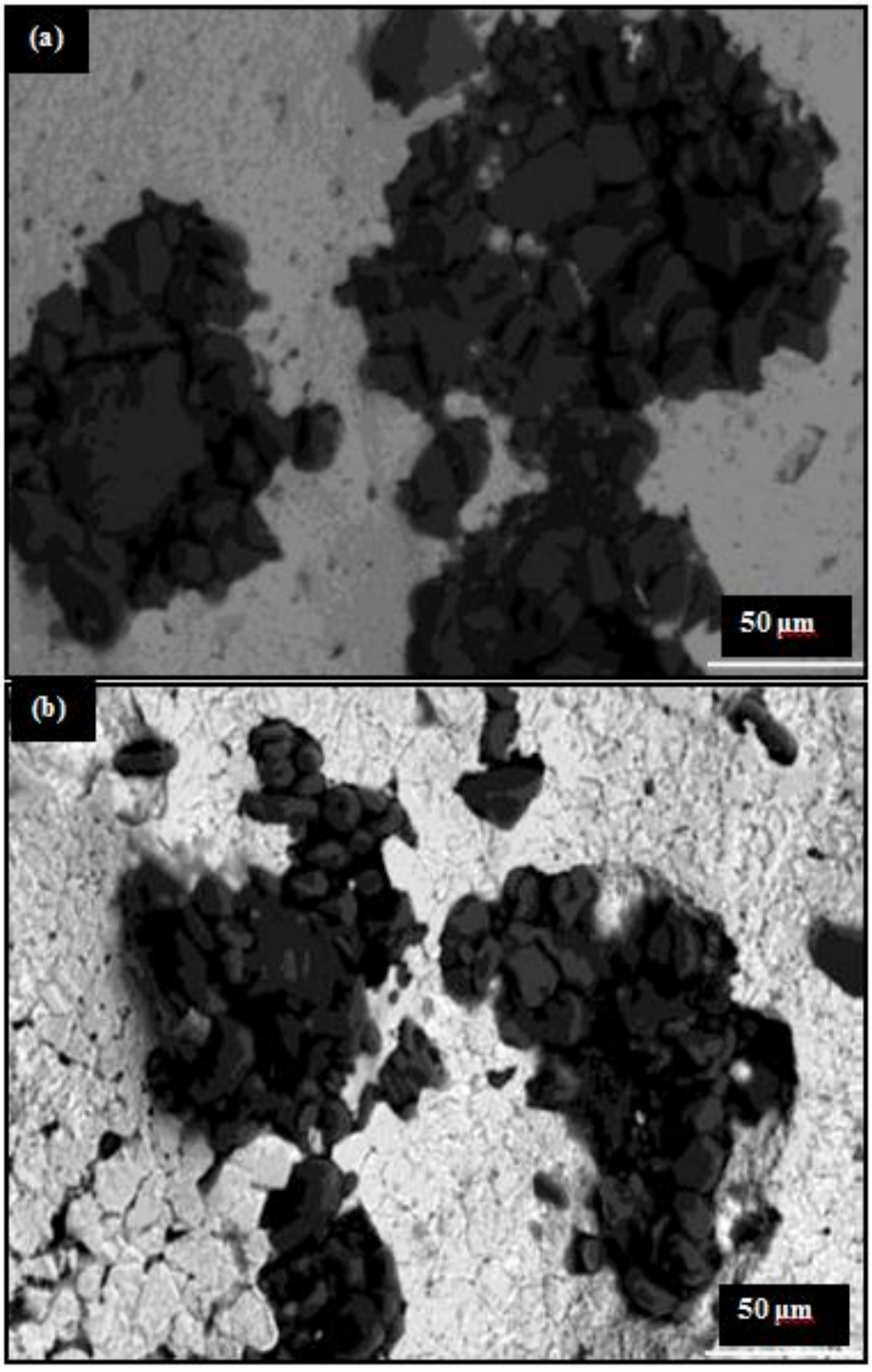

Fig. 5.5. Optical image of diffused c-BN at temperature at (a) 750 ºC and (b) 850 ºC for ½ hour soaking time

Fig. 5.6 to Fig. 5.9 shows the optical image of diffused c-BN at temperature of 750 ºC and 850 ºC for 1 hour and 2 hours of soaking time. At 750 ºC, when the

soaking time increased to 1 hour, a very nominal diffusion was observed, while after 2 hours, c-BN diffused entirely on the surface; refer Fig. 5.4 and Fig. 5.5. On the other hand, at 850 ºC, with a soaking time of 1 hour, the c-BN diffused in the surface, and after 2 hours, a very thick layer of c-BN particles spread in the surface; refer Fig. 5.6 and Fig. 5.7. The diffusion of c-BN was observed and the distribution of c-BN on the whole surface has occurred. At low-temperature diffusion of c-BN was less and at high temperature, the dissemination of c-BN was more. But, when more temperature were applied more than 2 hours of soaking time, the sample behaves more brittle and its dimensions changed, which deteriorate the mechanical properties.

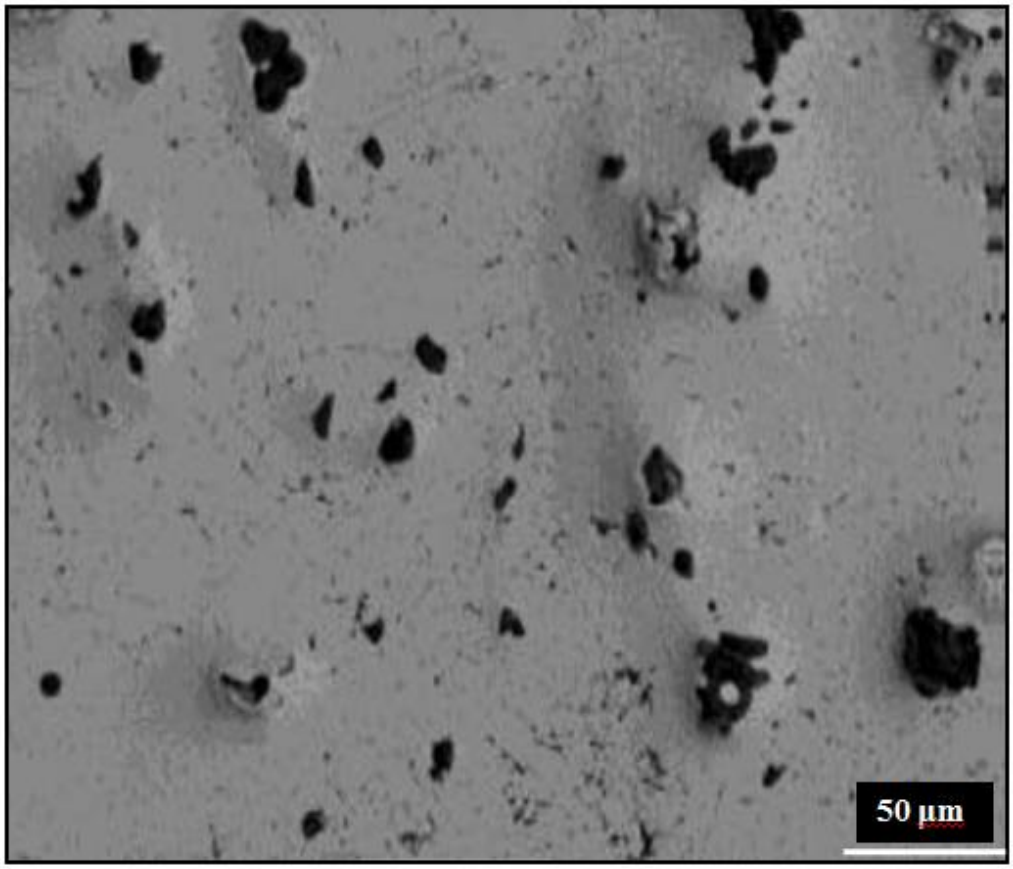

Fig. 5.6. Optical image of diffused c-BN at 750 ºC for 1 hour of processing time

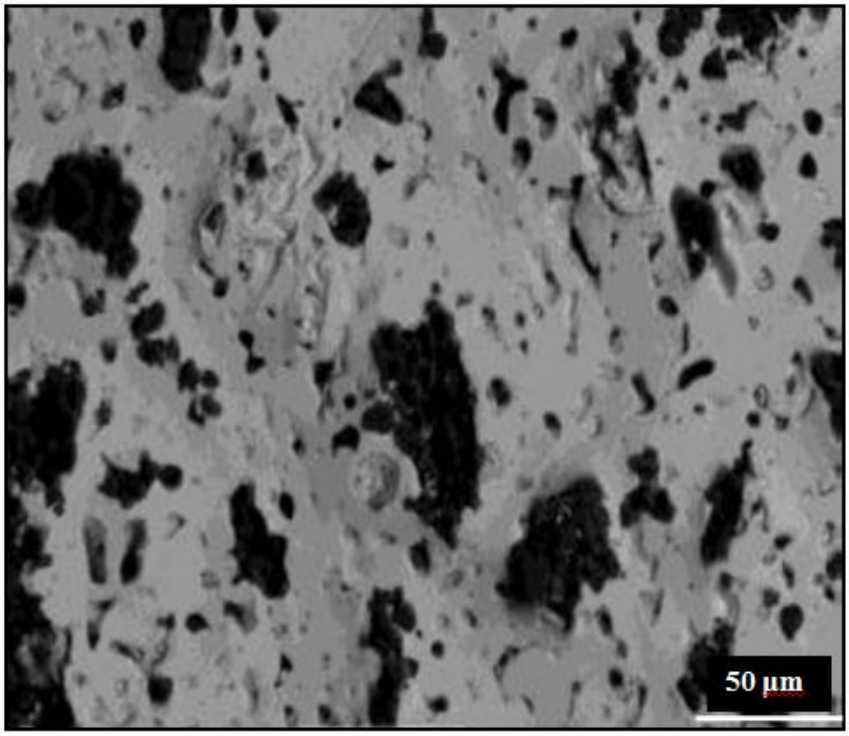

Fig. 5.7. Optical image of diffused c-BN at 750 ºC for 2 hours of processing time

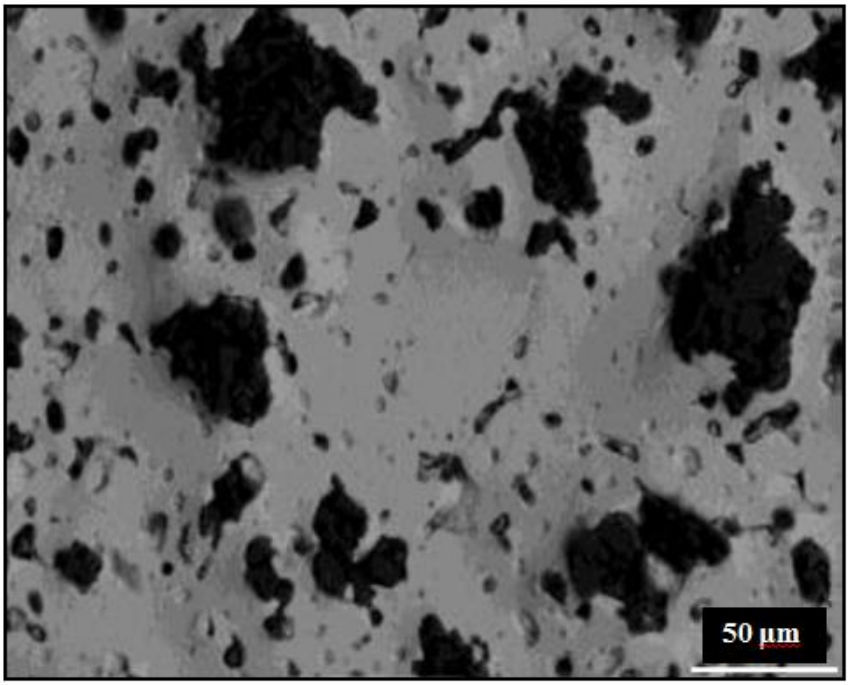

Fig. 5.8. Optical image of diffused c-BN at 850 ºC for 1 hour of processing time

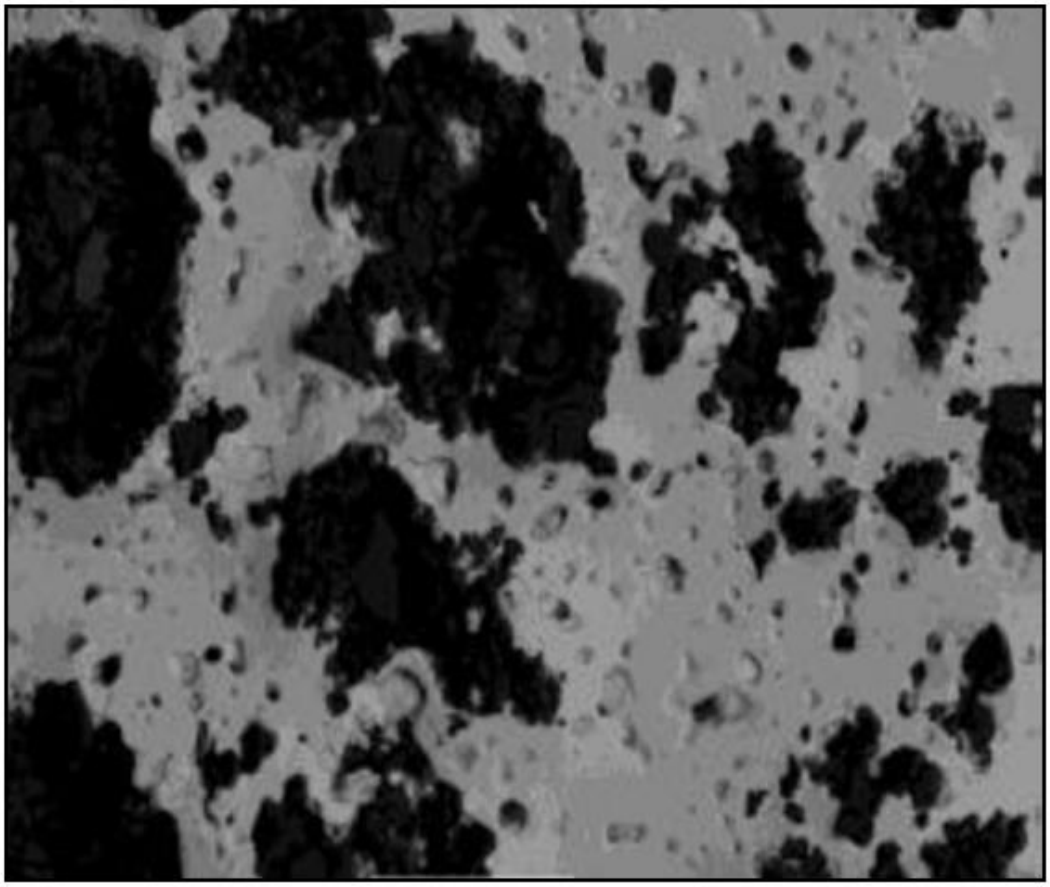

Fig. 5.9. Optical image of diffused c-BN at 850 ºC for 2 hours of processing time

5.2. Effect of Process parameters on Structural porosities

The effect of processing parameters and time on the formation of structural porosities were alos studied. Fig. 5.10 shows the variation of strutural porosities with repect to difussion temprature and processing time. It can be seen that processing time have significant effect on the structural porosities. With the incarse in time/soaking hours, the porosities decrased. This is attributed because, with the incrase in soaking time, the difussion layer become more compact and densified, which prevents the formation of pores in the structure. On the otherhand, the difussion temprature have also significant effect on the porosities genration.At low temprature (750 ºC) for 1 h of soaking time, the porosities are 10.35% and at 850 ºC, the porosities are 5.57 %.

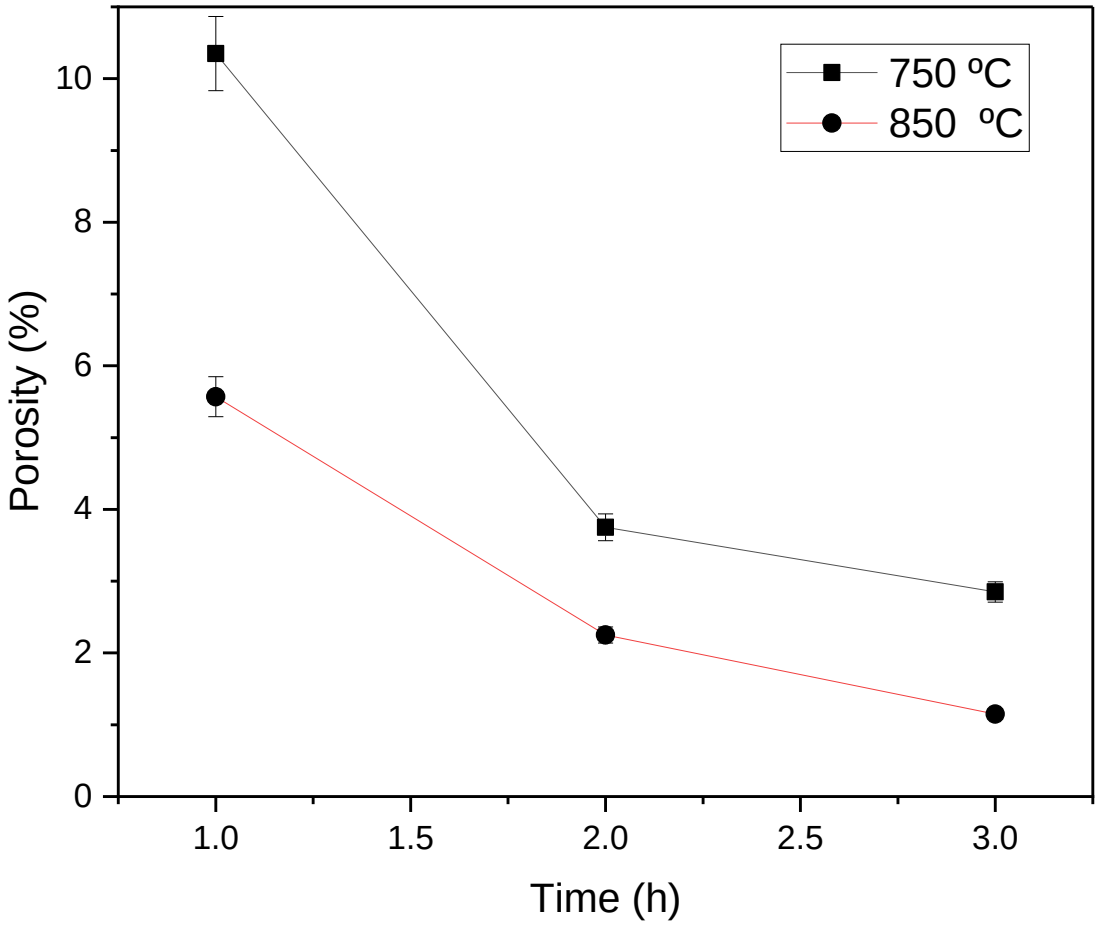

Fig. 5.10. Variation of structural porosities with respect of diffusion time and temperature

5.3. Parametric Optimization using Taguchi's Methodology

5.3.1. Taguchi Design of Experiment

The approach used to identify and analyze all possible conditions in a multiple factor experiment is known as experiment design (DOE). Taguchi approach has also been used to improve output features by choosing parameters of the process and their levels in engineering problems. It is a combined type of mathematical and statistical methods used for improving processes and product creation. This approach provides optimum parameter combinations with minimal variability. The nature of the experimental flow chart by Taguchi shows in Fig. 5.11.

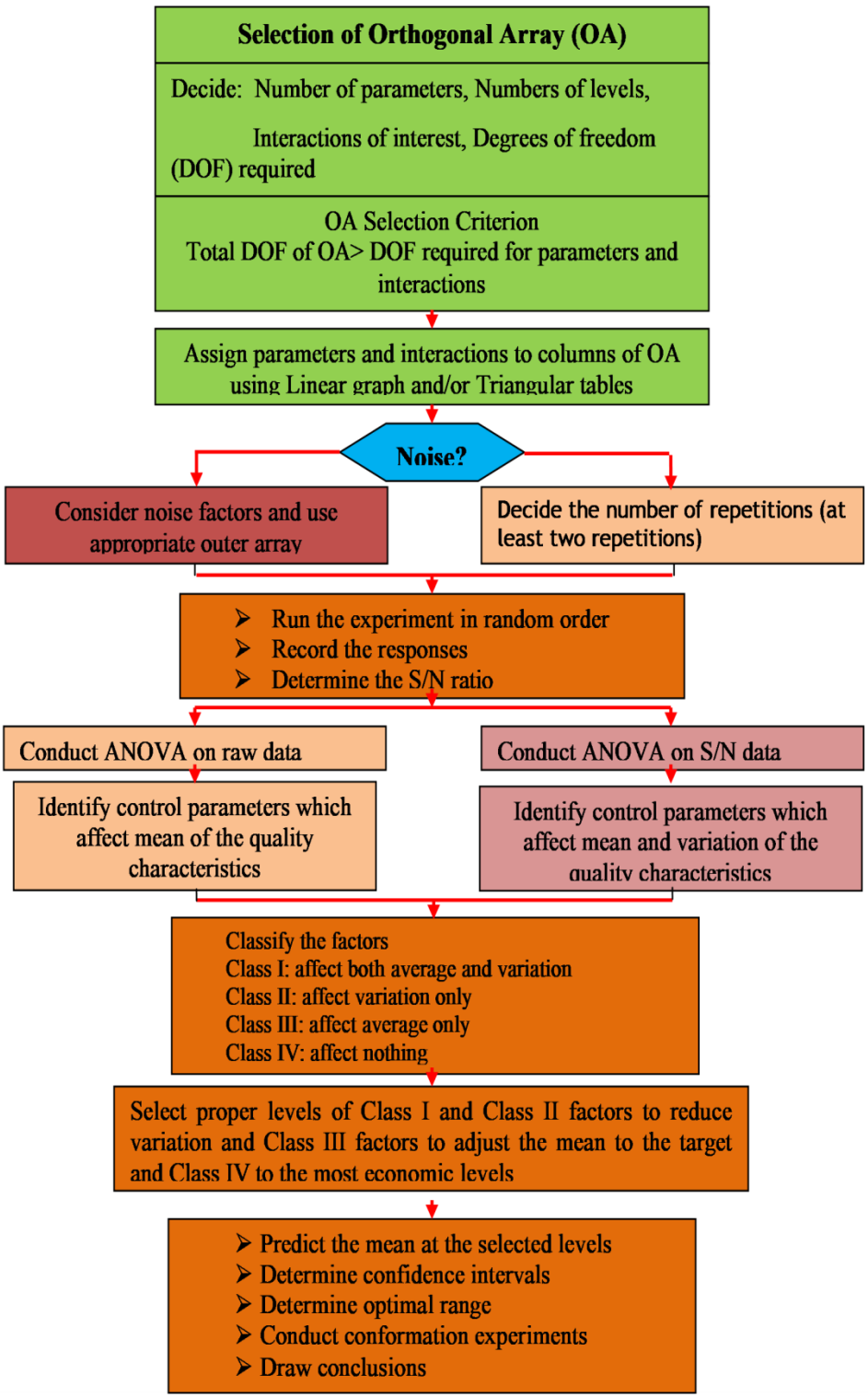

Fig. 5.11.Flow chart of DOE methodology

Dr. Taguchi in 1960 has developed the techniques for quality improvement and reduced operational costs in manufacturing industries by optimizing the process

of engineering experimentation. As per Taguchi's philosophy, the quality of the product can only be improved at the initial stage of its production and should not be tested at the final stage of the product. The different Orthogonal Arrays (OAs) were developed by Taguchi to minimize the effects of noise factors to create robust product design [156-157]. The technique is applied to the study with the following steps shown in Fig.5.11.

5.3.2. Taguchi Procedure for Experimental Design and Analysis

Taguchi's DOE technique proposed the design matrix of experimental trial runs based on the orthogonal array depending upon the number of parameters and their levels. As per Taguchi, many OAs were suggested to suit the combination of parameters and their levels. On the basis of the appropriate design matrix, experiments can be performed to get the inference about the quality.

The standard two-level, three-level and five-level arrays as reported by Prakash et al. [156] are:

a) Two-level arrays: L_4, L_8, L_{12}, L_{16}, L_{32}

b) Three-level arrays: L_9, L_{18}, L_{27}

c) Five-level array: L_{25}

The number as a subscript in the array designation indicates the number of trials in that array. The degree of freedom (DOF) available in an OA is:

$$f_{L_N} = N - 1$$

Where f_{L_N} = total degrees of freedom of an OA

L_N =OA designation

N = number of trials

When a particular OA is selected for an experiment, the following inequality must be satisfied as reported by [156]:

$f_{L_N} \geq$ Total DOF is required for parameters and interactions.

Depending on the number of levels in the parameters and total DOF required for the experiment, a suitable OA is selected.

Taguchi's methodology classified signal to noise (S/N) ratio as objective functions into three categories, namely, lower-the-better, higher-the-better, or nominal the better. Accordingly, the loss functions are narrated below:

a) Higher-the-Better

$$\frac{S}{N}\text{ratio} = -10\log\left(\frac{1}{n}\sum_{i=1}^{n}\frac{1}{y_{ij}^2}\right)$$

b) Lower-the-Better

$$\frac{S}{N}\text{ratio} = -10\log\left(\frac{1}{n}\sum_{i=1}^{n}y_{ij}^2\right)$$

Where y_{ij} = i^{th} replicate of j^{th} response, n = number of replicates = 1, 2,….,n; j =1, 2,…,k.

c) Nominal-the- Better

$$\frac{S}{N}\text{ratio} = 10\log\left(\frac{\bar{y}^2}{s^2}\right)$$

Where,

$$\bar{y} = \frac{y_1 + y_2 + y_3 \ldots\ldots\ldots\ldots\ldots + y_n}{n}$$

and

$$s^2 = \frac{\sum(y_i - \bar{y})^2}{n-1}$$

A nominal-the-best type of problem is one where minimization of the mean squared error around a specific target value is desired.

In the present study, surface microhardness and diffusion layer thickness needs to be maximized hence the "higher the better" type responses are selected.

A statistical analysis of variance (ANOVA) can be performed to determine the effect of process parameters on the performance measure. The optimum conditions can be found out by observing the minimum or maximum points for the performance measures from S/N plots. The optimum conditions identified through the analysis are required to be confirmed by confirmation experiments. The response variable fitted using a polynomial quadratic equation to correlate each response variable to the independent input parameters. The mathematical model of each response is generated and described in the form of second-order non-linear Eq. as below

$$Y = \beta_o + \sum_{i=1}^{n} \beta_i X_i + \sum_{i=1}^{n} \beta_i X_{ii}^2 + \sum_{i=1}^{n} \beta_i \, j \, X_i \sum_{i=1}^{n} \beta_i X_i \, X_j$$

Where Y is the corresponding response; X_i is the input parameter; X_{ii}^2 and $X_iX_j$are the squares and interaction terms of these input parameters; β_o, β_i, β_{ij}, and β_{ii} are the regression coefficients of parameters. The analyses were made using three-dimensional response surface plots constructed for each polynomial equation with Minitab-16 software (Minitab, Inc.). After achieving the optimum conditions for performance measures, the final step is to verify the performance at optimum conditions. After predicting the performance measures at optimum conditions, comparisons can be made with the experimental value of performance measures to check the percentage improvement in performance measures.

5.3.3. Scheme of Experimentation using Taguchi's Methodology

As per Taguchi's experimental design philosophy, a set of 3 levels assigned to each process parameter has 2 degrees of freedom (DOF). This gives a total of 9 DOF for 3 process parameters selected in this work. Thus a total of 8 DOF for the factors

and interaction between the selected parameters has not been considered for the present experiments. The nearest 3 levels orthogonal array available satisfying the criterion of selecting the OA is L-9 having 8 DOF. For each trial in the L-9 array, the levels of the process parameters are indicated in Table 5.2. The objective was to study the effects of some of the main parameters of the developed process on the quality characteristics with minimum experimentation.

Table 5.2.The L_9 (3^3) OA (parameters assigned) with response

Exp. No.	Run Order	Diffusion Time (h)	Diffusion Temp. (°C)	Diffusion Thickness (µm)		Micro-hardness (Hv)	
				Mean	S/N ratio	Mean	S/N ratio
1	2	1.0	750	5.0	13.98	372.75	50.88
2	6	1.0	850	35.0	30.88	905.25	58.59
3	7	1.0	950	43.3	32.74	692.25	56.26
4	1	1.5	750	9.0	19.08	532.50	53.98
5	5	1.5	850	78.3	37.88	1251.375	61.40
6	9	1.5	950	64.3	36.17	1027.725	59.69
7	3	2.0	750	61.7	35.80	985.125	59.32
8	4	2.0	850	98.3	39.85	1570.875	63.38
9	8	2.0	950	76.7	37.69	1224.75	61.21

Taguchi parametric design methodology was adopted and the experimentation has been planned using standard L-9 OA. Three input parameters (Diffusion time, Diffusion temperature and size of c-BN powder) were studied at five levels. These three were selected on the basis of literature review. Out of these three diffusion time and temperature were having significant effect on diffusion layer thickness and micro hardness as output parameters. Diffusion time was selected as ½, 1, 2, 3 and 5 hours, and diffusion temperature was selected as 550^o C to 950^o C in the range of 100^o C. Third input parameter was chosen as size of c-BN 5 µm and 50 µm. Which is proven to be non-significant in case of 50 µm as no diffusion was observed at this size. The main effects were plotted to know the effect of various parameters on the selected

quality characteristics. The selected parameters were optimized based on the maximum S/N ratio approach. Confirmation experiments were conducted for optimal quality characteristics. After gathering the experimental data results based on the orthogonal array (OA) L-9 runs, analysis has been carried out using the MINITAB-16 software. During the analysis, the Signal-to-Noise ratio (S/N ratio) was tabulated, main effect plots were extracted to reveal the effect of various input parameters on surface characteristics. The analysis of variance (ANOVA) has been carried out to determine the significant parameters and percentage contribution of each towards achieving output response.

5.3.4. Effect of Process Parameters on the Diffusion layer

The observed average of means and S/N ratios for the diffusion layer obtained after experimentation is shown in Table 5.3. The effect of time (h) and the temperature has been studied on diffusion layer thickness (DLT) by observing the mean and S/N ratios plots. The Higher-the-better type criterion was selected for analyzing the effect of input parameters on DLT. The average value of mean (raw data) and S/N ratio for DLT at different levels of input parameters are depicted in Table 5.4 and Table 5.5 respectively.

Table 5.3.The L_9 (3^3) OA (parameters assigned) with response DLT

Exp. No.	Run Order	Diffusion Time (h)	Diffusion Temp. (°C)	Diffusion layer Thickness (µm)	
				Mean	S/N ratio
1	2	1.0	750	5.0	13.98
2	6	1.0	850	35.0	30.88
3	7	1.0	950	43.3	32.74
4	1	1.5	750	9.0	19.08
5	5	1.5	850	78.3	37.88
6	9	1.5	950	64.3	36.17
7	3	2.0	750	61.7	35.80
8	4	2.0	850	98.3	39.85
9	8	2.0	950	76.7	37.69

Table 5.4. Response table for means of DLT

Level	**Diffusion Time (h)**	**Diffusion Temp. (ºC)**
1	27.78	25.22
2	50.56	70.56
3	78.89	61.44
Delta	51.11	45.33
Rank	2	1

Table 5.5. Response table for S/N ratio of DLT

Level	**Diffusion Time (h)**	**Diffusion Temp. (ºC)**
1	25.87	22.96
2	31.04	36.2
3	37.78	35.53
Delta	11.92	13.25
Rank	2	1

The DLT is dependent on energy and the microstructural change undergone by the workpiece during the diffusion process. In the diffusion process, the energy transfer is a function of the amount of heat supplied by time and temperature.

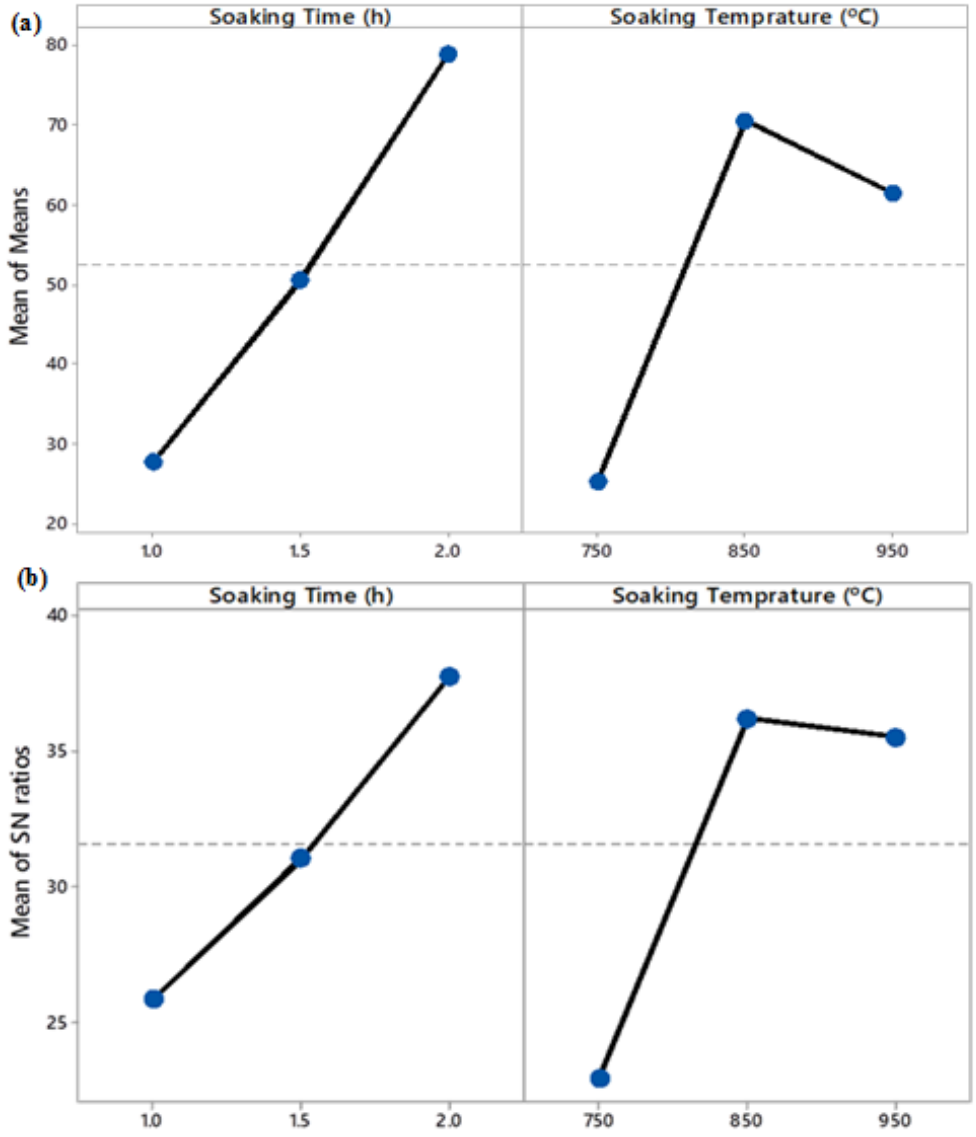

Fig. 5.12. (a) Mean and (b) S/N ration Plot of DLT with respect to input process parameters

Fig. 5.12(a) and (b) shows the average of raw data and S/N ratios for DLT at various levels of input process parameters. It has been observed that the DLT increased with the increase in diffusion time (h). The response trend of mean and S/N ratios is matching with each other. At low soaking time 1 h, the average DLT is low because the steel surface does not reach to the re-crystallization stage, which resists the diffusion of c-BN particles. However, the DLT is high at soaking time 2 h. This is attributed because, at the higher soaking time, the steel surface absorbs more c-BN

particles because at this steel surface reached to re-crystallization stage. On the other hand, the DLT first increased with the increase in diffusion temperature (ºC) up to 850 ºC temperature and then start decreased if diffusion temperature increased further. At 850 ºC, the D2 steel undergone through the re-crystallization phase and get soften owing to that c-BN particles were reinforced into the substrate surface up to few microns. At 950 ºC, the D2 steel undergone through shape change and failed the geometric configuration of the sample.

At 750 ºC of soaking temperature and 1 hour of soaking time, a very small diffusion layer was observed. The diffusion layer was measured up to 5 μm thick. At 850 ºC of soaking temperature and 1 hour of soaking time, a very thick diffusion layer was obtained. The diffusion layer was measured up to 35 μm thick. At950 ºC of soaking temperature and 1 hour of soaking time, a very thick diffusion layer was obtained, but the sample gets oxidized and changes its shape and profile. The diffusion layer was measured up to 43 μm thick. When the soaking time increased, the diffusion thickness increased. Still, small diffusion was observed at 750 ºC of soaking temperature and 1.5 hours. The diffusion layer was measured up to 9 μm thick. At850 ºC of soaking temperature and 1.5 hours of soaking time, a very thick diffusion layer was obtained. The diffusion layer was measured up to 78 μm thick. The best optical condition for the high diffusion layer is the high soaking temperature (2 h) and moderate soaking temperature (850 ºC).

Fig. 5.13(a) and (b) represents contour plot and 3D surface plot for DLT with respect to soaking time and soking temprature. The DLT increased with soaking time and have liner relation. The DLT has long-linear behavior with soaking temprature. Further, to investigate the significance of each input parameter ANOVA has been performed. Table 5.6 represents the analysis of variance for surface roughness.

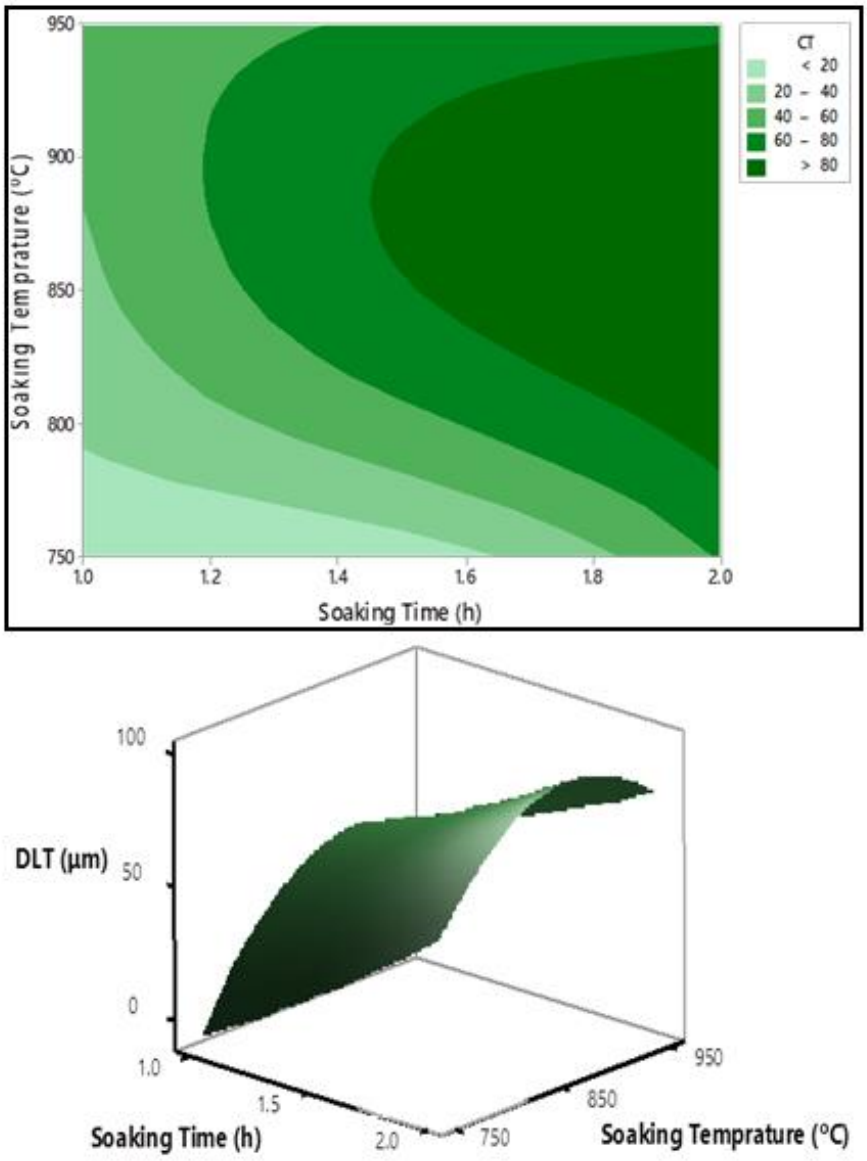

Fig. 5.13. (a) Contour plot and (b) 3D surface plot of DLT with respect to shocking time and temperature

The table depicts the factors, degree of freedom (DOF), sequential sum square error (Seq SS), adjusted sum square error (Adj SS), adjusted mean square error (Adj MS), F statistic, p-values, and percentage contribution (%) in columns. The p-value of lack of fit should be less than 0.05 for significant parameters, and certainly indicate that there is a statistically insignificant lack of fit at 95% confidence level. However, the p-value of the regression model and it's all terms have a p-value less than 0.05, hence they are statistically significant at 95% confidence, and thus the model

adequately represents the experimental data. From the ANOVA analysis, it has been observed that all the input process parameters have a significant contribution toward the DLT. Soaking time is a highly significant parameter with a 48.40% contribution. The soaking temperature has 42.52 contributions. The percentage contribution of error is 9% only.

Table 5.6. Analysis of variance of DLT

Factors	DOF	Seq SS	Adj MS	F	P	%
Soaking Time (h)	2	3934	1967	10.77	0.025	48.40*
Soaking temperature (°C)	2	3450.2	1725.1	9.44	0.031	42.52*
Residual Error	4	730.7	182.7			9.00
Total	8	8114.8				
***Significant Terms**						

5.3.5. Effect of Input Process parameters on micro-hardness

The observed average of means and S/N ratios for micro-hardness (H_μ) obtained after experimentation is shown in Table 5.7. The effect of time (h) and the temperature has been studied on H_μ by observing the mean and S/N ratios plots. The Higher-the-better type criterion was selected for analyzing the effect of input parameters on H_μ. The average value of mean (raw data) and S/N ratio for H_μ at different levels of input parameters are depicted in Table 5.8 and Table 5.9 respectively.

Table 5.7.The L_9 (3^3) OA (parameters assigned) with response Micro-hardness

Exp. No.	Run Order	Diffusion Time (h)	Diffusion Temp. (ºC)	Micro-hardness (H_μ)	
				Mean	S/N ratio
1	2	1.0	750	372.75	50.88
2	6	1.0	850	905.25	58.59
3	7	1.0	950	692.25	56.26
4	1	1.5	750	532.5	53.98
5	5	1.5	850	1251.375	61.40
6	9	1.5	950	1027.725	59.69
7	3	2.0	750	985.125	59.32
8	4	2.0	850	1570.875	63.38
9	8	2.0	950	1224.75	61.21

Table 5.8. Response table for means of H_μ

Level	Diffusion Time (h)	Diffusion Temp. (ºC)
1	616.7	591.7
2	880	1166.7
3	1183.3	921.7
Delta	566.7	575
Rank	2	1

Table 5.9.Response table for S/N ratio of H_μ

Level	Diffusion Time (h)	Diffusion Temp. (ºC)
1	55.24	54.73
2	58.36	61.12
3	61.3	59.05
Delta	6.06	6.39
Rank	2	1

The micro-hardness (H_μ) is dependent on microstructural change undergone by the work piece during the diffusion process. In the diffusion process, the microstructural changes depend upon the input heat energy transfer is a function of time and temperature. Fig. 5.14(a) and (b) shows the average of raw data and S/N ratios for H_μ at various levels of input process parameters. It has been observed that the H_μ increased with the increase in diffusion time (h). The response trend of mean and S/N ratios is matching with each other. At low soaking time 1 hour, the average DLT is low because the steel surface does not reach to the re-crystallization stage, which resists the diffusion of c-BN particles. So that hardness of the obtained surface was low. However, the H_μ is high at soaking time 2 hours. This is attributed because, at the higher soaking time, the steel surface absorbs more c-BN particles because at this steel surface reached the re-crystallization stage. Due to diffusion, the surface becomes more brittle and harder. On the other hand, the H_μ first increased with the increase in diffusion temperature (ºC) up to 850 ºC temperature and then start decreased if diffusion temperature increased further. At 850 ºC, the D2 steel undergone through the re-crystallization phase and get soften owing to that c-BN particles were reinforced into the substrate surface up to few microns. As a result surface hardness increased. At 950 ºC, the D2 steel undergone through shape change and failed the geometric configuration of the sample. As a result surface hardness decreased.

At 750 ºC of soaking temperature and 1 hour of soaking time, a very small diffusion layer was observed as a result no significant increase in the microhardness (H_μ) was observed. The $H_\mu$was measured around 350 HV.

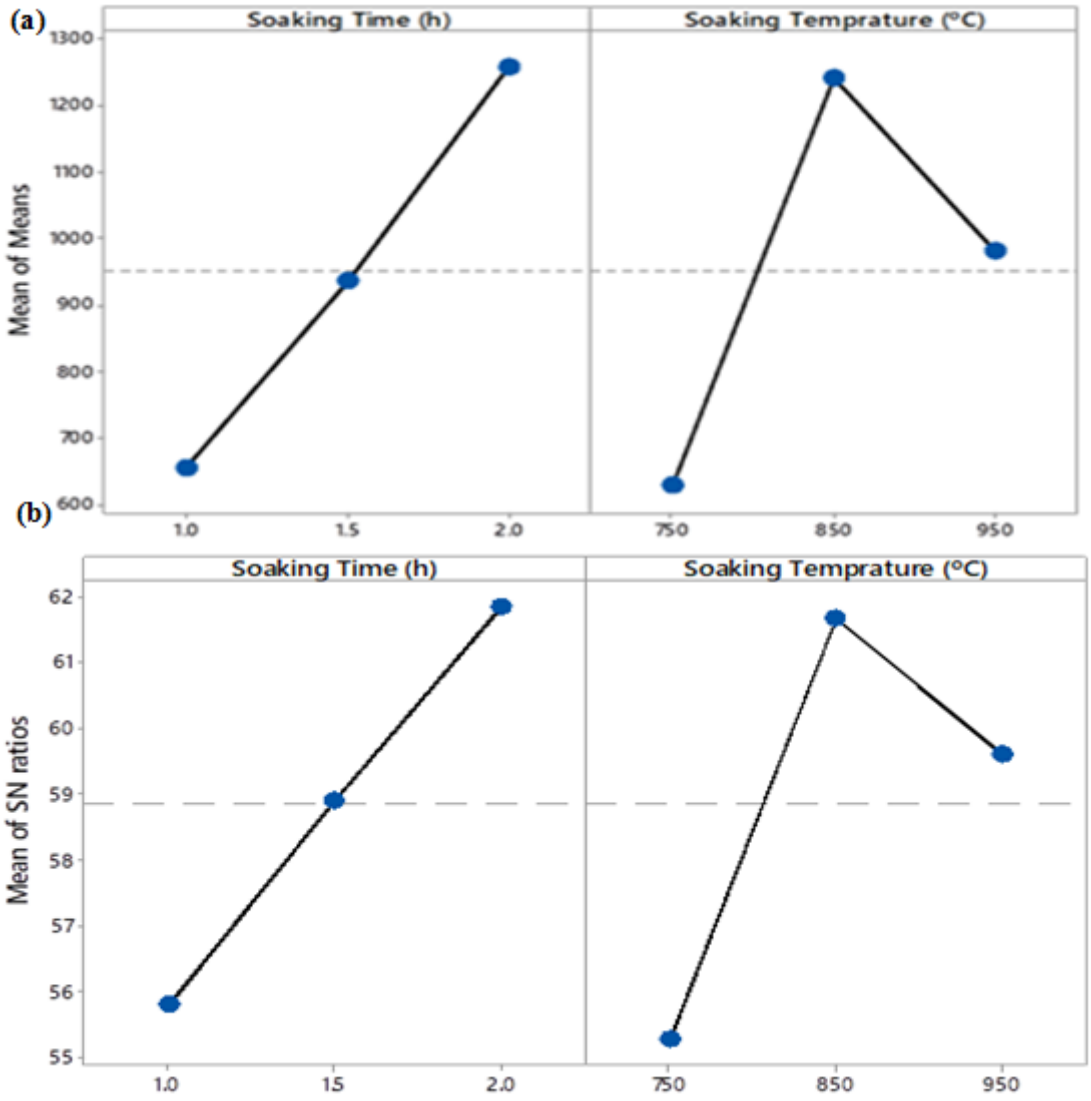

Fig. 5.14. (a) Mean and (b) S/N ratio Plot of H_{μ} with respect to input process parameters

At 850 ºC of soaking temperature and 1 hour of soaking time, a thick diffusion layer was obtained, which improved the surface properties. The H_{μ} was measured around 850 HV. At 950 ºC of soaking temperature and 1 hour of soaking time, a very thick diffusion layer was obtained, but the sample gets oxidized and changes its shape and profile. As a result, mechanical properties were destroyed. The H_{μ} was measured around 650 HV. When the soaking time increased, the diffusion thickness increased, which improved the mechanical properties of the surface. Still, small diffusion was observed at 750 ºC of soaking temperature and 1.5 hours. As a result, a slight

improvement in the microhardness of the surface was measured. The $H_\mu$was measured around 500 HV. At850 ºC of soaking temperature and 1.5 hours of soaking time, a very thick diffusion layer was obtained and the surface became very hard and brittle. The H_μ was measured around 1475 HV. The best optical condition for high surface hardness is the high soaking temperature (2 h) and moderate soaking temperature (850 ºC).

Fig. 5.15 (a) and (b) represents contour plot and 3D surface plot for H_μ with respect to soaking time and soking temprature. The H_μ increased with soaking time and have a linear relation. The H_μ has lon-linear behavior with soaking temprature. Further, to investigate the significance of each input parameter ANOVA has been performed. Table 5.10 represents the analysis of variance for surface roughness. The table depicts the factors, degree of freedom (DOF), sequential sum square error (Seq SS), adjusted sum square error (Adj SS), adjusted mean square error (Adj MS), F statistic, p-values, and percentage contribution (%) in columns. The p-value of lack of fit should be less than 0.05 for significant parameters, and certainly indicate that there is a statistically insignificant lack of fit at 95% confidence level. However, the p-value of the regression model and it's all terms have a p-value less than 0.05, hence they are statistically significant at 95% confidence, and thus the model adequately represents the experimental data. From the ANOVA analysis, it has been observed that all the input process parameters have a significant contribution toward the DLT. Soaking time is a highly significant parameter with a 48.40% contribution. The soaking temperature has 42.52 contributions. The percentage contribution of error is 9% only.

Table 5.10. Analysis of variance of H_μ

Factors	DOF	Seq SS	Adj MS	F	P	%
Soaking Time (h)	2	482467	241233	51.65	0.001	48.21*
Soaking temperature (ºC)	2	499550	249775	53.48	0.001	49.92*
Residual Error	4	18683	4671			1.87
Total	8	1000700				
***Significant Terms**						

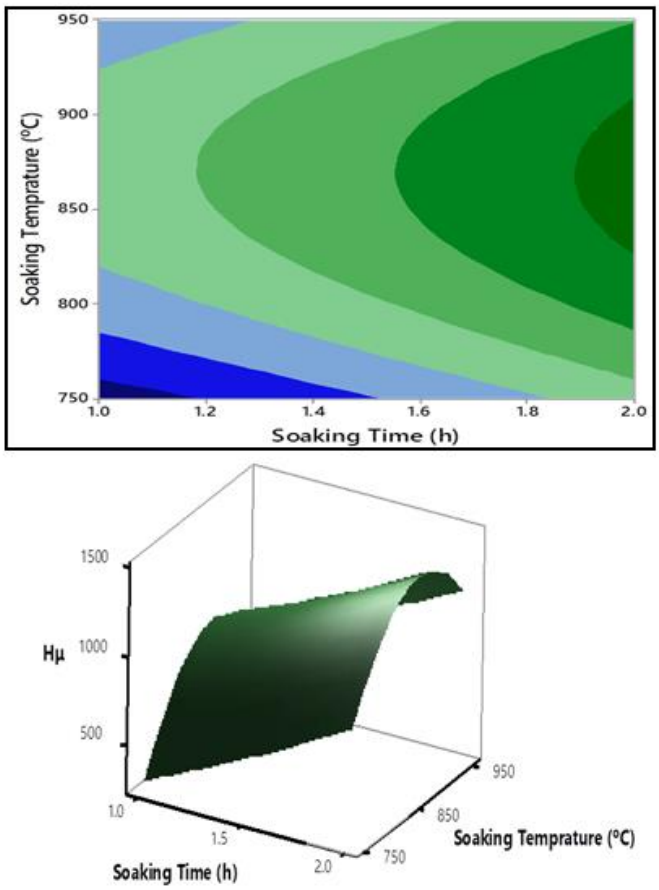

Fig. 5.15. (a) Contour plot and (b) 3D surface plot of H_μ with respect to shocking time and temperature

5.3.6. Confirmation of experiments

For the verification of optimal solutions obtained using Taguchi's methodology, confirmation test has been conducted for optimal solutions. Table 5.11 shows the optimal condition predicted for DLT and H_μ response using Taguchi's methodology and also shows the confidence interval for both response in which the optimal value should lies. Table 5.11 shows the confirmation experiments for a different factor combination. The tests were repeated three times and average values were compared with the predicted solutions.

Table 5.11. Confirmation test

Soaking Time (h)	Soakig Temp (ºC)	Predicted		Confirmation		% Error	
		DLT (µm)	H_μ (HV)	DLT (µm)	H_μ (HV)	DLT (µm)	H_μ (HV)
2	750	97	1551	98	1575	1.02	1.54
1	850	38	947.85	35	905	857	4.64

5.4. Microstructure analysis

Fig.5.16 shows the SEM-micrograph of microstructure of the diffused layer and substrate surface. Form the SEM micrograph, a clear picture of diffused c-BN was observed on the D2-steel surface.

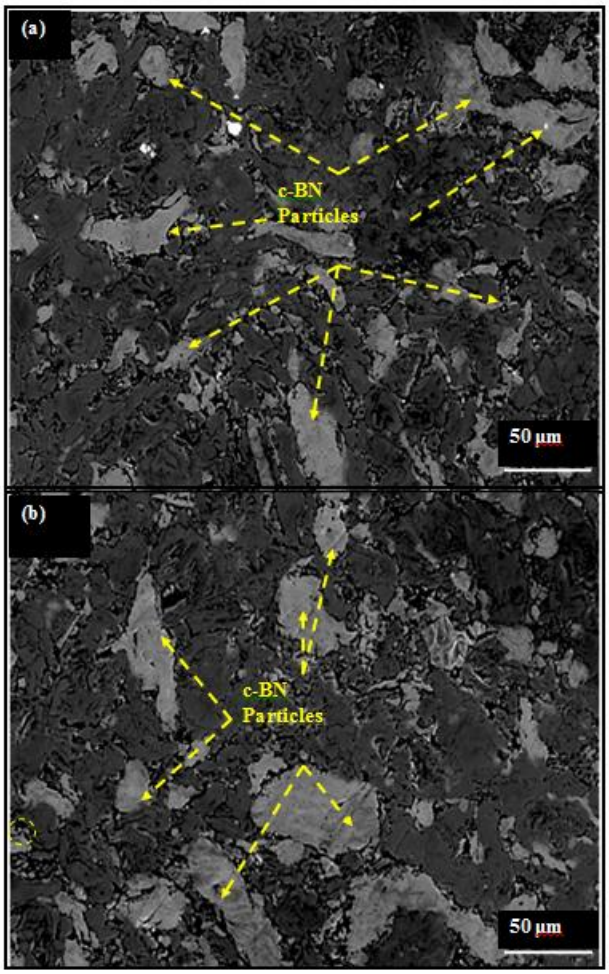

Fig. 5.16. SEM micrograph of diffused top surface at (a) 750 ºC for 2 hours (b) 850 ºC for 1 hour

The diffused c-BN can be identified with bright grey color and the dark portion was identified as a substrate surface. Grain boundaries of c-BN diffused particles were clearly seen. It can be seen that the c-BN particles were agglomerated and appeared in the matrix if D2 steel in the size of 10 μm to 50 μm. Yellow color arrows highlighted the diffusion of c-BN. From Fig. 5.16(a) and (b) it was found that the distribution of c-BN was higher in the samples prepared at 850 ºC for 1 hour. From the microstructure examination, it can be seen that a highly dense surface was obtained. Due to grain size difference between D2 steel and c-BN particles, during solidification, re-crystallization takes place and c-BN diffused in the D2-steel matrix.

Fig.5.17 shows the cross-section micrograph of the diffused layer. Form both samples micrograph, a clear picture of the diffusion zone, thickness, and the interface was identified. It is evident from Fig. 5.17 (a) that as-prepared surface composite prepared at 750 ºC for 2 hours comprised of unevenly distributed micro-cracks and micro-holes of different sizes. The c-BN particles were diffused in D2 steel substrate up to 50 μm depth at operating condition of at 750 ºC for 2 hours. It is evident from Fig. 5.17 (b) that the as-prepared layer at 850 ºC for 1 hour comparatively thicker zone. The c-BN particles were diffused in D2 steel substrate up to 90 μm depth at operating condition of at 850 ºC for 1 hour. At higher temperatures, the D2 steel surface becomes soft and this allows c-BN to diffuse deeper in the layer. The c-BN particles in layer can be clearly seen in the cross-section micrograph, which conferred and confirmed the diffusion of c-BN particles.

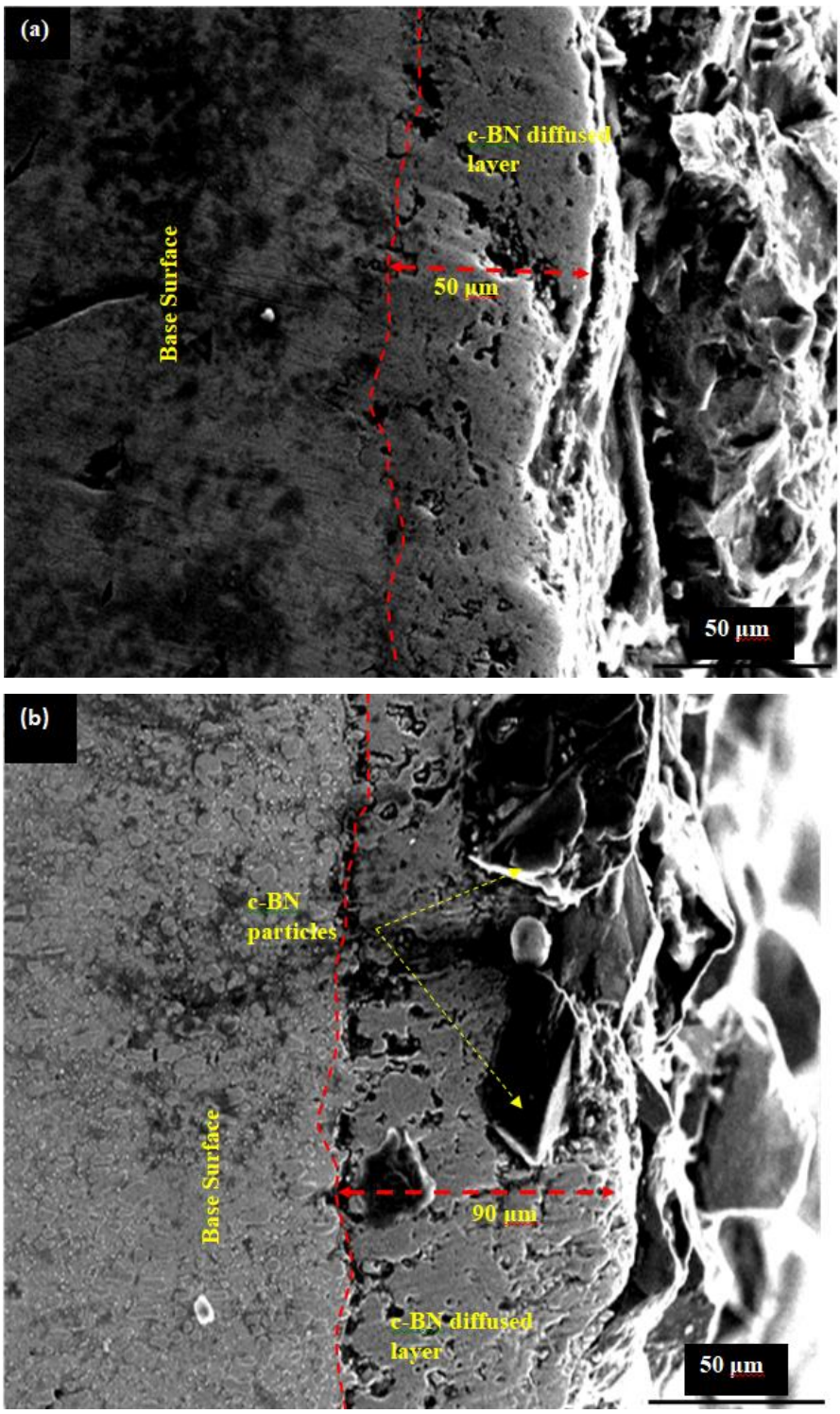

Fig.5.17. Cross-section SEM micrograph of diffused layer at (a) 750 ºC for 2 hours and (b) 850 ºC for 1 hour

Fig. 5.18 and 5.19 show the EDS analysis of the diffused layer of c-BN at 750 ºC for 2 hours and 850 ºC for 1 hour, respectively. The EDS spectrum of substrate confirms that major substrate elements (Fe, C) are present in the peaks.

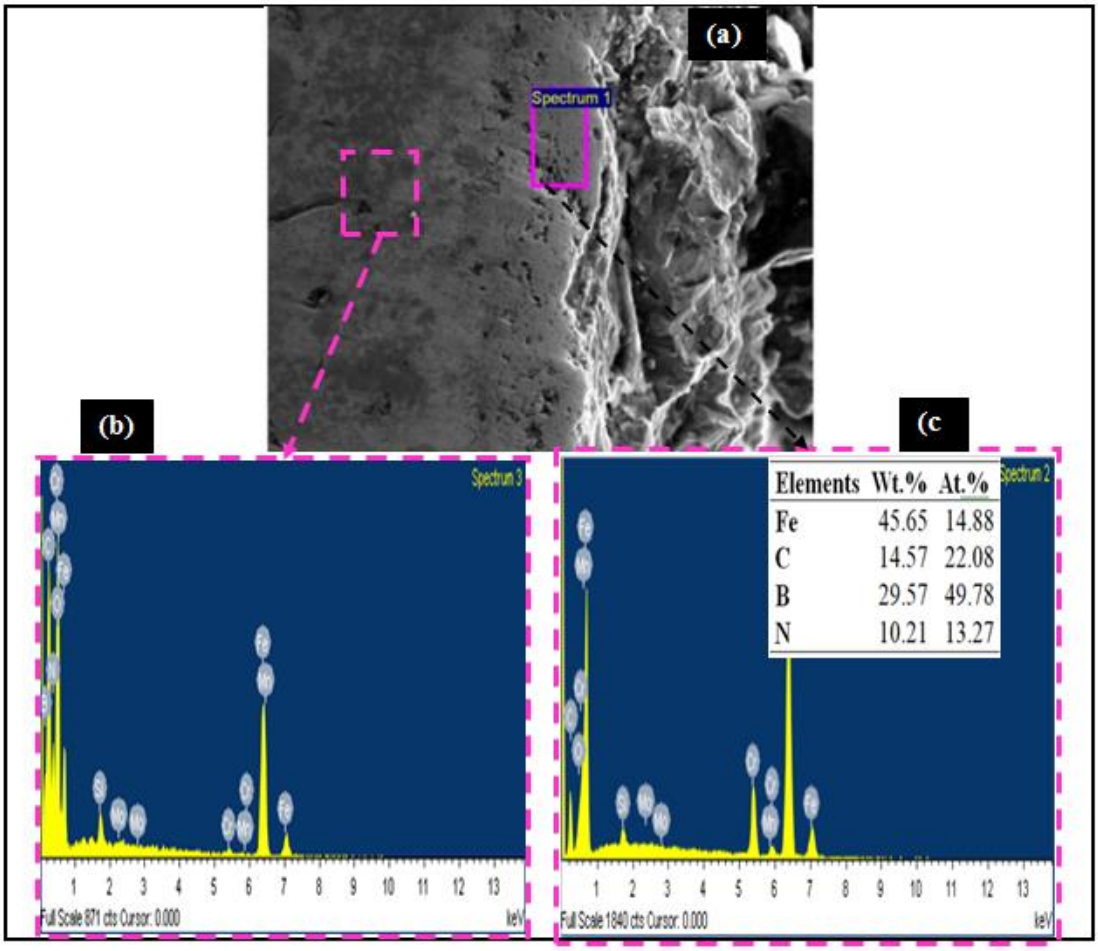

Fig. 5.18.EDS spectrum of the EDS spectrum of c-BN layer at 750 ºC for 2 hours

On the other hand, the EDS spectrum of c-BN particles shows the increase of elements such as boron and nitride, which confirmed that only high purity c-BN were reinforced. At750 ºC for 2 hours, the elemental wt. % of C, B, N, and Fe was 14.57, 29.57, 10.21, and 45.65%. The intensity of c-BN diffusion increased with temperature; refer Fig. 5.15. At850 ºC for 1 hour, the elemental wt. % of C, B, N, and Fe was 18.15, 35.65, 14.54, and 31.66%; refer Fig. 5.17.

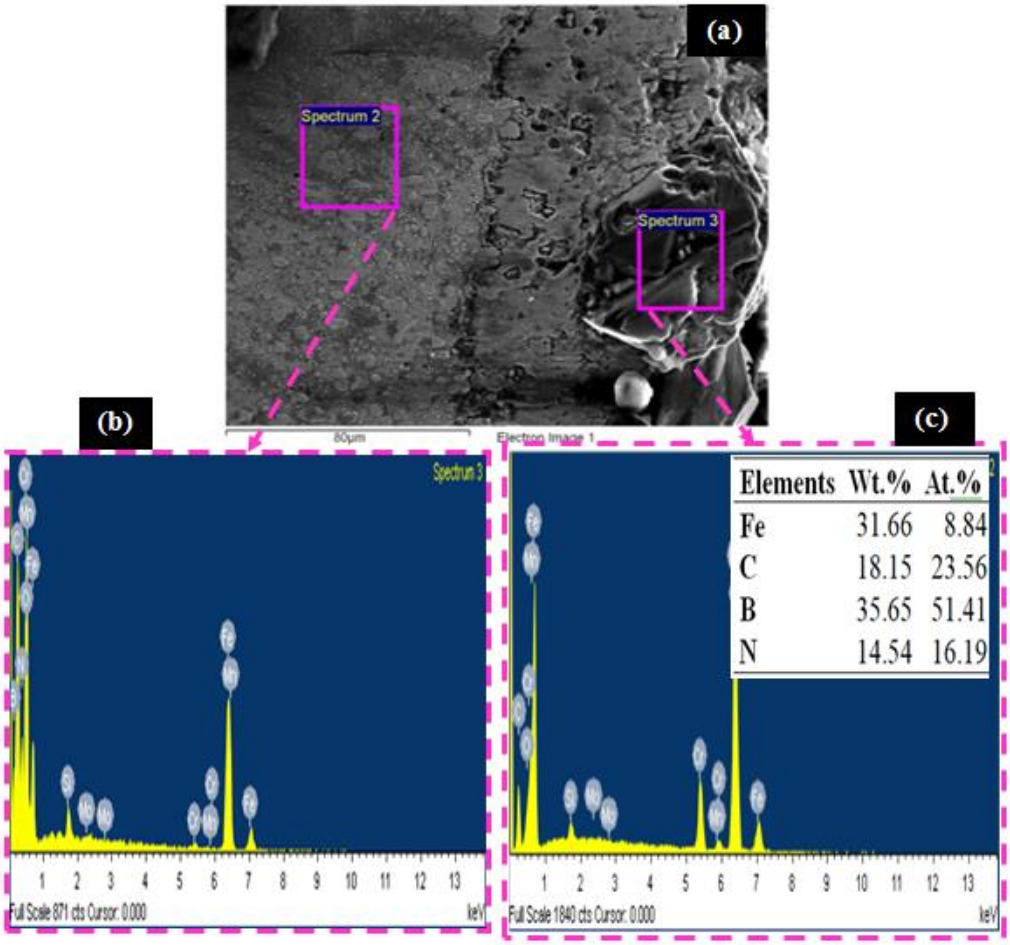

Fig. 5.19.EDS spectrum of the EDS spectrum of c-BN layer at 850 ºC for 1 hours

Fig. 5.20 (a) shows the EDS line scan along the c-BN diffused layer developed at 850 ºC for 1 hour and (b) shows the EDS line scan along the c-BN diffused layer developed at 750 ºC for 2 hours . From the line scan it can be seen that base elements of D2-steel such as iron (Fe) was uniformly form the top to bottom. But, distribution of c-BN particles can be seen only in the region of diffused layer only.

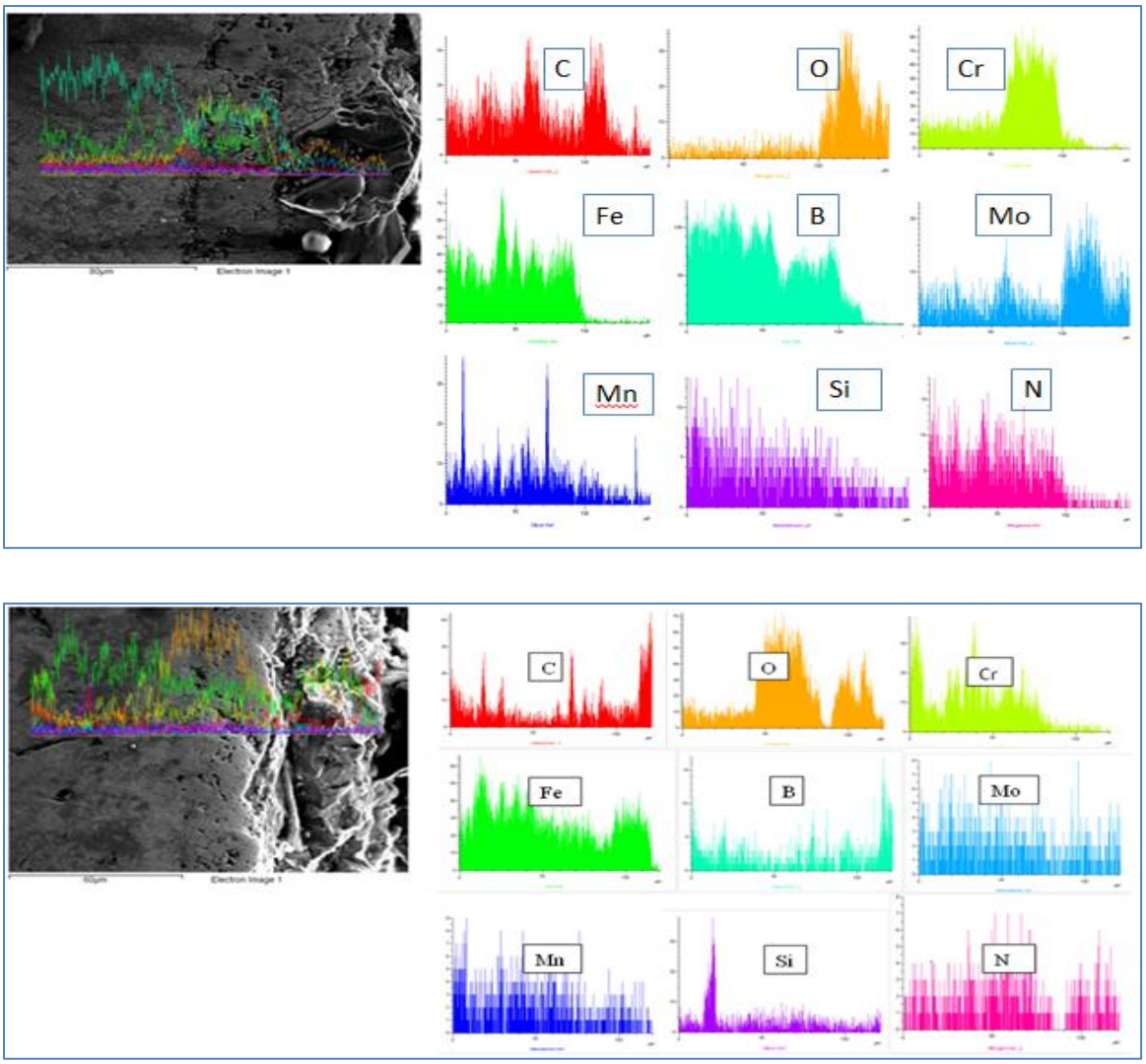

Fig. 5.20. (a) EDS line scan of c-BN diffused layer developed at 850 ºC for 1 hour and (b) EDS line scan of c-BN diffused layer developed at 750 ºC for 2 hours

5.5. Micro-hardness analysis

Fig. 5.21 shows the variation of surface micro-hardness across the diffused c-BN layer. From the obtained results, it can be seen that the hardness of composite samples was improved considerably as compared to raw samples. The average of five readings was taken, and the mean hardness was determined.

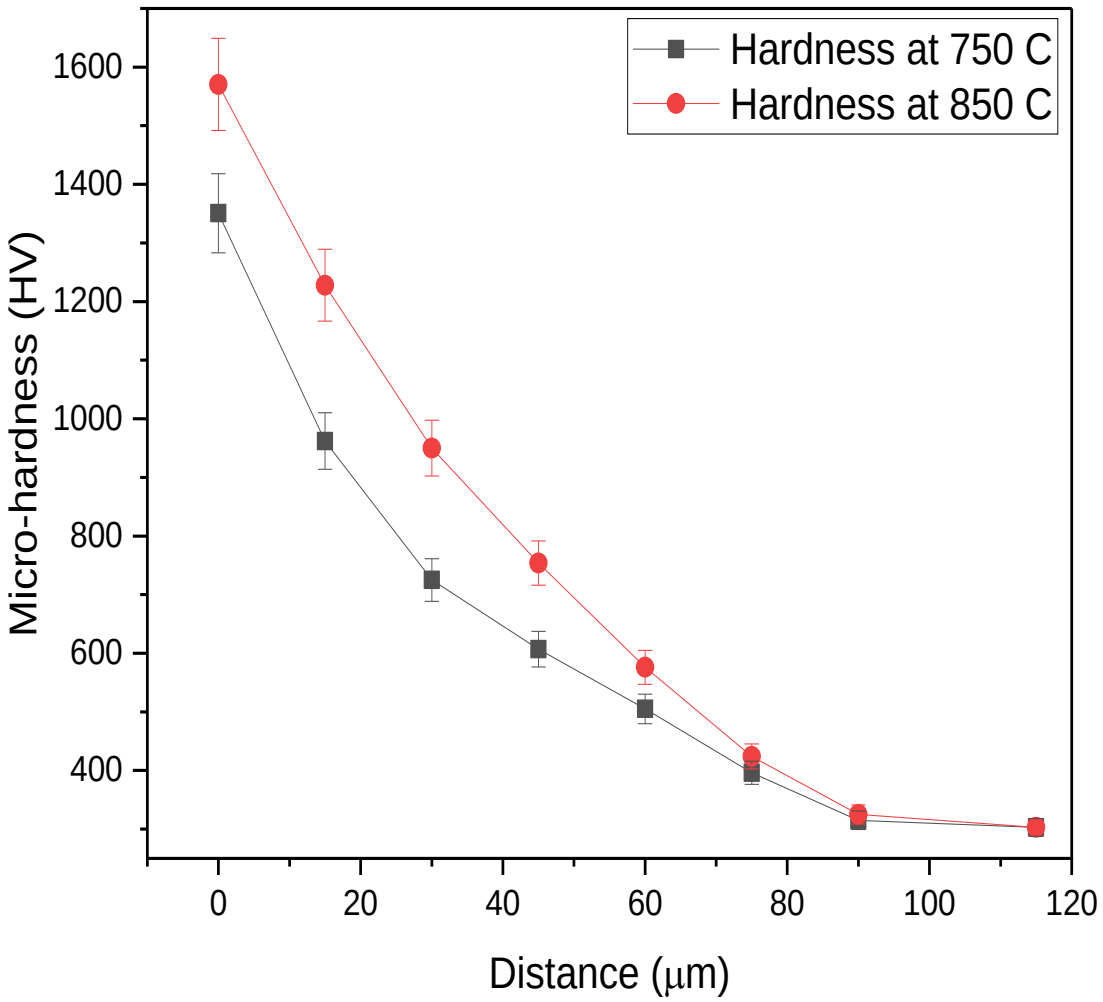

Fig. 5.21. Micro-hardness versus the distance away from the top surface to substrate

Fig. 5.22 shows the indent image on the un-treated, D2-steel work peice surface. The micro-hardness for un-treated work peice was measured around 303 HV; refer Fig. 5.22 (a). The c-BN-reinforced layer developed at 850 ºC for 1 hour was 1570 HV, which is 418.2% higher as compared to raw samples hardness 303 HV; refer Fig. 5.22 (b).

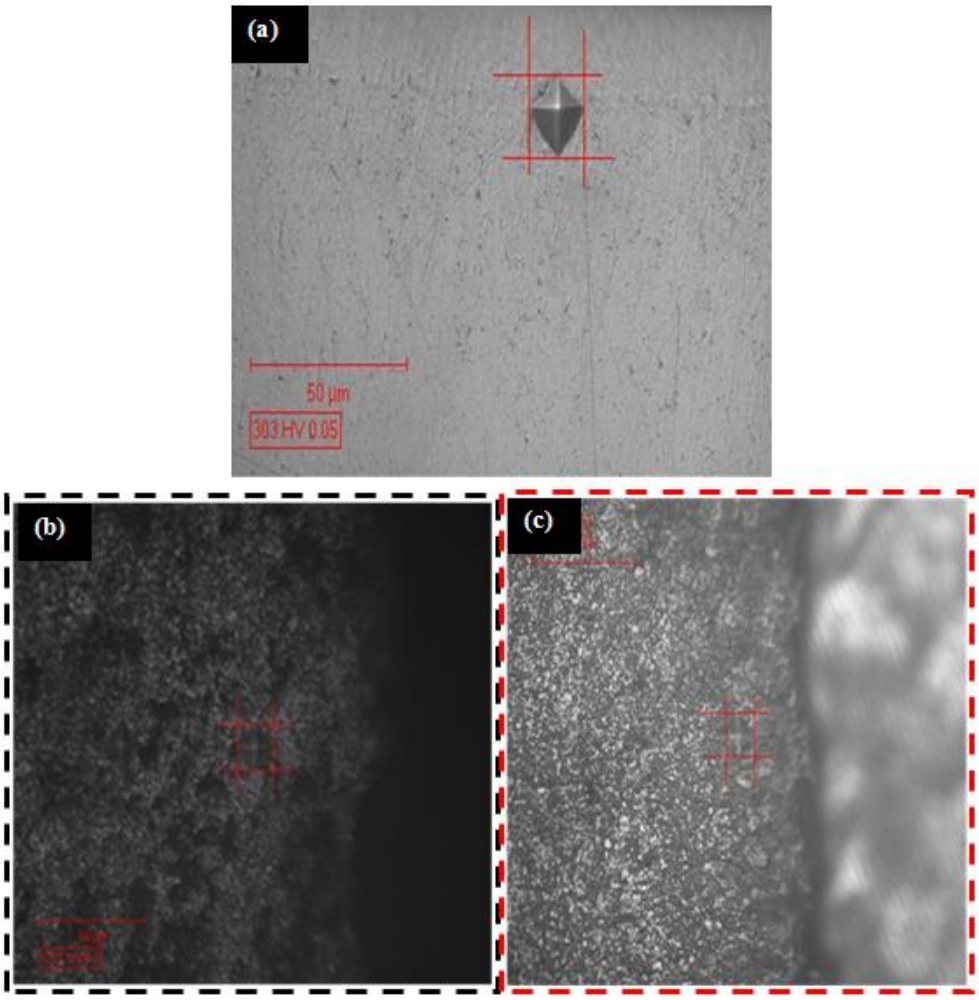

Fig. 5.22. Micro-hardness of (a) un-treated surface, (b) samples at 750 ºC for 2 hours, and (c) samples at 850 ºC for 1 hour

When samples were prepared at 850 ºC for 2 hours, the hardness decreased because the sample loosed its dimensions accuracy and started to dilate. The mean hardness of c-BN-reinforced surface composite developed at 750 ºC for 2 hours was measured around 1350 HV, which was 345.54% higher as compared to the untreated sample (303 HV); refer Fig. 5.22 (c). This is because the top surface of the as-developed surface comprised c-BN hard particles, which enhanced the surface properties of the D2 steel surface. Similarly, in the case of diffusion of c-BN at 750 ºC for 3 hours, the samples loosed its dimensions accuracy and started to dilate. This is because the top surface of the as-developed surface contains c-BN hard particles, un-melted particles, and structural porosity; thus, results in low surface hardness.

5.6. Wear resistance

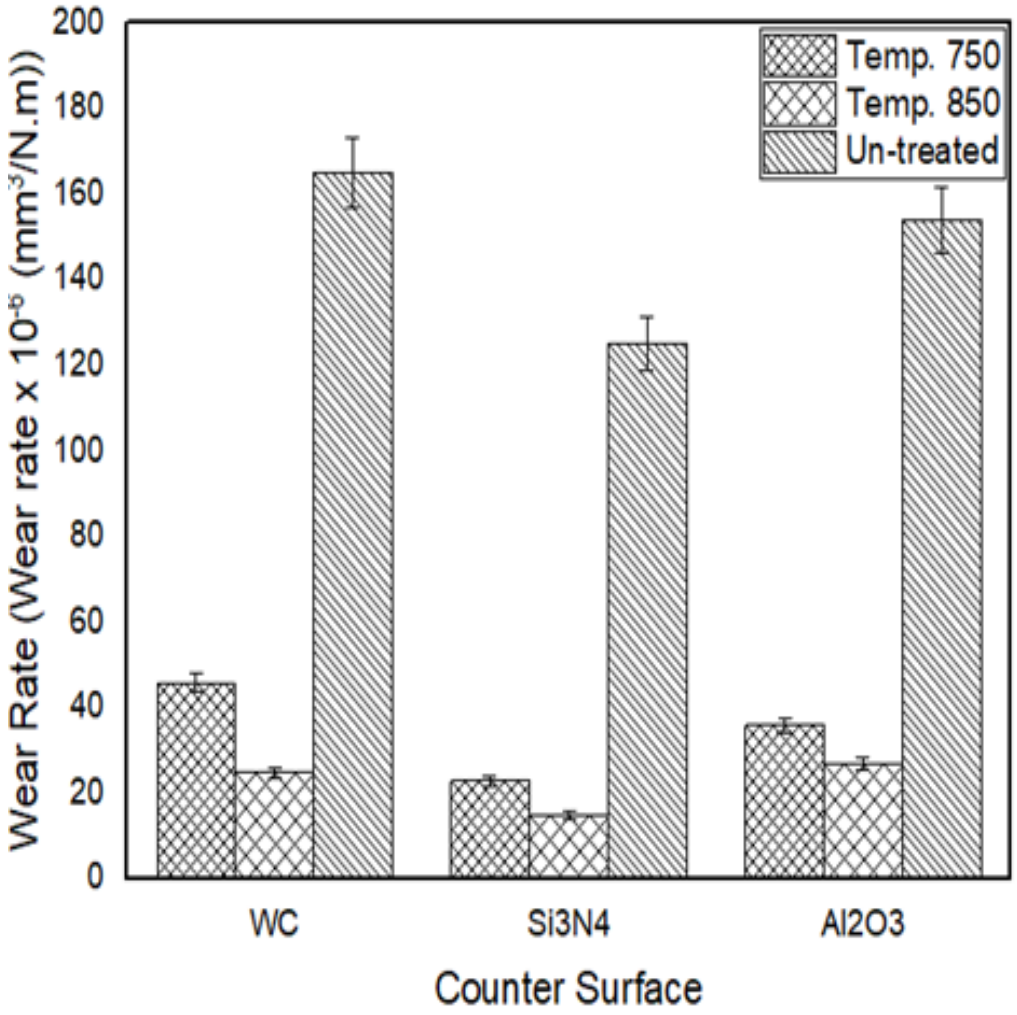

Fig. 5.23.Wear rate of un-treated surface, c-BN diffused samples at 750 ºC for 2 hours, and 850 ºC for 1 hour against WC, Si_3N_4, and Al_2O_3 counter surface

The wear resistance of the untreated surface and c-BN diffused samples was determined in terms of wear rate and coefficient friction. Fig.5.23 and Fig. 5.24 shows the wear rate and average coefficient of friction of un-treated surface and c-BN diffused samples at 750 ºC for 2 hours, and 850 ºC for 1 hour against WC, Si_3N_4, and Al_2O_3 counter surface. The WC, Si_3N_4, and Al_2O_3 counter-surface have the hardness in the range of 2700 HV, 1600-2000 HV, and 1700-2200 HV, respectively. Fig. 5.21 shows the wear rate. It can be seen that all samples showed higher wear against the

WC counter surface and lower wear rate against the Si_3N_4 counter surface. This is because Si_3N_4 provides sufficient lubrication and results in less friction [37].

Un-treated samples have the highest wear rate in comparison to c-BN diffused samples. This is because an untreated specimen has a low surface hardness and deteriorates faster at the contact with the more robust surface of counter surfaces. There was noted that the untreated samples have the highest wear rate against the WC counter surface. The sample prepared at 850 ºC for 1 hour demonstrated the lowest wear rate because of its higher surface hardness. Generally, the c-BN may have a better surface resistance to abrasion [37].Fig.5.24 shows the coefficient of friction (COF) of sample un-treated surface and c-BN diffused samples at 750 ºC for 2 hours and 850 ºC for 1 hour against WC, Si_3N_4, and Al_2O_3 counter surface.

It can be seen in Fig. 5.24 that the un-treated samples have the highest COF against the Si_3N_4 counter surface and COF against the WC counter surface. The c-BN diffused samples also have similar properties such as high COF against Si_3N_4 counter surface as compared to WC and Al_2O_3. The failure has been due to fracturing and removal of c-BN particles from the surface. Yet, the c-BN particles are not physically missed but they were reinforced in the surface. Thus, they were removed against high strength surface generating accentuated wear. A similar observation was found in the literature [20, 36].

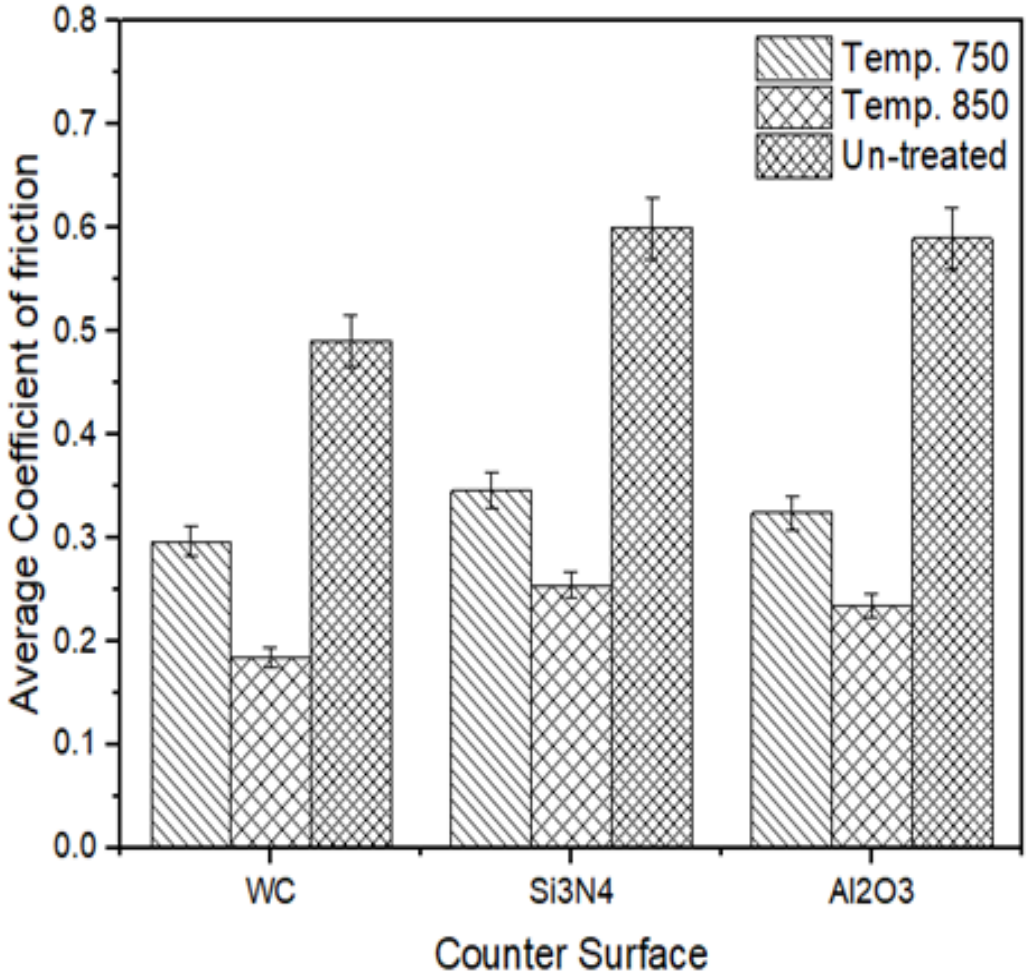

Fig. 5.24. Average COF of un-treated surface, c-BN diffused samples at 750 ºC for 2 hours, and 850 ºC for 1 hour against WC, Si_3N_4, and Al_2O_3 counter surface

Fig.5.25 and 5.26 show the SEM morphology of the worn surface of counter plates WC and un-treated sample pins. Form the SEM micrographs, it can be seen that the WC-counter surface is not worn-out against, refer Fig. 5.25. Moreover, deposition materials from the un-treated pin were observed. The un-treated pin has a low surface hardness and failed against the WC-counter tool. Ploughing and robbing of an untreated surface can be seen against the hard surface of the WC-counter tool, refer Fig. 5.26.

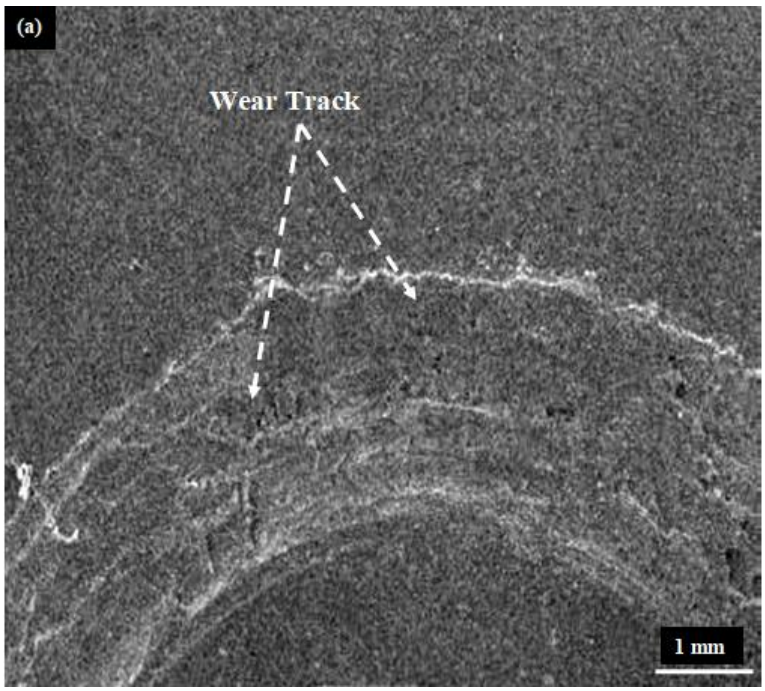

Fig. 5.25. SEM images of worn-out WC counter surface against the un-treated pin

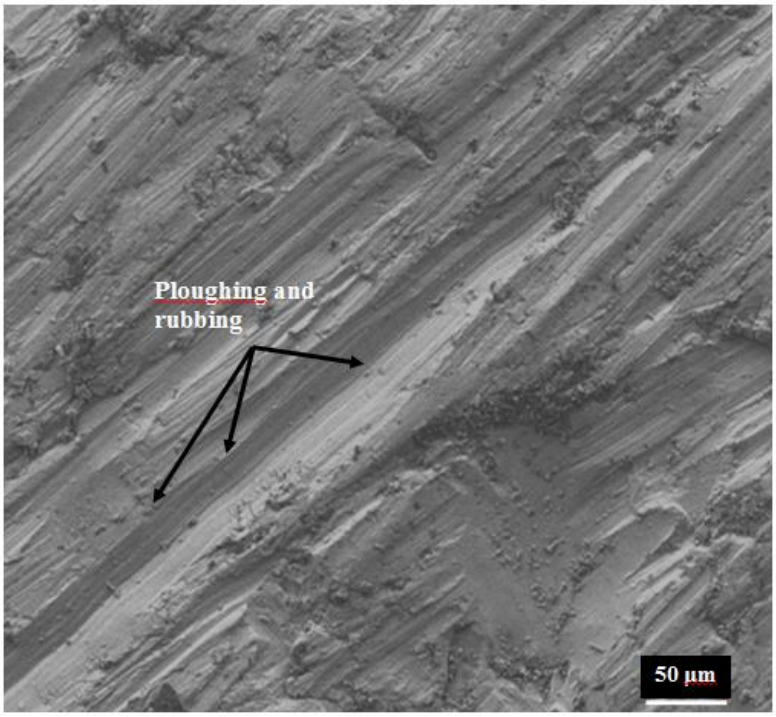

Fig. 5.26. SEM images of worn-out surface of pin against WC counter surface

Fig.5.27 and 5.28 show the SEM morphology of the worn surface of counter plates WC and un-treated sample pins. The wear track of the WC-counter surface

against the sample prepared at 750 ºC for 2 hours showed that the rubbing and disposition c-BN abraded debris, refer Fig. 5.25. This is because the sample has hardness value (1350 HV) lower as compared to WC (2700 HV). There, the c-BN particles were removed from the layer and started running against the counter surface.

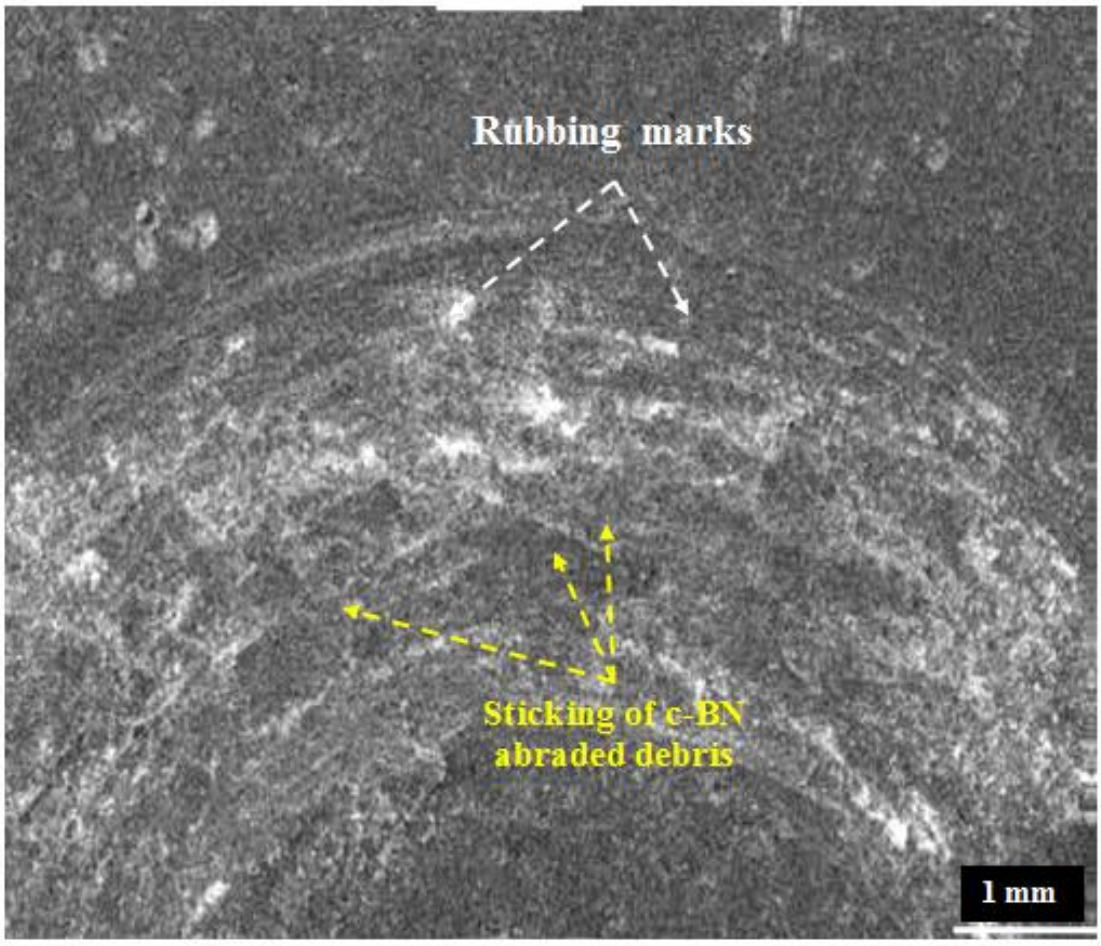

Fig. 5.27. SEM images of worn-out WC counter surface

On the other hand, craters and scratch marks were observed on the SEM image of the worn surface of pin prepared at 750 ºC, refer Fig. 5.28. Micro-sized pits were devolved on the surface and sub-moron sized debris were gathered in these micro pits, owing to the removal of c-BN particles. It can be attributed to the formation of an adherent transfer of the c-BN layer on the sample surface, probably as a result of WC oxidation. The wear resistance was increased on the pin sample prepared at 750 ºC

with almost 82.75% by diffusion of c-BN in D2 steel. This results in rubbing both surface counter and pin.

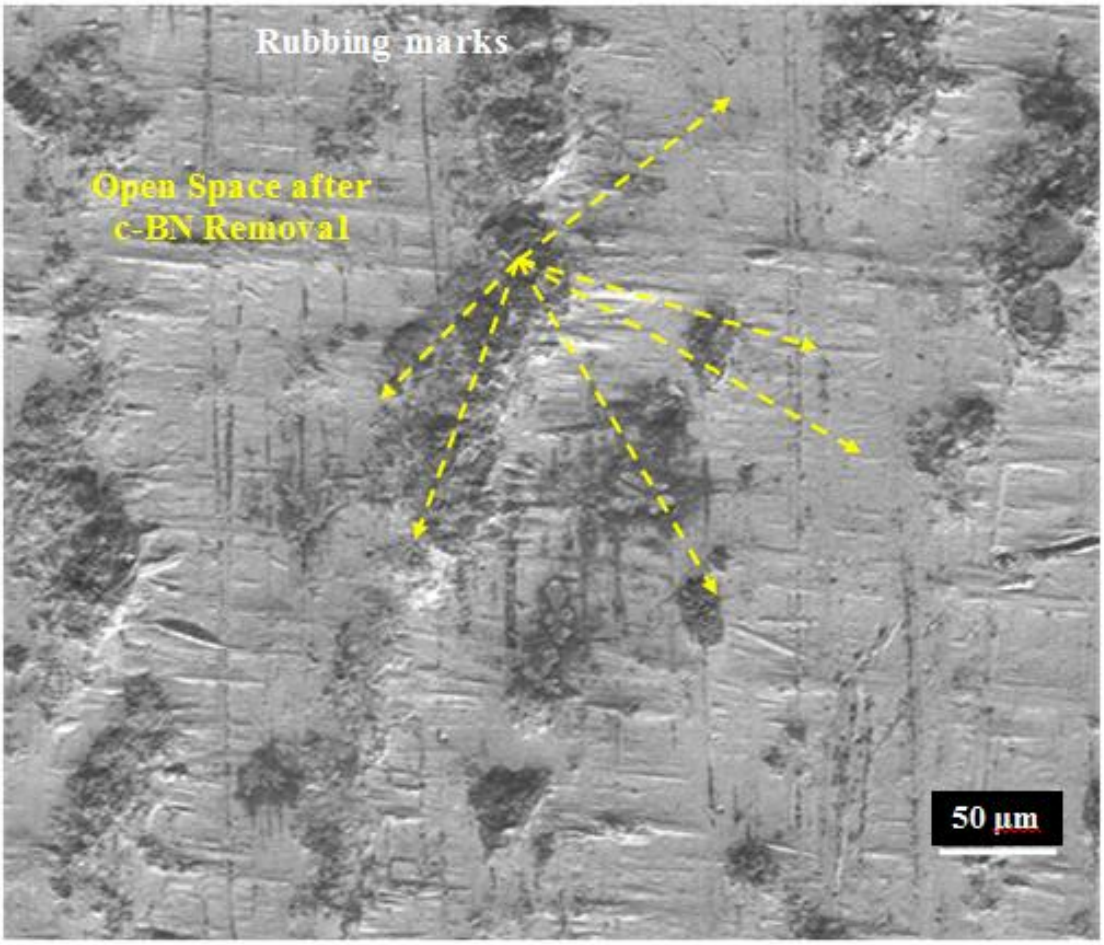

Fig. 5.28. SEM images of worn-out treated c-BN diffused pin treated at 750ºC for 2 hours

Fig. 5.29 and Fig. 5.30 show the SEM morphology of the worn surface of counter plates WC and un-treated sample pins. The wear track of WC-counter surface against sample prepared at 850 ºC for 1 hour showed slightly more rubbing and less disposition of c-BN abraded debris, refer Fig. 5.29. This is because the sample is highly dense and less amount of c-BN particles were removed from the layer and started running against the counter surface. On the other hand, comparatively fewer craters and scratch marks were seen from the SEM image of the worn surface of the pin sample prepared at 850 ºC, refer Fig. 5.30. The wear resistance was increased on the pin sample made at 850 ºC with almost 89.65% by diffusion of c-BN in D2 steel.

The results show that the sample made at process parameters of 850 ºC for 1 hour is best and exhibit high wear resistance as compared to the sample prepared at 750 ºC for 2 hours. The as-proposed technology can be used for the development of a c-BN diffused D2 steel tool for high-temperature machining applications.

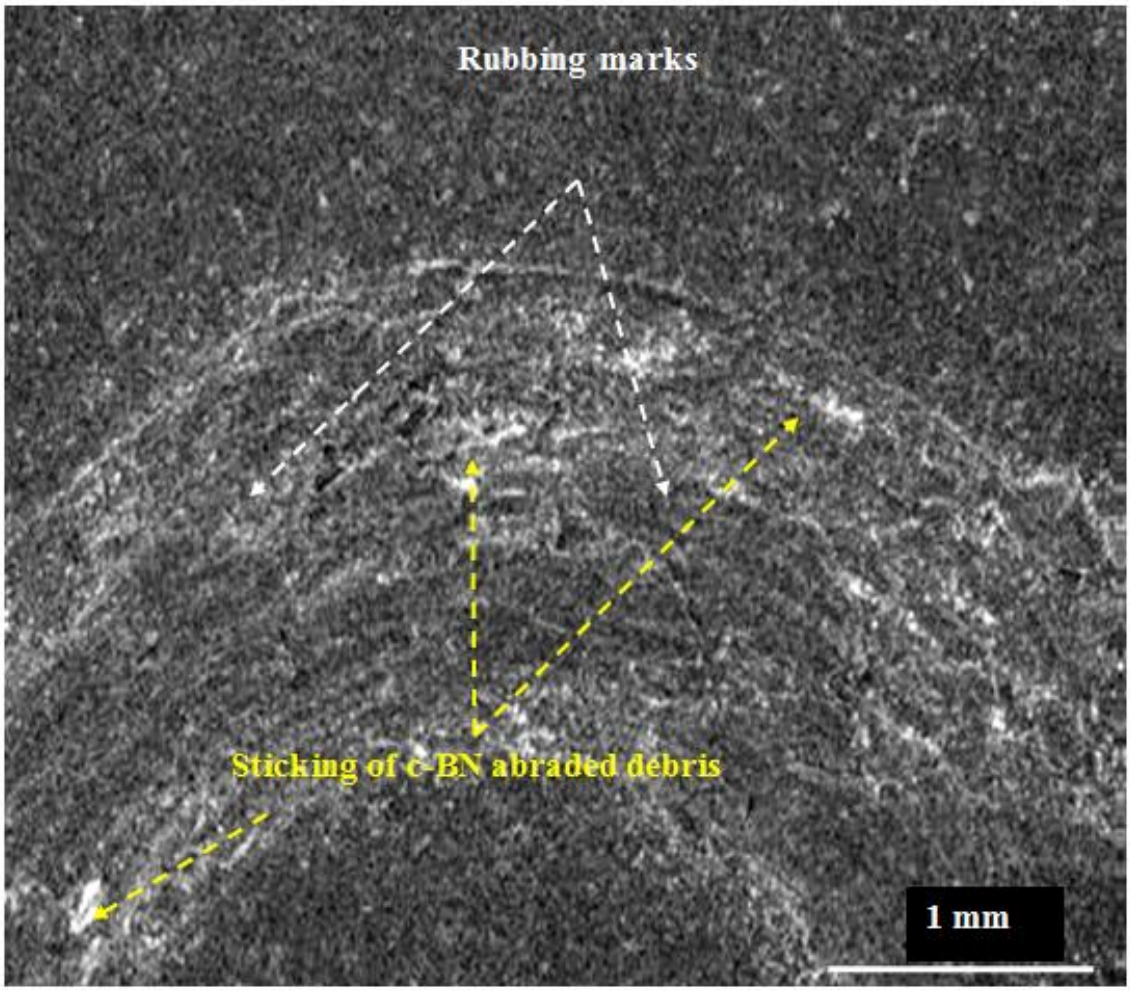

Fig. 5.29. SEM images of worn-out counter surface

Fig. 5. 30. SEM images of c-BN diffused pin treated at 850ºC for 1 hour

5.7. Erosion Analysis

Air jet erosion test was performed in order to simulate actual heat resistant condition such as coal-fired boiler conditions by utilizing the solid particle erosion test rig. The erosive wear behavior and comparison of bare sample (D2 steel substrate). The samples image after erosion test is shown in Fig. 5.31. It was found during this investigation that the scars produced on the specimen were of different type due to a constant strike of eroded material at various angles. Elliptic shape was formed at 45° and 60°, while the angle of impingement at 90° shaped a circular scar. Upon analysis of specimens, the dark gray colored ring is clear. Furthermore, it was found that, relative to the eroded region, the region was rough. Erosion after the air jet erosion test was performed, the volume loss (mm^3/g) due to erosion was determined by optical profilometer and after that the data were measured using the change of

volume process. In order to calculate the mean erosive wear depth of an eroded scar, an erosive wear depth was measured in six different arbitrary positions.

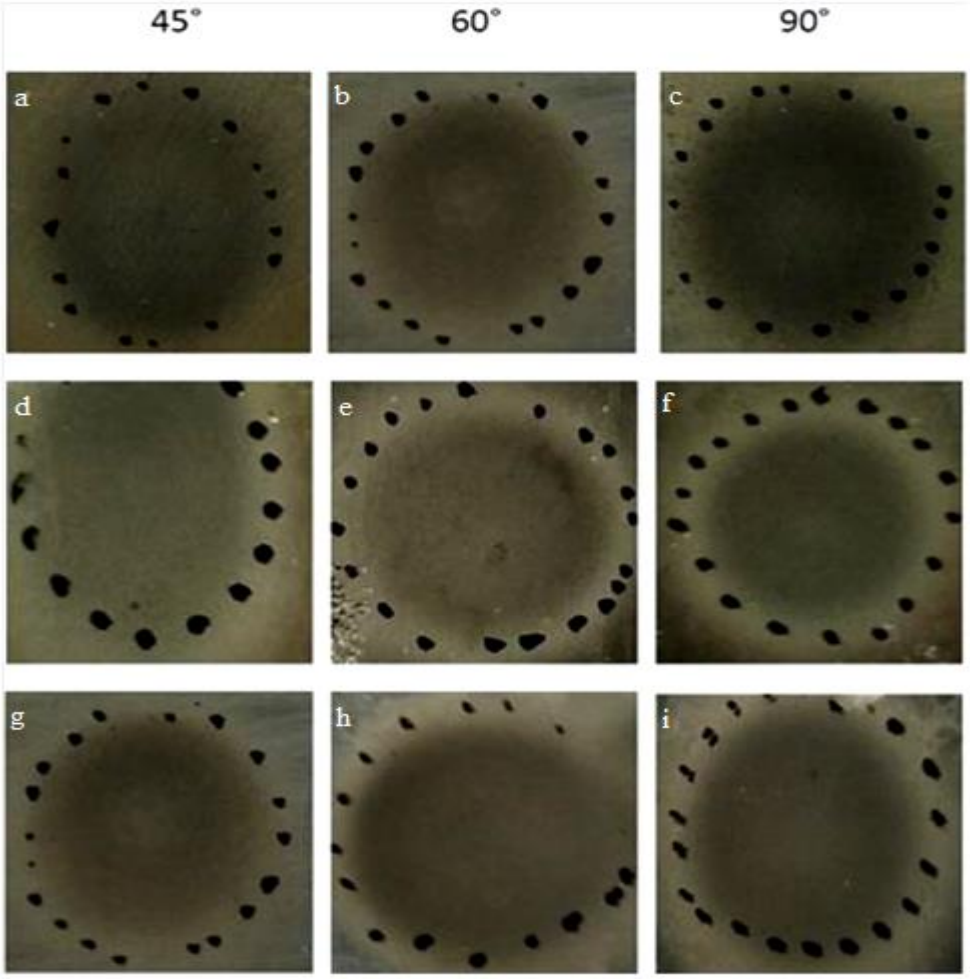

Fig. 5.31. Surface macrographs of eroded samples of bare and c-BN diffused as steel standard at impact angles of 45°, 60° and 90° subjected to elevated temperature erosive wear studies in simulated coal-fired boiler conditions (a-c) bare D2-steel, (d-f) c-BN at 750 ºC, and (g-i) c-BN at 850 ºC

The erosive wear data was collected for bare sample and thermal diffused samples. The volume erosion rate (mm^3/g) at an impact angle of 45°of bare specimen was 0.0065 mm^3/g, at 750 °C 0.00054 mm^3/g, and Sample-II at 850 °C as 0.00047 mm^3/g. The volume erosion rate (mm^3/g) at an impact angle of 60°of bare specimen was 0.0055 mm^3/g, sample-I at 750 °C 0.00051 mm^3/g, and Sample-II at 850 °C as 0.00039 mm3/g. The volume erosion rate (mm^3/g) at an impact angle of 90°of bare specimen was 0.0048 mm^3/g, sample-I at 750 °C 0.00045 mm^3/g, and Sample-II as

0.00035 mm^3/g. Fig. 5.32 to 5.35 show the comparative analysis of erosion rate of sample-I and sample-II in comparison with un-treated/base sample. Form the Figures, it can be seen that the sample-II has less erosion rate as compared to bare and sample-I. It is because, sample-II possessed high surface hardness and high strength to abrasion, which prevents the surface from erosion failure. The sample-II is suitable for high temperature applications.

From above displayed column charts, it can be examined that the volume erosion rate of bare sample un-treated steel substrate was maximum at an impingement angle of 45° which was simultaneously reducing as the angle of impingement increases, that means the volume erosion rate was reduced at impingement angle 60° and minimal erosion rate at impingement angle of 90°. This behavior is similar to the ductile materials. Whereas, the behavior of volume erosion rate was opposite on sample-I and sample-II. That means the volume erosion rate on treated specimens was maximum at impingement angle of 90° which was then reduced at impingement angle of 60° and then minimal at impingement angle of 45°.Fig. 5.32 to Fig. 5.34 shows the erosion rate of un-treated, Sample-I at 750 °C, and Sample-II at 850 °C.

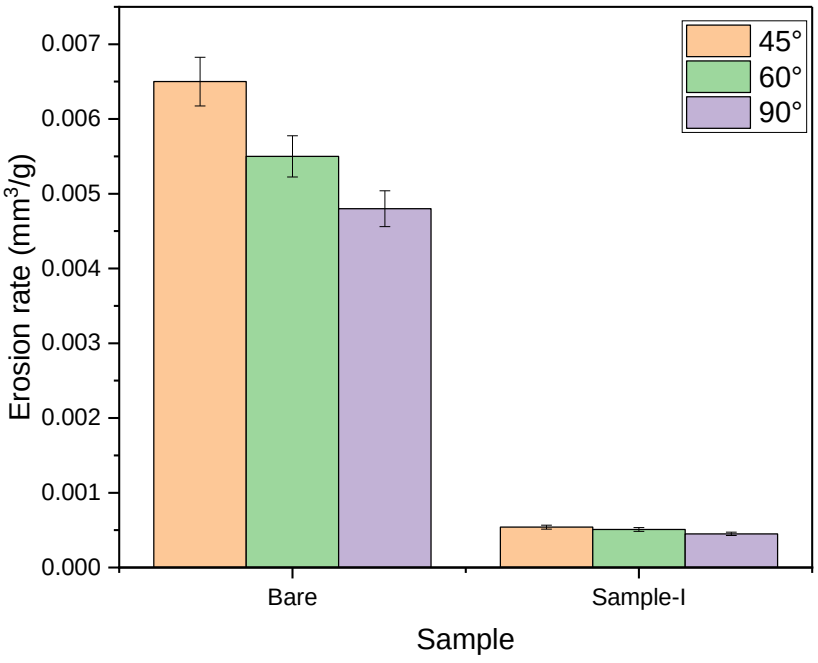

Fig. 5.32. Erosion rate of Sample-I at 750 °C as compared to bare sample (particle velocity = 30 m/s, erodent feed rate = 2 gm/min)

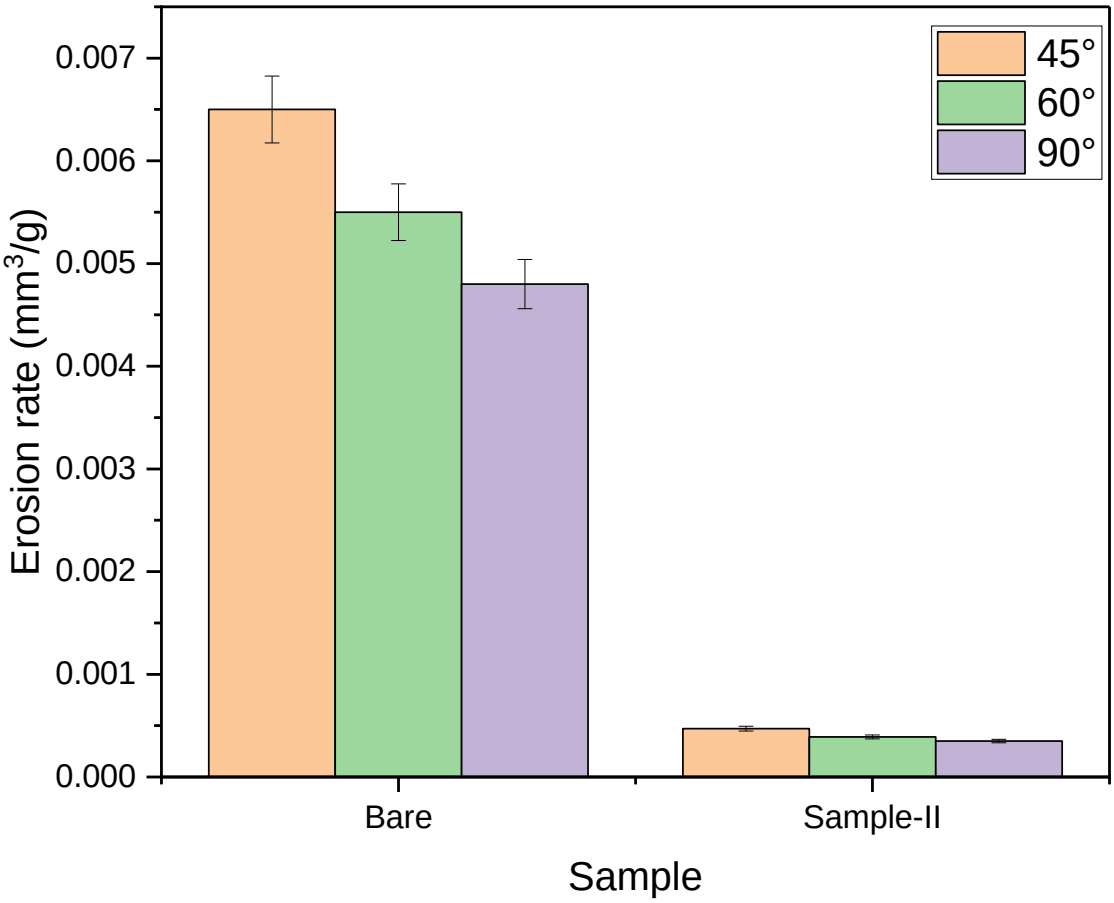

Fig. 5.33. Erosion rate of Sample-II at 850 °C as compared to bare sample (particle velocity = 30 m/s, erodent feed rate = 2 gm/min)

Therefore, based on the present investigated data the volume erosion rates at impingement angles of 45°, 60° and 90° can be arranged in the following order:

Untreated sample>Sample-I at 750 °C **>Sample-II** at 850 °C

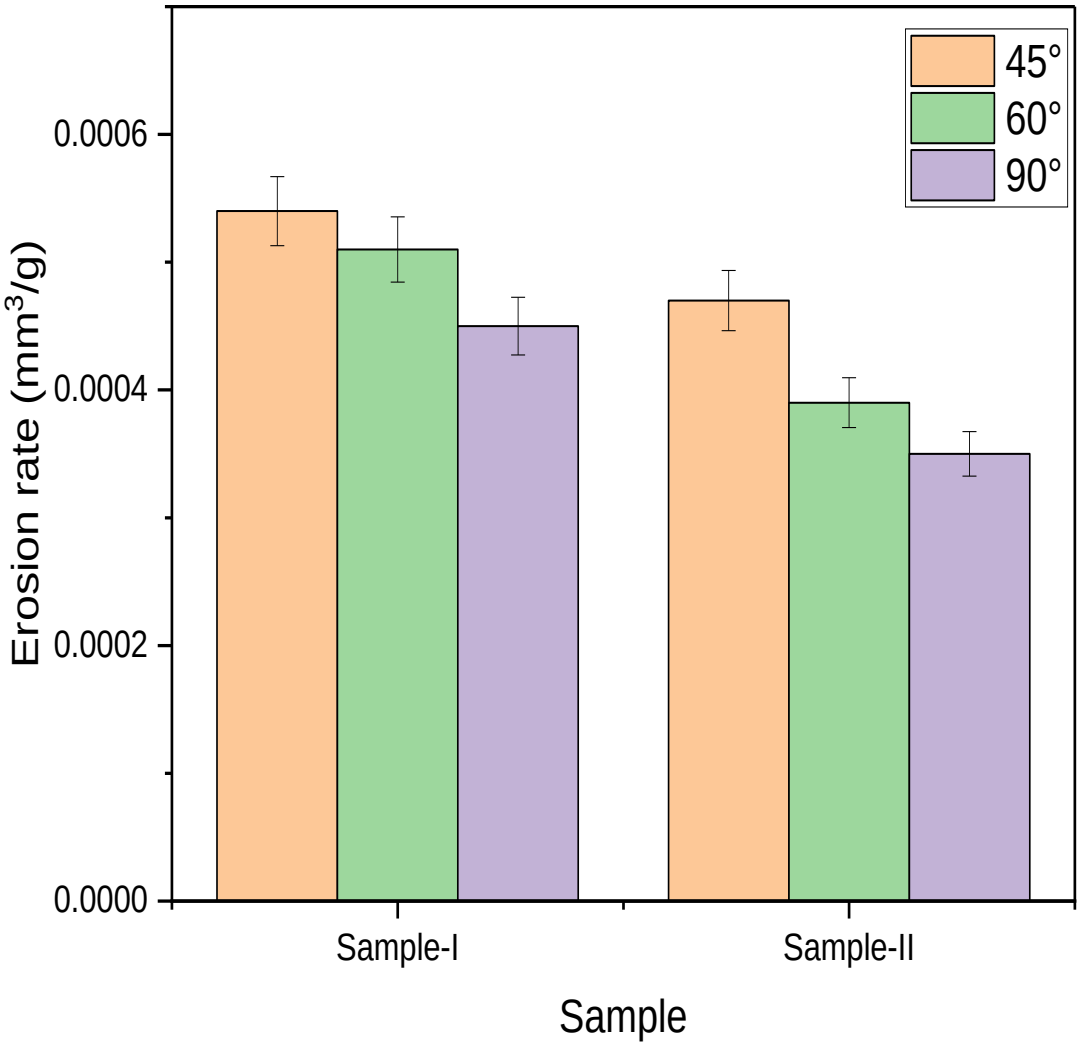

Fig. 5.34. Erosion rate of Sample-I at 750 °C as compared to sample-II at 850 °C (particle velocity = 30 m/s, erodent feed rate = 2 gm/min)

The sample which has high erosion rate has low erosion resistance and those have low erosion rate have high erosion resistance. On the basis of erosion rate, it can be claimed that the erosion resistance of bare sample was minimum at an impingement angle of 45° which was simultaneously increasing as the angle of impingement increases, that means the volume erosion rate was increased at impingement angle 60° and maximum erosion resistance at impingement angle of 90°. This behavior is similar to the ductile materials. Whereas, the behavior of erosion resistance was opposite on sample-I and sample-II. That means the erosion resistance on diffused samples were maximum at impingement angle of 90° which was then increases at impingement angle of 60° and then maximum at impingement angle of

45°. Therefore, based on the present investigated data the erosion resistance at impingement angles of 45°, 60° and 90° can be arranged in the following order:

Sample-II at 850 °C **>Sample-I** at 750 °C **>Un-treated base Steel**

CHAPTER 6

CONCLUSIONS AND SCOPE FOR FUTURE RESEARCH WORK

In the present research work, the application thermal diffusion has been successfully used to deposit the c-BN layer on the steel surface to enhance the mechanical and wear resistance of steel for high temperature applications.

6.1.Conclusions

After inclusive analysis of the presented work, the major conclusions can be drawn as below:

1. A rich layer of c-BN has been successfully deposited on the steel surface for high temperature applications.
2. The best optimal condition for the diffusion of c-BN on the D2-steel surface was 750 ºC for 2 hours and 850 ºC for 1 hour.
3. The diffusion layer thickness was measured in the range of 50-90 μm, which exhibits high surface hardness.
4. EDS analysis showed that c-BN particles were uniformly diffused in the layer.
5. The diffusion layer exhibits a very low percentage of structural porosities ~ 1.5%.
6. The average hardness of the samples manufactured at 750 ºC for 2 hours and 850 ºC for 1 hour was measured around 1350HV and 1570HV, respectively. The improvement in the hardness for these samples was 345.44% and 418.2%, respectively, as compared to untreated samples 303HV.
7. The novel manufactured surface composite showed excellent wear resistance characteristics. These samples revealed slightly lower wear resistance against WC, Al_2O_3 counter surfaces, and the best wear rate against Si_3N_4 counter surface. Overall, the wear resistance of pin surface treated at 850 ºC for 1 hour was improved with almost 89.65% by diffusion of c-BN in D2 steel, when comparing to untreated pin samples.

8. Erosion resistance of diffused samples was maximum at an impingement angle of 90° which was then increasing at an impingement angle of 60° and then maximum at an impingement angle of 45°. Therefore, based on the present investigated data the erosion resistance at impingement angles of 45°, 60°, and 90° can be arranged in the following order " **Sample-II** at 850 °C **>Sample-I** at 750 °C **Un-treated base Steel".**

9. In summary, the present research study shows that the c-BN diffused layer has the potential for tailoring hard and wear-resistant features for high-temperature applications like machine tool and turbine blade, and boiler coating.

6.2. Scope for Future Research Work

Analysis of the results acquired from the current work advocates quite a few possible extensions to the research. A few of them are listed:

1. Further experiments could be conducted with 50 ^{o}C temperature range as input parameter and compared with existing samples of 100 ^{o}C range.

2. In this research, an experimental investigation on the effects of c-BN powder on the surface characteristics has been studied. However, there is a scope for the use of powder particles of other materials such as Al_2O_3, polycrystalline diamond (PCD), and other hard materials.

3. There is a scope on finite element modeling and analysis to simulate the diffusion process for a better understanding of phenomena and predict the thermal stresses.

4. The diffusion of c-BN using PVD and other advanced coating techniques can be compared on the basis of cost analysis.

5. The corrosion resistance of c-BN diffused layer can be studied in the future.

References

[1]. Galedari, S. A., Mahdavi, A., Azarmi, F., Huang, Y., & McDonald, A. (2019). A Comprehensive Review of Corrosion Resistance of Thermally-Sprayed and Thermally-Diffused Protective Coatings on Steel Structures. *Journal of Thermal Spray Technology, 28(4),* 645-677.

[2]. Zhuravlev, G. M., Gvozdev, A. E., Cheglov, A. E., Sergeev, N. N., & Gubanov, O. M. (2017). Maximum plastic strengthening in tool steels. *Steel in Translation, 47(6),* 399-411.

[3]. Podgornik, B., Paulin, I., Zajec, B., Jacobson, S., & Leskovšek, V. (2016). Deep cryogenic treatment of tool steels. *Journal of Materials Processing Technology, 229,* 398-406.

[4]. Huang, J. Y., Zhu, Y. T., Liao, X. Z., Beyerlein, I. J., Bourke, M. A., & Mitchell, T. E. (2003). Microstructure of cryogenic treated M2 tool steel. *Materials Science and Engineering: A*, *339*(1-2), 241-244.

[5]. Lima, J. G., Avila, R. F., Abrao, A. M., Faustino, M., & Davim, J. P. (2005). Hard turning: AISI 4340 high strength low alloy steel and AISI D2 cold work tool steel. *Journal of Materials Processing Technology*, *169*(3), 388-395.

[6]. Roberts, G. A., Kennedy, R., & Krauss, G. (1998). *Tool steels*. ASM international.

[7]. Isik, Y. (2007). Investigating the machinability of tool steels in turning operations. *Materials & design*, *28*(5), 1417-1424.

[8]. Qamar, S. Z. (2009). Effect of heat treatment on mechanical properties of H11 tool steel. *Journal of Achievements in materials and manufacturing engineering*, *35*(2), 115-120.

[9]. Guo, L. Q., Qin, S. X., Yang, B. J., Liang, D., & Qiao, L. J. (2017). Effect of hydrogen on semiconductive properties of passive film on ferrite and austenite phases in a duplex stainless steel. *Scientific Reports*, *7*(1), 1-6.

[10]. Totten, G. E. (2017). *Tribology and Wear of Tool Steels*.

[11]. Akbarzadeh, A., & Naghdy, S. (2013). Hot workability of a high carbon high chromium tool steel. *Materials & Design*, *46*, 654-659.

[12]. Persson, A., Hogmark, S., & Bergström, J. (2005). Thermal fatigue cracking of surface engineered hot work tool steels. *Surface and Coatings Technology*, *191*(2-3), 216-227.

[13]. Gräfen, W., & Edenhofer, B. (2005). New developments in thermo-chemical diffusion processes. *Surface and Coatings Technology*, *200*(5-6), 1830-1836.

[14]. Jurči, P., & Hudáková, M. (2011). Diffusion boronizing of H11 hot work tool steel. *Journal of Materials Engineering and Performance*, *20*(7), 1180-1187.

[15]. Rutherford, K. L., Bull, S. J., Doyle, E. D., & Hutchings, I. M. (1996). Laboratory characterisation of the wear behaviour of PVD-coated tool steels and correlation with cutting tool performance. *Surface and Coatings Technology*, *80*(1-2), 176-180.

[16]. F. Hermanek, Thermal Spray Terminology and Company Origins, ASM International, Materials Park, 2001

[17]. P. Fauchais, A. Vardelle, Thermal Sprayed Coatings Used Against Corrosion and Corrosive Wear, INTECH Open Access Publisher, 2012

[18]. Galedari, S. A., Mahdavi, A., Azarmi, F., Huang, Y., & McDonald, A. (2019). A comprehensive review of corrosion resistance of thermally-sprayed and thermally-diffused protective coatings on steel structures. *Journal of Thermal Spray Technology*, *28*(4), 645-677.

[19]. J.R. Davis, Handbook of Thermal Spray Technology, ASM international, Materials Park, 2004

[20]. A. Pardo, P. Casaju´ s, M. Mohedano, A.E. Coy, F. Viejo, B. Torres, and E. Matykina, Corrosion Protection of Mg/Al Alloys by Thermal Sprayed Aluminum Coatings, *Applied Surface Science*., 2009, 255(15), p 6968-6977.

[21]. R.M. Trommer and C.P. Bergmann, Flame Spray Technology: Method for Production of Nanopowders, Springer, Berlin, 2015, p 7-10ISBN 978-3-662-47162-3.

[22]. E. Pfender, Plasma Jet Behavior and Modeling Associated with the Plasma Spray Process, Thin Solid Films, 1994, 238(2), p 228-241.

[23]. A.S. Kang, G. Singh, and V. Chawla, Some Problems Associated with Thermal Sprayed Ha Coatings: A Review, *International Journal of Surface Engineering Materials and Technology*, 2013, 3, p 10-20.

[24]. J. Wang and J. Villafuerte, Low Pressure Cold Spray of Tungsten Carbide Composite Coatings, *Adv. Mater. Processes*, 2009, 167(2), p 54-57.

[25]. E. Irissou, J.G. Legoux, B. Arsenault, and C. Moreau, Investigation of Al-Al_2O_3 Cold Spray Coating Formation and Properties, J. *Thermal Spray Technology*, 2007, 16(5-6), p 661-668.

[26]. N. Melendez and A. McDonald, Development of WC-based metal matrix composite coatings using low-pressure cold gas dynamic spraying, *Surface Coatings and Technology*, 2013, 214, p 101-109.

[27]. A. Papyrin, V. Kosarev, S. Klinkov, A. Alkhimov, and V.M. Fomin, *Cold Spray Technology*, *Elsevier*, Amsterdam, 2006.

[28]. J. Davis, Surface Engineering for Corrosion and Wear Resistance, 1st ed., ASM International, Materials Park, 2001, p 1-43.

[29]. P. Dearnley, Surface engineering with diffusion technologies, Introduction to Surface Engineering, Cambridge University Press, Cambridge, 2015, p 35-115

[30]. X. Liu, H. Wang, D. Li, and Y. Wu, Study on Kinetics of Carbide Growth by Thermal Diffusion Process, *Surface Coatings and Technology* ,2006, 201, p 2414-2418

[31]. J.R. Nicholls, Designing Oxidation-Resistant Coatings, JOM, 2000, 52, p 28-35

[32]. Wang, H., Xie, G., Zhu, Z., Ying, Z., & Zeng, Y. (2014). Enhanced tribological performance of the multi-layer graphene filled poly (vinyl chloride) composites. *Composites Part A: Applied Science and Manufacturing*, *67*, 268-273.

[33]. Holleck, H. (1986). Material selection for hard coatings. *Journal of Vacuum Science & Technology A: Vacuum, Surfaces, and Films, 4(6),* 2661-2669.

[34]. Liu, Y., Bhowmick, S., & Yakobson, B. I. (2011). BN white graphene with "colorful" edges: The energies and morphology. *Nano letters*, *11(8)*, 3113-3116.

[35]. Pakdel, A., Zhi, C., Bando, Y., & Golberg, D. (2012). Low-dimensional boron nitride nanomaterials. *Materials Today, 15(6),* 256-265.

[36]. Fernandes, F. A. P., Heck, S. C., Picone, C. A., & Casteletti, L. C. (2020). On the wear and corrosion of plasma nitrided AISI H13. *Surface and Coatings Technology, 381*, 125216.

[37]. P. Dearnley, Surface engineering with diffusion technologies, Introduction to Surface Engineering, Cambridge University Press, Cambridge, 2015, p 35-115

[38]. Sopko, J., & Simhan, K. (1974). U.S. Patent No. 3,850,679. Washington, DC: U.S. Patent and Trademark Office.

[39]. Mittemeijer, E. J., & Somers, M. A. (2015). Thermochemical surface engineering of steels. Woodhead Publishing.

[40]. K.L. Choy, Chemical Vapor Deposition of Coatings, Prog. Mater Sci., 2003, 48, p 57-170

[41]. E.J. Mittemeijer and M.A.J. Somers, Ed., Thermochemical Surface Engineering of Steels, 1st ed., Elsevier—Woodhead Publishing, Cambridge, 2014

[42]. E. Medvedovski, F. Chinski, and J. Stewart, Wear- and Corrosion- Resistant Boride-Based Coatings Obtained Through Thermal Diffusion CVD Processing, *Advanced Engineering Materials, 2014, 16(6),* p 713-728

[43]. A. Mahdavi, E. Medvedovski, G. Mendoza, and A. McDonald, Corrosion Resistance of Boronized, Aluminized, and Chromized Thermal Diffusion-Coated Steels in Simulated High Temperature Recovery Boiler Conditions, Coatings, 2018, 8(8), p 257.

[44]. E. Medvedovski, Formation of Corrosion–Resistant Thermal Diffusion Boride Coatings, *Advanced Engineering Materials* 2016, 18(1), p 11-33

[45]. E. Medvedovski, J. Jiang, and M. Robertson, Iron Boride-Based Thermal Diffusion Coatings for Tribo-Corrosion Oil Production Applications, Ceram. Int., 2016, 42(2), p 3190-3211

[46]. R. Telle, L.S. Sigl, and K. Takagi, Boride-Based Hard Materials, Handbook of Ceramic Hard Materials, R. Riedel, Ed., Wiley, Weinheim, 2000, p 802-945

[47]. P. Dearnley and T. Bell, Engineering the Surface with Boron Based Materials, *Surface Engineering, 1985,* 1(3), p 203-217

[48]. A.K. Sinha, Boriding (Boronizing); ASM Handbook, Heat Treating, 1991, 4, p 437

[49]. R. Petrova and N. Suwattananont, Surface Modification of Ferrous Alloys with Boron, J. *Electron. Mateials., 2005, 34(5),* p 575-582

[50]. N. Suwattananont and R. Petrova, Oxidation Kinetics of Boronized Low Carbon Steel AISI, 1018, Oxid. Met., 2008, 70, p 307-315

[51]. R. Petrova, N. Suwattananont, and V. Samardzic, The Effect of Boronizing on Metallic Alloys for Automotive Applications, J. Mater. Eng. Perform., 2008, 17(3), p 340-345.

[52]. A.K. Cheetham and P. Day, Solid State Chemistry: Techniques, Oxford Science Publications, Oxford, UK, 1991

[53]. H. Donald and B. Jenkins, Thermodynamics of the Relationship Between Lattice Energy and Lattice Enthalpy, *J. Chemical Educ., 2005, 82(6),* p 950-952

[54]. M. Ladd, Crystal Structures: Lattices and Solids in Stereoview. Horwood Series in Chemical Science, Elsevier, Chichester, *Journal of Thermal Spray Tech (2019) 28*:645–677

[55]. H.J. Grabke and M. Schutze, Oxidation of Intermetallics, Wiley- VCH Verlag GmbH, Berlin, 1998

[56]. N.V. Bangaru and R.C. Krutenat, Diffusion Coatings of Steels: Formation Mechanism and Microstructure of Aluminized Heat-Resistant Stainless Steels, *Journal of Vac. Science and Technoogy. B, 1984, 2(4),* p 806-815

[57]. V. Voka´l, V. Rohr, M.J. Pomeroy, and M. Schu¨tze, Corrosion of Alloys and Their Diffusion Aluminide Coatings by KCl:K2SO4 Deposits at 650_C in Air, *Material Corrosion, 2008, 59(5),* p 374-379

[58]. S. Kiamehr, T.N. Lomholt, K.V. Dahl, T.L. Christiansen, and M.A. Somers, Application of Aluminum Diffusion Coatings to Mitigatethe KCl-Induced High-Temperature Corrosion, *Material Corrosion* 2017, 68(1), p 82-94

[59]. D. Wang, Corrosion Behavior of Chromized and/or Aluminized 225Cr-1Mo Steel in Medium-BTU Coal Gasifier Environments, *Surface Coatings and Technology* 1988, 36(1-2), p 49-60

[60]. C.Y. Bai, M.D. Ger, and M.S. Wu, Corrosion Behaviors and Contact Resistances of the Low-Carbon Steel Bipolar Plate with a Chromized Coating Containing Carbides and Nitrides, *Int. J. Hydrog. Energy, 2009, 34(16),* p 6778-6789.

[61]. Christiansen, T., & Somers, M. A. (2005). Low temperature gaseous nitriding and carburising of stainless steel. *Surface Engineering*, *21*(5-6), 445-455.

[62]. Suh, B. S., & Lee, W. J. (1997). Surface hardening of AISI 316L stainless steel using plasma carburizing. *Thin Solid Films*, *295*(1-2), 185-192.

[63]. Tsujikawa, M., Yoshida, D., Yamauchi, N., Ueda, N., Sone, T., & Tanaka, S. (2005). Surface material design of 316 stainless steel by combination of low temperature carburizing and nitriding. *Surface and Coatings Technology*, *200*(1-4), 507-511.

[64]. Sun, Y., Li, X., & Bell, T. (1999). Low temperature plasma carburising of austenitic stainless steels for improved wear and corrosion resistance. *Surface Engineering*, *15*(1), 49-54.

[65]. Ganesh, P., Giri, R., Kaul, R., Sankar, P. R., Tiwari, P., Atulkar, A., ...& Kukreja, L. M. (2012). Studies on pitting corrosion and sensitization in laser rapid manufactured specimens of type 316L stainless steel. *Materials & Design*, *39*, 509-521.

[66]. Da Silva, G. F., Tavares, S. S. M., Pardal, J. M., Silva, M. R. D., & De Abreu, H. F. G. (2011). Influence of heat treatments on toughness and sensitization of a Ti-alloyed supermartensitic stainless steel. *Journal of Materials Science*, *46*(24), 7737-7744.

[67]. Edenhofer, B., Joritz, D., Rink, M., & Voges, K. (2015). Carburizing of steels. In *Thermochemical Surface Engineering of Steels* (pp. 485-553). Woodhead Publishing.

[68]. Beer, O. (2018). Experiences in Heat Treatment of Heat Resistant Carburizing Bearing Steels. *HTM Journal of Heat Treatment and Materials*, *73*(1), 27-40.

[69]. Schuster, J., Bruder, E., & Müller, C. (2012). Plasma nitriding of steels with severely plastic deformed surfaces. *Journal of Materials Science*, *47*(22), 7908-7913.

[70]. Flodström, I. (2012). Nitrocarburizing and high temperature nitriding of steels in bearing applications.

[71]. Stechyshyn, M. S., Martynyuk, A. V., Bilyk, Y. M., Oleksandrenko, V. P., & Stechyshyna, N. M. (2017). Influence of the ionic nitriding of steels in glow discharge on the structure and properties of the coatings. *Materials Science*, *53*(3), 343-350.

[72]. Genel, K., Demirkol, M., & Capa, M. (2000). Effect of ion nitriding on fatigue behaviour of AISI 4140 steel. *Materials Science and Engineering: A*, *279*(1-2), 207-216.

[73]. Muraleedharan, T. M., & Meletis, E. I. (1992). Surface modification of pure titanium and Ti□ 6A1□ 4V by intensified plasma ion nitriding. *Thin Solid Films*, *221*(1-2), 104-113.

[74]. Möller, W., Parascandola, S., Telbizova, T., Günzel, R., & Richter, E. (2001). Surface processes and diffusion mechanisms of ion nitriding of stainless steel and aluminium. *Surface and Coatings Technology*, *136*(1-3), 73-79.

[75]. Hudis, M. (1973). Study of ion- nitriding. *Journal of Applied Physics*, *44*(4), 1489-1496.

[76]. Fernandes, F. A. P., Neto, A. L., Casteletti, L. C., & De Oliveira, A. M. (2008). ION NITRIDING AND NITROCARBURIZING. *Heat Treating Progress*, 41.

[77]. Sirin, S. Y., Sirin, K., & Kaluc, E. (2008). Effect of the ion nitriding surface hardening process on fatigue behavior of AISI 4340 steel. *Materials Characterization*, *59*(4), 351-358.

[78]. Borges, C. F. M., Hennecke, S., & Pfender, E. (2000). Decreasing chromium precipitation in AISI 304 stainless steel during the plasma-nitriding process. *Surface and Coatings Technology*, *123*(2-3), 112-121.

[79]. Rolinski, E., Sharp, G., Cowgill, D. F., & Peterman, D. J. (1998). Ion nitriding of titanium alpha plus beta alloy for fusion reactor applications. *Journal of nuclear materials*, *252*(3), 200-208.

[80]. Chong, S. O., & Kim, S. J. (2019). Characterization of cavitation-erosion resistance of plasma ion nitrided 316L stainless steel under shock wave in seawater. *Journal of nanoscience and nanotechnology*, *19*(7), 3943-3949.

[81]. Chong, S. O., & Kim, S. J. (2019). Characterization of cavitation-erosion resistance of plasma ion nitrided 316L stainless steel under shock wave in seawater. *Journal of nanoscience and nanotechnology*, *19*(7), 3943-3949.

[82]. Zhang, X., Wang, J., Fan, H., & Pan, D. (2018). Erosion–corrosion resistance properties of 316L austenitic stainless steels after low-temperature liquid nitriding. *Applied Surface Science*, *440*, 755-762.

[83]. Kumar, R., Bhardwaj, D., & Sharma, Y. C. (2018). A Review on Plasma Ion Nitriding (PIN) Process. *i-Manager's Journal on Material Science*, *6*(1), 31.

[84]. Khusainov, Y. G., & Ramazanov, K. N. (2019). Local ion nitriding of martensitic structural steel in plasma of glow discharge with hollow cathode. *Inorganic Materials: Applied Research*, *10*(3), 544-548.

[85]. Lopes, H. S. M., Moreto, J. A., Manfrinato, M. D., Cruz, N. C. D., Rangel, E. C., & Rossino, L. S. (2016). Micro abrasive wear behaviour study of carburization and ion plasma nitriding of P20 steel. *Materials Research*, *19*(3), 686-694.

[86]. Ramazanov, R., Vafin, R., Asylbaev, A., & Nikolaev, A. (2019, November). Effect of applying a magnetic field in ion nitriding on probe characteristics of glow discharge, microhardness and R6M5 steel structure. In *Journal of Physics: Conference Series* (Vol. 1393, No. 1, p. 012121). IOP Publishing.

[87]. De Las Heras, E., Ybarra, G., Lamas, D., Cabo, A., Dalibon, E. L., & Brühl, S. P. (2017). Plasma nitriding of 316L stainless steel in two different N2-H2 atmospheres-Influence on microstructure and corrosion resistance. *Surface and Coatings Technology*, *313*, 47-54.

[88]. Borgioli, F., Galvanetto, E., & Bacci, T. (2020). Effects of Surface Modification by Means of Low-Temperature Plasma Nitriding on Wetting and Corrosion Behavior of Austenitic Stainless Steel. *Coatings*, *10*(2), 98.

[89]. Tyunkov, A. V., Golosov, D. A., Zolotukhin, D. B., Nikonenko, A. V., Oks, E. M., Yushkov, Y. G., & Yakovlev, E. V. (2020). Nitriding of titanium in electron beam excited plasma in medium vacuum. *Surface and Coatings Technology*, *383*, 125241.

[90]. Burdovitsin, V. A., Golosov, D. A., Oks, E. M., Tyunkov, A. V., Yushkov, Y. G., Zolotukhin, D. B., & Zavadsky, S. M. (2019). Electron beam nitriding of titanium in medium vacuum. *Surface and Coatings Technology*, *358*, 726-731.

[91]. Zhao, G. H., Aune, R. E., & Espallargas, N. (2016). Tribocorrosion studies of metallic biomaterials: The effect of plasma nitriding and DLC surface modifications. *journal of the mechanical behavior of biomedical materials*, *63*, 100-114.

[92]. Wang, Q., Zhang, X., Huang, C., & Luo, Y. (2017). Ion Nitriding CoCrMo Alloy for Orthopedic Applications Studied by X-Ray Photoelectron

Spectroscopy Analysis and Tribocorrosion Behavior. *Journal of Tribology*, *139*(1).

[93]. Hacisalihoglu, I., Yildiz, F., & Alsaran, A. (2017). Wear performance of different nitride-based coatings on plasma nitrided AISI M2 tool steel in dry and lubricated conditions. *Wear*, *384*, 159-168.

[94]. Pilarska, M., Frączek, T., & Maźniak, K. (2018). The Role of Complementary Potential in Plasma Nitriding Processes of Technical Titanium. *Archives of Metallurgy and Materials*, *63*.

[95]. Farghali, A., & Aizawa, T. (2018). Nitrogen supersaturation process in the AISI420 martensitic stainless steels by low temperature plasma nitriding. *ISIJ International*, *58*(3), 401-407.

[96]. Arbilei, M. N., & Hamed, J. M. (2018). Liquid Nitriding of Stainless Steel 316L to improve fatigue properties for Orthopedic Screws. *Al-Nahrain Journal for Engineering Sciences*, *21*(4), 508-515.

[97]. Galeano-Osorio, D. S., Vargas, S., Vélez, J. M., Mello, A., Tanaka, M. N., & Castano, C. E. (2020). Hemocompatibility of plasma nitrided 316L stainless steel: Effect of Processing Temperature. *Applied Surface Science*, *509*, 144704.

[98]. Hussein, M. A., Kumar, A. M., Yilbas, B. S., & Al-Aqeeli, N. (2017). Laser nitriding of the newly developed Ti-20Nb-13Zr at.% biomaterial alloy to enhance its mechanical and corrosion properties in simulated body fluid. *Journal of Materials Engineering and Performance*, *26*(11), 5553-5562.

[99]. Yang, X., Meng, Y., & Tian, Y. (2016). Controllable friction and wear of nitrided steel under the lubrication of [DMIm] PF6/PC solution via electrochemical potential. *Wear*, *360*, 104-113.

[100]. Kumar, A., Kaur, M., Singh, S., Joseph, A., Jhala, G., & Bhandari, S. (2018). High-temperature tribological studies of plasma-nitrided tool steels. *Surface Engineering*, *34*(8), 620-633.

[101]. Fabijanic, D., Timokhina, I., Beladi, H., & Hodgson, P. (2017). The nitrocarburising response of low temperature bainite steel. *Metals*, *7*(7), 234.

[102]. Kusmanov, S. A., Dyakov, I. G., Kusmanova, Y. V., & Belkin, P. N. (2016). Surface modification of low-carbon steels by plasma electrolytic nitrocarburising. *Plasma Chemistry and Plasma Processing*, *36*(5), 1271-1286.

[103]. Jiang, L., Luo, H., & Zhao, C. (2018). Nitrocarburising of AISI 316 stainless steel at low temperature. *Surface Engineering*, *34*(3), 205-210.

[104]. Alphonsa, J., Mukherjee, S., & Raja, V. S. (2018). Study of plasma nitriding and nitrocarburising of AISI 430F stainless steel for high hardness and corrosion resistance. *Corrosion Engineering, Science and Technology*, *53*(sup1), 51-58.

[105]. Velkavrh, I., Ausserer, F., Klien, S., Voyer, J., Diem, A., Trausmuth, A., ...& Lingenhöle, K. (2017). Optimisation of plasma nitrocarburising for reducing wear in dry sliding contacts. In *Key Engineering Materials* (Vol. 721, pp. 389-393). Trans Tech Publications Ltd.

[106]. Kusmanov, S., Kusmanova, I., Tambovskiy, I., Belkin, P., & Parfenyuk, V. (2019). Anodic plasma electrolytic nitrocarburising of Ti6Al4 V alloy (SMT31). *Surface Engineering*, *35(3)*, 199-204.

[107]. Tambovskiy, I. V., Kusmanov, S. A., Korableva, S. S., Silkin, S. A., Sevostyanov, N. V., Komissarova, M. R., & Belkin, P. N. (2017). Anodic plasma electrolytic nitrocarburising of VT22 titanium alloy in carbamide and ammonium chloride electrolyte. *Surface Engineering and Applied Electrochemistry*, *53*(5), 407-412.

[108]. Branzei, M., Cojocaru, M. O., Druga, L. N., Tudose, F., & Trusca, R. (2018). Non-Toxic Environment for Ferritic Nitrocarburising Process. *REVISTA DE CHIMIE*, *69*(9), 2416-2419.

[109]. Caliari, D., Timelli, G., & Vanzo, F. (2018). Nitrocarburising of annealed and severe plastically deformed 16MnCr5 steel. *Surface Engineering*, *34*(7), 536-546.

[110]. Fernandes, F. A. P., Casteletti, L. C., & Gallego, J. (2016). Low Temperature Plasma Nitriding and Nitrocarburising of a Superaustenitic Stainless Steel. *Materials Performance and Characterization*, *5*(5), 664-674.

[111]. Godzsák, M., Pekker, P., Cora, I., & Veres, Z. (2016). Investigation of the intermediate layers formed by austenitic nitrocarburising. *International Journal of Microstructure and Materials Properties*, *11*(1-2), 34-47.

[112]. Liu, R. L., & Yan, M. F. (2017). Effects of rare earths on nanocrystalline for nitrocarburised layer of stainless steel. *Materials Science and Technology*, *33*(11), 1346-1351.

[113]. Göhring, H., Kante, S., Leineweber, A., & Mittemeijer, E. J. (2016). Microstructural development and crystallographic properties of decomposing Fe–N–C compound layers. *International Journal of Materials Research*, *107*(3), 203-216.

[114]. Velkavrh, I., Äusserer, F., Klien, S., Voyer, J., Lingenhöle, K., Kafexhiu, F., ...& Hofer, F. (2019). Influence of surface properties of nitrocarburised and oxidised steel on its tribological behaviour. *Tribologie und Schmierungstechnik*, *66*(1), 25-33.

[115]. VASILESCU, M., & DOBRESCU, M. (2019). The Importance of Nitrogen in the Heat Treating of Ferrous and Non-Ferrous Metals and Alloys. *The Annals of "Dunarea de Jos" University of Galati. Fascicle IX, Metallurgy and Materials Science*, *42*(1), 31-35.

[116]. Tambovskiy, I. V., Kusmanov, S. A., Korableva, S. S., Tambovskaya, M. I., Komissarova, M. R., & Belkin, P. N. (2019). Increasing wear resistance of Ti6Al4V alloy by anodic saturation with carbon and nitrogen. In *BALTTRIB'2019: proceedings of X international scientific conference, Vytautas Magnus University, Agriculture Academy, Kaunas, Lithuania, 14-16 November 2019, 2019, p. 42-47*.

[117]. Derakhshandeh, S. M. R., Hadavi, S. M. M., Eshraghi, M. J., Javaheri, M., & Mozafari, M. (2017). Improved electrochemical performance of nitrocarburised stainless steel by hydrogenated amorphous carbon thin films for bone tissue engineering. *IET Nanobiotechnology*, *11*(6), 656-660.

[118]. Xiao, J., Huang, Y., Zhou, Q., Wang, J., & He, X. (2019). Room temperature nanoindentation creep of nitrocarburised AISI 4140 steel. *Surface Engineering*, *35*(8), 719-727.

[119]. Velkavrh, I., Ausserer, F., Klien, S., Voyer, J., Diem, A., Lingenhöle, K., ...& Schröttner, H. (2018). Properties of nitrocarburised and oxidised steel surfaces and the correlation with their tribological behaviour under unlubricated sliding conditions. *Wear*, *410*, 127-141.

[120]. Dong, Y., Zheng, K., Fuentes, G., & Dong, H. (2018). Low adhesion effect of novel duplex NC/WC: C coatings against ductile materials at elevated temperatures. *Materials Letters*, *220*, 32-35.

[121]. Krzysztof Gocman, Tadeusz Kadoski Waldemar Mróz, SylwiaBurdyska, Artur Prokopiuk.Structural and mechanical properties of boron nitride thin films deposited on steel substrates by pulsed laser deposition.Journal of *KONES Powertrain and Transport*, Vol. 18, No. 1 2011.

[122]. Wang, W., Wang, D., & Han, F. (2019). Improvement of corrosion resistance of twinning-induced plasticity steel by hot-dipping aluminum with subsequent thermal diffusion treatment. *Materials Letters*, 248, 60-64.

[123]. Rosa, R., Veronesi, P., & Casagrande, A. (2020). On the effect of steel substrate alloying elements on the in-situ formation of intermediate thermal diffusion barrier layers. *Materials Chemistry and Physics*, 240, 122231.

[124]. Khairallah, S. A., & Anderson, A. (2014). Mesoscopic simulation model of selective laser melting of stainless steel powder. Journal of *Materials Processing Technology*, *214(11),* 2627-2636.

[125]. Zhang, X. Y., Jiang, L., Huang, X. B., Ma, Y., Fan, A. L., & Tang, B. (2012). Improvement of antibacterial properties of stainless steel by combining plasma cu and thermal diffusion. Wuji Cailiao Xuebao(*Journal of Inorganic Materials*), *27(5),* 519-523.

[126]. Medvedovski, E. (2016). Formation of Corrosion- Resistant Thermal Diffusion Boride Coatings. *Advanced Engineering Materials, 18(1),* 11-33.

[127]. Ghadi, A., Soltanieh, M., Saghafian, H., & Yang, Z. G. (2016). Investigation of chromium and vanadium carbide composite coatings on CK45 steel by Thermal Reactive Diffusion. *Surface and Coatings technology*, 289, 1-10.

[128]. Huang, Z. T., & Tian, W. H. (2014). Effects of Mo Contents in Matrix on Microstructure and Properties of Vanadium Carbide Coating Formed by Thermal Diffusion Treatment. Journal of *Iron and Steel Research International, 21(1),* 104-108.

[129]. Hollis, K. J., Hawley, M. E., & Dickerson, P. O. (2012). Characterization of Thermal Diffusion Related Properties in Plasma Sprayed Zirconium Coatings. Journal of *thermal spray technology*, *21(3-4),* 409-415.

[130]. Liu, Z. H., Zhang, D. Q., Sing, S. L., Chua, C. K., & Loh, L. E. (2014). Interfacial characterization of SLM parts in multi-material processing: Metallurgical diffusion between 316L stainless steel and C18400 copper alloy. *Materials Characterization, 94*, 116-125.

[131]. Ozbek, I., & Bindal, C. (2011). Kinetics of borided AISI M2 high speed steel. *Vacuum, 86(4),* 391-397.

[132]. Kania, H., & Sipa, J. (2019). Zinc coating deposition with new thermal diffusion process on low carbon steel substrates. *Hutnik, Wiadomości Hutnicze, 86(1*).

[133]. Ganji, O., Sajjadi, S. A., Yang, Z. G., Mirjalili, M., & Najari, M. R. (2020). On the formation and properties of chromium carbide and vanadium carbide coatings produced on W1 tool steel through thermal reactive diffusion (TRD). *Ceramics International*.

[134]. Sabetghadam, H., Hanzaki, A. Z., & Araee, A. (2010). Diffusion bonding of 410 stainless steel to copper using a nickel interlayer. *Materials Characterization, 61(6),* 626-634.

[135]. Dashkevich, V., Usherenko, Y., Matvienko, I., & Ivashko, V. (2019). Combined Technology of Electro-Spark Alloying and Thermal Diffusion Boriding of Steel. In Proceedings of the 12th *International Scientific and Practical Conference. Volume III* (Vol. 24, p. 26).

[136]. Fähsing, D., Oskay, C., Meißner, T. M., & Galetz, M. C. (2018). Corrosion testing of diffusion-coated steel in molten salt for concentrated solar power tower systems. *Surface and Coatings Technology, 354*, 46-55.

[137]. Uhlmann, E., Hinzmann, D., Kropidlowksi, K., Meier, P., Prasol, L., & Woydt, M. (2018). Substitution of commercially coated tungsten carbide tools in dry cylindrical turning process by HiPIMS coated niobium carbide cutting inserts. *Surface and Coatings Technology, 354*, 112-118.

[138]. Kikuchi, S., Iwamae, S., Akebono, H., Komotori, J., & Misaka, Y. (2018). Improvement of the electrochemical characteristics of medium carbon steel using atmospheric-controlled induction-heating fine particle peening. *Surface and Coatings Technology, 354,* 76-82.

[139]. Gan, Z., Yu, G., He, X., & Li, S. (2017). Numerical simulation of thermal behavior and multicomponent mass transfer in direct laser deposition of Co-base alloy on steel. International Journal of *Heat and Mass Transfer*, *104*, 28-38.

[140]. Maruno, H., & Nishimoto, A. (2018). Adhesion and durability of multi-interlayered diamond-like carbon films deposited on aluminum alloy. *Surface and Coatings Technology*, *354*, 134-144.

[141]. Biesuz, M., & Sglavo, V. M. (2016). Chromium and vanadium carbide and nitride coatings obtained by TRD techniques on UNI 42CrMoS4 (AISI 4140) steel. *Surface and Coatings Technology*, *286*, 319-326.

[142]. Rayane, K., Allaoui, O., & Allaoui, A. (2017). Effect of diffusion annealing on borides layers produced on XC38 steel. *Acta Physica Polonica A*, *132(3)*, 521-523.

[143]. Ortiz-Domínguez, M., Campos-Silva, I., Hernandez-Sanchez, E., Nava-Sánchez, J. L., Martinez-Trinidad, J., Jiménez-Reyes, M. Y., & Damián-Mejía, O. (2011). Estimation of Fe2B growth on low-carbon steel based on two diffusion models. *International Journal of Materials Research*, *102(4)*, 429-434.

[144]. Strahin, B. L., Shreeram, D. D., & Doll, G. L. (2017). Properties and tribological performance of vanadium carbide coatings on AISI 52100 steel deposited by thermoreactive diffusion. *JOM*, *69(7)*, 1160-1164.

[145]. H. Cesur, B. Kaftanoglu, A. Kalkanli, B. Oral. Deposition of boron nitride coatings on steel substrate by RF magnetron sputtering.Proceedings of *the 7th International Conference,Coatings in Manufacturing Engineerin*g, 1-3 October 2008, Chalkidiki, Greece.

[146]. Liu, Z., Gong, Y., Zhou, W., Ma, L., Yu, J., Idrobo, J. C., ...& Ajayan, P. M. (2013). Ultrathin high-temperature oxidation-resistant coatings of hexagonal boron nitride. *Nature communications*, *4(1)*, 1-8.

[147]. Song, X., Gao, J., Nie, Y., Gao, T., Sun, J., Ma, D., ...& Rümmeli, M. H. (2015). Chemical vapor deposition growth of large-scale hexagonal boron nitride with controllable orientation. *Nano Research, 8(10),* 3164-3176.

[148]. Campos-Silva, I., & Ortíz-Domínguez, M. (2010). Modelling the growth of Fe2B layers obtained by the paste boriding process in AISI 1018 steel. *International Journal of Microstructure and Materials Properties, 5(1),* 26-38.

[149]. Kulka, M., Makuch, N., & Pertek, A. (2013). Microstructure and properties of laser-borided 41Cr4 steel. *Optics & Laser Technology, 45,* 308-318.

[150]. Chaus, A. S., Pokorný, P., Čaplovič, Ľ., Sitkevich, M. V., & Peterka, J. (2018). Complex fine-scale diffusion coating formed at low temperature on high-speed steel substrate. *Applied Surface Science, 437,* 257-270.

[151]. Suri, A. K., Subramanian, C., Sonber, J. K., & Murthy, T. C. (2010). Synthesis and consolidation of boron carbide: a review. *International Materials Reviews, 55(1),* 4-40.

[152]. Zhong, Z., Hinoki, T., Jung, H. C., Park, Y. H., & Kohyama, A. (2010). Microstructure and mechanical properties of diffusion bonded SiC/steel joint using W/Ni interlayer. *Materials & Design, 31(3),* 1070-1076.

[153]. Pramanik, A., Basak, A. K., & Prakash, C. (2019). Understanding the wire electrical discharge machining of Ti6Al4V alloy. *Heliyon, 5(4),* e01473.

[154]. Pramanik, A., Islam, M. N., Basak, A. K., Dong, Y., Littlefair, G., & Prakash, C. (2019). Optimizing dimensional accuracy of titanium alloy features produced by wire electrical discharge machining. *Materials and Manufacturing Processes, 34(10),* 1083-1090.

[155]. Singh, S., & Prakash, C. (2020). Effect of cryogenic treatment on the microstructure, mechanical properties and finishability of β-TNTZ alloy for orthopedic applications. *Materials Letters*, 128461.

[156]. Prakash, C. Surface modification of phase titanium alloy by powder mixed EDM and determination of optimal surface texture for medical implants. *Ph.D Dissertation, Panjab University*, 2016

[157]. Patnaik, A., & Bhatt, A. D. (2011). Mechanical and dry sliding wear characterization of epoxy–TiO2 particulate filled functionally graded composites materials using Taguchi design of experiment. *Materials & Design, 32(2),* 615-627.

[158]. Xiuju Song et al.(2015) Chemical vapour deposition growth of large-scale hexagonal boron nitride with controllable orientation. *Nano Research*,2015,DOI:10.1007/s12274-015-0816-9.

[159]. J. L. Andujar,E. Bertran, and M. C. Polo (1997). Plasma-enhanced chemical vapor deposition of boron nitride thin films from B2H6–H2–NH3 and B2H6–N2 gas mixtures.1997.

[160]. Halil Caliskan, Bilal Kursuncu, Sevki Yilmaz Guven, Abdullah Cahit Karaoglanli, Mustafa Sabri Gok and Akgun Alsaran (2016). Effect of boron nitride coating on wear behavior of carbide cutting tools in milling of inconel 718. Machining, Joining and Modifications of Advanced Materials. *Advanced Structured Materials 61*, DOI 10.1007/978-981-10-1082-8_2.

[161]. M. Kandeva, A. Vencl, E. Assenova, D. Karastoyanov and T. Grozdanova (2014). Abrasive wear of chemical nickel coatings with boron nitride nano-particles. *Proceedings of the 11th International Conference "THE-A" Coatings in Manufacturing Engineering*. 1-3 October 2014, Thessaloniki, Greece.

[162]. Tharajak, J. Palathai and Sombatsompop N (2012). Tribological Properties of Flame Sprayed Hexagonal Boron Nitride/Polyetheretherketone Coatings. *Advanced Materials Research Vol. 410* (2012) pp 333-336.

[163]. Henrik Pedersen, Mikhail Chubarov, Hans Högberg, Jens Jensen and Anne Henry (2012). On the effect of water and oxygen in chemical vapor deposition of boron nitride. *Thin Solid Films, (520),* 18, 5889-5893.

[164]. K.P. Budna , P.H. Mayrhofer , J. Neidhardt , É. Hegedũs , I. Kovács ,L. Tóth , B. Pécz , C. Mitterer (2007). Effect of nitrogen-incorporation on structure, properties and performancecof magnetron sputtered CrB2. *Surface & Coatings Technology,202* (2008) 3088–3093.

[165]. Andenet Alemu ,Alex Freundlich , Nacer Badi , Chris Boney and Abdelhak Bensaoula (2010) . Low temperature deposited boron nitride thin films for a robust anti-reflection coating of solar cells. *Solar Energy Materials & Solar Cells, 94* (2010) 921–923.

[166]. T. Wittkowski, J. Jorzick, K. Jung, and B. Hillebrands (1999). Elastic properties of thin h-BN films investigated by Brillouin light scattering. http://www.physik.uni-kl.de/w_hilleb, *Thin Solid Films*, in press.

[167]. Quan Li, R.Q. Zhang, L.D. Marks, W.J. Zhang, I. Bello (2002). Reactivity of different tBN environments serving as reaction sites in cBN film deposition. *Diamond and Related Materials, 11* (2002) 1416–1421.

[168]. S. Nakhaie, J. M. Wofford, T. Schumann, U. Jahn, M. Ramsteiner, M. Hanke, J. M. J. Lopes,and H. Riechert (2015). Synthesis of atomically thin hexagonal boron nitride films on nickel foils by molecular beam epitaxy. *Applied Physics Letters 106*, 213108.

[169]. Alan F. Jankowski, Jeffrey P. Hayes, Daniel M. Makowiecki and Mark A. McKeman (1997). *International Conference on Metallurgical Coatings and Thin Films*. A@ 21-25, San Diego, CA.

CERTIFICATE OF PUBLICATION OF PAPERS FOR PH.D.

This is to certify that Mr. Harminder Singh Saggu pursuing Ph.D. (**Part Time**) programme in Department of Mechanical Engineering with Registration Number 41500104 under the Guidance of Dr. Amardeep Singh Kang and co-supervision of Dr. Chander Prakash and Dr. C. I. Pruncu has the following Publications / Letter of Acceptance in the Referred Journals / Conferences mentioned thereby fulfilling the minimum programme requirements as per the UGC.

SNO.	TITLE OF PAPER WITH AUTHOR NAMES	NAME OF JOURNAL / CONFERENCE	PUBLISHED DATE	ISSN NO/ VOL NO, ISSUE NO	RDP REMARKS
1.	Development and characterization of cubic boron nitride based surface composite on D2 tool steel using thermal diffusion.	Materials Today: Proceedings	14 March 2020	Materials Today: Proceedings 26 (2020) 2099–2102	
2.	Experimental investigation on the surface hardness and tribological	Materials Today: Proceedings	15 July 2020	2214-7853 doi.org/10.1016/j.matpr.2020.06.390	

	properties of c-BN diffused D2 steel				
3.	Synthesis of cubic boron nitride diffused-D2 steel surface composite by thermo-chemical diffusion process to enhance the wear resistance.	Materials Research Express	02 September 2020.	Mater. Res. Express 7(9) (2020) 096503	

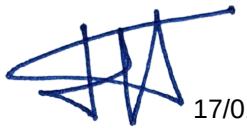

17/01/2021 Regd No: 41500104, harminder.saggu@lpu.co.in

Signature of Candidate with Date, Registration No, Email ID

17/01/2021 UID:24367

Signature of Guide with Date & UID

17/01/2021 UID: 21503

Signature of Co-Guide with Date & UID